The John A. Blume Earthquake Engineering Center

Department of Civil Engineering
Stanford University

PROBABILISTIC SITE-DEPENDENT RESPONSE SPECTRA

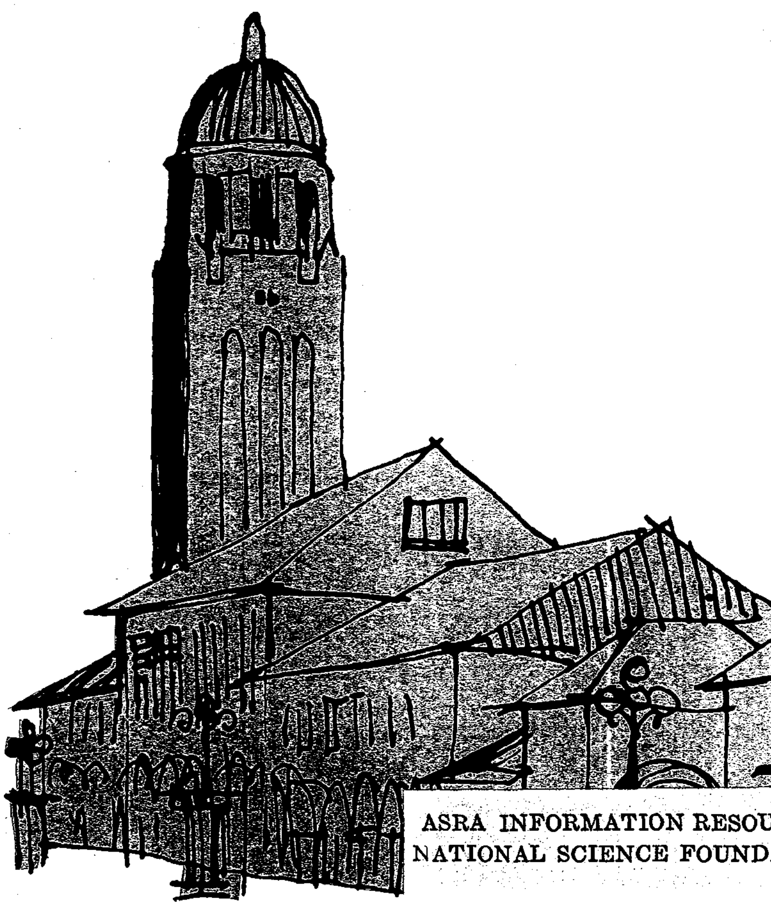

by

Anne S. Kiremidjian
Haresh C. Shah

This research was partially supported by
The National Science Foundation
Grant GI-39122
and
Banco Central de Nicaragua

Report No. 29
April 1978

The John A. Blume Earthquake Engineering Center was established to promote research and education in earthquake engineering. Through its activities our understanding of earthquakes and their effects on mankind's facilities and structures is improving. The Center conducts research, provides instruction, publishes reports and articles, conducts seminars and conferences, and provides financial support for students. The Center is named for Dr. John A. Blume, a well-known consulting engineer and Stanford alumnus.

Address

The John A. Blume Earthquake Engineering Center
Department of Civil Engineering
Stanford University
Stanford, California 94305

50272-101

REPORT DOCUMENTATION PAGE	1. REPORT NO. NSF/RA-780322	2.	3. Recipient's Accession No. PB290353

4. Title and Subtitle
Probabilistic Site-Dependent Response Spectra (Report No. 29)

5. Report Date
April 1978

6.

7. Author(s)
A.S. Kiremidjian, H.C. Shah

8. Performing Organization Rept. No.
29

9. Performing Organization Name and Address
Stanford University
Department of Civil Engineering
The John A. Blume Earthquake Engineering Center
Stanford, California 94305

10. Project/Task/Work Unit No.

11. Contract(C) or Grant(G) No.
(C)
(G) GI39122

12. Sponsoring Organization Name and Address
Applied Science and Research Applications (ASRA)
National Science Foundation
1800 G Street, N.W.
Washington, DC 20550

13. Type of Report & Period Covered

14.

15. Supplementary Notes

16. Abstract (Limit: 200 words)
Effects of local soil conditions on the PGA, the frequency content, and the amplification factor are investigated. Analysis goals are to obtain peak ground motion modification parameters for correcting the probability distributions on the peak ground acceleration values for the site of interest; to develop site dependent response spectral shapes (or dynamic amplification factors) and probability distributions of the latter for three basic soil types; and to develop probability distributions on response spectra at a given location for the three different soil types and from them to obtain design response spectra for a specified risk level. Some significant observations were: (1) Peak ground acceleration from a given earthquake, whose epicenter is within 25 km from the site of interest, diminishes in value by factors of 1.0, 0.75, and 0.60 as the local site conditions change from firm ground to intermediate soils, to alluvial soils; (2) Probability distributions on peak ground acceleration for soil classes 0 and 1 can be derived from the distribution for soil class 2 by applying the soil factors of K_0 and K_1; (3) Spectral shapes for the three soil types described by classes 0, 1, and 2 are found to be statistically independent of peak ground acceleration; and (4) The stochastic behavior of dynamic amplification factors is found to be best represented by the gamma distribution.

17. Document Analysis a. Descriptors

Earthquakes	Seismic surveys	Soils
Seismology	Hazards	Soil analysis

b. Identifiers/Open-Ended Terms
Response spectra
Probabilistic response spectra

c. COSATI Field/Group

18. Availability Statement	19. Security Class (This Report)	21. No. of Pages
NTIS.		93
	20. Security Class (This Page)	22. Price A05-A01

(See ANSI-Z39.18) See Instructions on Reverse OPTIONAL FORM 272 (4-77) (Formerly NTIS-35) Department of Commerce

PROBABILISTIC SITE-DEPENDENT RESPONSE SPECTRA

by

Anne Setian Kiremidjian
Haresh C. Shah

This research was partially supported by the National Science Foundation Grant GI-39122 and Banco Central de Nicaragua.

ia

ACKNOWLEDGMENTS

The authors of this report would like to thank Professor T. C. Zutty and Dr. C. P. Mortgat for the many helpful discussions and suggestions.

The partial support provided by the National Science Foundation Grant GI-39122 and Banco Central de Nicaragua is greatfully acknowledged.

TABLE OF CONTENTS

CHAPTER 1

INTRODUCTION

Earthquake ground motion has been observed to be altered by the various types of soils encountered along the path of energy propagation. Changes occur due to the different soil layers, the depth of the soil layer to bedrock, irregularities within a soil layer, different densities, shear wave velocities, and natural periods of the soil. Furthermore, the effect of the local soil on the ground motion will depend on the strength of the initial energy release, its frequency characteristics and its duration.

Awareness of the local soil condition problem has lead to the study of its influence on the different ground motion parameters. Some of the first efforts to study the changes in the intensity of ground motion were made by Wood (19) in his study of damage distribution and the intensity of shaking in San Francisco during the April 19, 1906 earthquake. The relationship between damage and ground conditions has been demonstrated by Duke (2). Gutenberg (4) and Kanai (9) have shown that small earthquakes and microtremors cause higher ground surface accelerations on soil deposits than on rock. Wiggins (19) has studied the effect of site conditions on the intensity of ground shaking by analyzing more than one hundred strong motion records. Differences in peak ground motion with soil depths and soil characteristics have been studied by Seed and Idriss (12) by considering earthquake records at sites approximately at the same distance from the epicenter. The primary conclusions from their study are that deep deposits of soft soils tend to produce ground motion with long-period characteristics, thus affecting long-period structures, and shallow deposits of stiff soils result in ground motions having predominantly short period characteristics that affect short period structures. Analytical models for considering soil effects on earthquake motion are also developed in the same study. In a later report by Seed and Idriss (13) it was observed that for great distant earthquakes, the incidence of structural damage for buildings in San Francisco is likely to be greatest for multi-story buildings underlain by deep deposits of clay. The structural damage potential for those buildings was found to be twice as high as for buildings with the same structural characteristics built on other types of foundation material. The potential for damage was estimated to be about three to four times as high as for structures sited on rock. Site dependent response spectra were developed by Seed, Ugas, and Lysmer (14). The mean and one standard deviation spectral shapes were analyzed for four different soil conditions ranging from deep cohesionless soils to rock.

A considerable amount of work has also been done in the area of the damage potential of soil; such as soil liquefaction and landslides. These topics will not be of primary concern in the present development, though their importance is recognized. They pertain to much more localized problems, and it would be difficult to include them in the general methodology of this development.

In the present chapter the effects of local soil conditions on the PGA, the frequency content and the amplification factor are investigated. Other methods such as analysis of microtremor data, analytical modeling of soils, or actual testing of soils are not considered. The goals of this analysis are threefold:

(1) To obtain peak ground motion modification parameters for correcting the probability distributions on the peak ground acceleration values for the site of interest.

(2) To develop site dependent response spectral shapes (or dynamic amplification factors) and probability distributions of the later for three basic soil types.

(3) To develop probability distributions on response spectra at a given location for the three different soil types and from them to obtain design response spectra for a specified risk level.

CHAPTER 2

SITE-DEPENDENT DISTRIBUTION ON PEAK GROUND ACCELERATION

2.1 Theoretical Development

The factors affecting earthquake ground motion have already been emphasized in the introduction. Of particular interest is the variation in peak ground acceleration values with different types of soils. Some previously developed models (11, 52) for obtaining the future peak ground acceleration at a site assume uniformity of the soil throughout the regions. In general however, the soil conditions can vary from deep soft alluvium to firm ground, and only rarely does one find continuous bedrock for foundation. Thus it is necessary to include the effects of local soil conditions in the peak ground acceleration forecast models. In the model used by Kiremidjian (11) the probability distribution of peak ground acceleration is determined at firm ground site and it would be difficult to generalize it to include all the possible travel paths of energy transmission with the numerous possible soil conditions encountered along the way. In such a case, the soil condition analysis would have to be done from the point of energy release and all modifications along the way would have to be incorporated. Such a method for analysis can be developed theoretically with the use of random generation models. However, the application of these models in practice may be very difficult. Consequently, the analysis in this development considers only the local site conditions and not the conditions along the wave travel path.

It is hypothesized that constants giving the relation between different classes of soil can be obtained and can be defined as follows:

$$k_i = \frac{\text{Peak Ground Acceleration of Soil Class i}}{\text{Peak Ground Acceleration of Firm Ground}} \qquad (1)$$

where i specifies a soil class other than firm ground. Equation (1) can be written as:

$$k_i = \frac{y_i}{y} \qquad (2)$$

where

y_i = peak ground acceleration for soil class i

y = peak ground acceleration for firm ground

or alternatively as

$$y_i = k_i y \qquad (3)$$

The cumulative probability distribution on peak ground acceleration for soil class i can be derived in its most general form as:

$$P[Y_i \leq y_i] = P[Yk_i \leq y_i] = P[Y \leq y_i/k_i] \qquad (4)$$

The form of Equation (4) is the same as the distribution for firm ground acceleration except for the dividing factor of k_i. Thus for any soil class, the cumulative distribution on peak ground acceleration can be obtained directly from the one for firm ground acceleration, but replacing the variable y by the variable y_i/k_i where k_i is the constant for the ith soil class. A direct application of the proposed modification will be shown later in this chapter.

2.2 Strong Motion Data

Strong motion records from 57 past major earthquakes in the Western United States have been collected by the Earthquake Engineering Research Laboratory of the California Institute of Technology (6). The 57 earthquake events are listed in Table 1. From these earthquakes 209 strong motion accelerograms were obtained at free field stations or at the basements of buildings.

Tables 2 to 4 give the earthquakes from which the records were taken, the magnitude of the earthquake, the distance from the epicenter to the recording station when available, and the peak acceleration for each horizontal component. Only the horizontal components of the records will be used in the subsequent analysis since it is felt that they are the primary cause of damage.

The data varies in Richter magnitude from 3.8 to 7.7, the majority of the earthquakes being in the range between 5.0 and 6.7, thus representing a fairly uniform sample of damaging earthquakes. This data will be used for two different purposes. First the peak ground acceleration values will be used to obtain the soil class factors described in the previous section. Second, the acceleration response spectra computed from the entire acceleration record (7) will be used in obtaining response spectrum shapes and probability distributions on response spectra for different soil conditions. One disadvantage of the data is that about 50% of it is from the February 9, 1971, San Fernando earthquake; this introduces a bias towards conditions encountered primarily in the San Fernando-Los Angeles area, and also contains peculiarities associated with that particular earthquake. Later in the discussion as assessment will be made of the degree of accuracy of the results obtained.

TABLE 1*

Data for Earthquakes Providing Strong Motion Records**

No.	Earthquake Area	Mo. Day Year	Time Time Zone	Lat. (N) ° ' "	Long. (W) ° ' "	Depth (km)	Mag.	Max. Int.
1	Long Beach, CA	Mar. 10, 1933	1754 PST	33 37 00	117 58 00	16.0	6.3	9
2	Southern Calif.	Oct. 2, 1933	0110 PST	33 47 00	118 08 00	16.0	5.4	6
3	Eureka, CA	Jul. 6, 1934	1449 PST	41 42 00	124 36 00			5
4	Lower Calif.	Dec. 30, 1934	0552 PST	32 15 00	115 30 00	16.0	6.5	9
5	Helena, Mt.	Oct. 31, 1935	1138 MST	46 37 00	111 58 00		6.0	8
6	Helena, Mt.	Oct. 31, 1935	1218 MST	46 37 00	111 58 00			3
7	Helena, Mt.	Nov. 21, 1935	2058 MST	46 36 00	112 00 00			6
8	Helena, Mt.	Nov. 28, 1935	0742 MST	46 37 00	111 58 00			6
9	Humboldt Bay, CA	Feb. 6, 1937	2042 PST	40 30 00	125 15 00			5
10	Imperial Valley, CA	Apr. 12, 1938	0825 PST	32 53 00	115 35 00	16.0	3.0	
11	Imperial Valley, CA	Jun. 5, 1938	1842 PST	32 54 00	115 13 00	16.0	5.0	
12	Imperial Valley, CA	Jun. 6, 1938	0435 PST	32 15 00	115 10 00	16.0	4.0	
13	Northwest Calif.	Sep. 11, 1938	2210 PST	40 18 00	124 48 00		5.5	6
14	Imperial Valley, CA	May 18, 1940	2037 PST	32 44 00	115 30 00	16.0	6.7	10
15	Northwest CA	Feb. 9, 1941	0145 PST	40 42 00	125 24 00		6.4	
16	Santa Barbara, CA	Jun. 30, 1941	2351 PST	34 22 00	119 35 00	16.0	5.9	8
17	Northern Calif.	Oct. 3, 1941	0813 PST	40 36 00	124 36 00			7
18	Torrance-Gardena, CA	Nov. 14, 1941	0042 PST	33 47 00	118 15 00	16.0	5.4	8
19	Borrego Valley, CA	Oct. 21, 1942	0822 PST	32 58 00	116 00 00	16.0	6.5	7
20	Northern Calif.	Mar. 9, 1949	0429 PST	37 06 00	121 18 00		5.3	7
21	Western Wash.	Apr. 13, 1949	1156 PST	47 06 00	122 42 00		7.1	8
22	Imperial Valley, CA	Jan. 23, 1951	2317 PST	32 59 00	115 44 00	16.0	5.6	7
23	Northwest Calif.	Oct. 7, 1951	2011 PST	40 17 00	124 48 00		5.8	7
24	Kern County, CA	Jul. 21, 1952	0453 PDT	35 00 00	119 01 00	16.0	7.7	11
25	Kern County, CA	Jul. 23, 1952	PDT	35 17 00	118 39 00			
26	Northern Calif.	Sep. 22, 1952	0441 PDT	40 12 00	124 25 00		5.5	7
27	Southern Calif.	Nov. 21, 1952	2346 PST	35 50 00	121 10 00			7
28	Imperial Valley, CA	Jun. 13, 1953	2017 PST	32 57 00	115 43 00	16.0	5.5	7
29	Wheeler Ridge, CA	Jan. 12, 1954	1534 PST	35 00 00	119 01 00	16.0	5.9	8
30	Central Calif.	Apr. 25, 1954	1233 PST	36 48 00	121 48 00		5.3	7
31	Lower Calif.	Nov. 12, 1954	0427 PST	31 30 00	116 00 00	16.0	6.3	5
32	Eureka, CA	Dec. 21, 1954	1156 PST	40 47 00	123 52 00		6.5	7
33	San Jose, CA	Sep. 4, 1955	1801 PST	37 22 00	121 47 00		5.8	7
34	Imperial County, CA	Dec. 16, 1955	2117 PST	33 00 00	115 30 00	16.0	4.3	
35	Imperial County, CA	Dec. 16, 1955	2142 PST	33 00 00	115 30 00	16.0	3.9	
36	Imperial County, CA	Dec. 16, 1955	2207 PST	33 00 00	115 30 00	16.0	5.4	7
37	El Alamo, Baja Calif.	Feb. 9, 1956	0633 PST	31 42 00	115 54 00	16.0	6.8	
38	El Alamo, Baja Calif.	Feb. 9, 1956	0725 PST	31 42 00	115 54 00		6.4	
39	Southern Calif.	Mar. 18, 1957	1056 PST	34 07 06	119 13 12	13.8	4.7	6
40	San Francisco, CA	Mar. 22, 1957	1048 PST	37 40 00	122 28 00		3.8	5
41	San Francisco, CA	Mar. 22, 1957	1144 PST	37 40 00	122 29 00		5.3	7
42	San Francisco, CA	Mar. 22, 1957	1515 PST	37 39 00	122 27 00		4.4	5
43	San Francisco, CA	Mar. 22, 1957	1627 PST	37 39 00	122 29 00		4.0	5
44	Central Calif.	Jan. 19, 1960	1926 PST	36 47 00	121 26 00		5.0	6
45	Northern Calif.	Jun. 5, 1960	1718 PST	40 49 00	124 53 00		5.7	6
46	Hollister, CA	Apr. 8, 1961	2323 PST	36 30 00	121 18 00	11.0	5.7	7
47	Northern Calif.	Sep. 4, 1962	0917 PST	40 58 00	124 12 00		5.0	6
48	Puget Sound, Wash.	Apr. 29, 1965	0729 PST	47 24 00	122 18 00		6.5	8
49	Southern Calif.	Jul. 15, 1965	2346 PST	34 29 06	118 31 18	15.1	4.0	6
50	Parkfield, CA	Jun. 27, 1966	2026 PST	35 57 18	120 29 54	6.0	5.6	7
51	Gulf of Calif.	Aug. 7, 1966	0936 PST	31 48 00	114 30 00	16.0	6.3	6
52	Northern Calif.	Sep. 12, 1966	0841 PST	39 24 00	120 06 00		6.3	7
53	Northern Calif.	Dec. 10, 1967	0407 PST	40 30 00	124 36 00		5.8	6
54	Northern Calif.	Dec. 18, 1967	0925 PST	37 00 36	121 47 18		5.2	6
55	Borrego Mtn., CA	Apr. 8, 1968	1830 PST	33 11 24	116 07 42	11.1	6.4	7
56	Lytle Creek, CA	Sep. 12, 1970	0630 PST	34 16 12	117 32 24	8.0	5.4	7
57	San Fernando, CA	Feb. 9, 1971	0600 PDT	34 24 42	118 24 00	13.0	6.4	11

* From Trifunac and Brady (54)

** Blanks indicate unavailable information. Many Southern California earthquakes have an assumed depth of 16 km.

2.3 Soil Correction Factors

When considering the peak ground acceleration from strong motion records, several factors must be taken into account. The peak ground acceleration value at a site will depend on the magnitude of the earthquake, the distance from the epicenter to the recording station, the soil condition at the site and the geological conditions along the energy propagation path. In general, the peak ground acceleration value has been shown (3) to decrease with increasing distance away from the epicenter, and to increase exponentially with Richter magnitude. Thus, in the analysis it is important to compare acceleration values recorded at the same distance from the epicenter and to be from earthquakes of comparable Richter magnitudes.

The first step in this analysis is to categorize the soil conditions in different groups. With the limited variety of strong motion records however, it is necessary to use as simple a classification as possible. For that purpose, three types of soil characteristics are defined in a manner similar to the one suggested by Trifunac and Brady (17).

Class 0: - soft alluvium deposits
Class 1: - intermediately stiff soils
Class 2: - firm ground or rocks

Other more detailed classifications have been used by Duke, et al (2), Wiggins (18) and Seed, et al (14). Duke's and Seed's classifications can be easily correlated to the one defined above (see Reference 17). Wiggins describes the soil types according to their shear wave velocity.

When sorting the data according to the above soil types, 258 accelerograms from 129 recording stations were found to belong to Class 0, 116 accelerograms from 58 stations were found to be best described by soil Class 1, and 44 accelerograms from 22 stations were found to have

TABLE 2

Strong Motion Earthquake Records for Soil Class 0

NO.	EERL NO.	LOCATION	DATE	RM	DIST. FROM EPI	DIRECTION	PGA CM/SEC²
1.	A001	El Centro,Imperial Valley	5.18.40	6.3	10km	SE	341.69
2.	A001	El Centro,Imperial Valley	5.18.40	6.3	10km	S90W	210.14
3.	A003	Atheneum,CIT,Pasadena	6.21.52	7.7	124km	SE	46.46
4.	A003	Atheneum,CIT,Pasadena	6.21.52	7.7	124km	S90W	52.06
5.	A004	Lincoln School Tunnel,Taft	6.21.52	7.7	55km	N21E	152.70
6.	A004	Lincoln School Tunnel,Taft	6.21.52	7.7	55km	S69E	175.94
7.	A005	Santa Barbara	6.21.52	7.7	89km	N43E	87.83
8.	A005	Santa Barbara	6.21.52	7.7	89km	S48E	128.61
9.	A006	Hollywood Storage Bldg. Basement,Los Angeles	6.21.52	7.7	120km	SW	54.07
10.	A006	Hollywood Storage Bldg. Basement,Los Angeles	6.21.52	7.7	120km	N90E	43.52
11.	A007	Hollywood Storage Bldg. P.E.Lot,Los Angeles	6.21.52	7.7	120km	SW	58.10
12.	A007	Hollywood Storage Bldg. P.E.Lot,Los Angeles	6.21.52	7.7	120km	N90E	41.24
13.	A010	Bank of Amer.,San Jose	9. 4.55		10km	N31W	100.16
14.	A010	Bank of Amer.,San Jose	9. 4.55		10km	N59E	105.80
15.	A011	El Centro,Imperial Valley	2. 9.56		118km	SW	32.42
16.	A011	El Centro,Imperial Valley	2. 9.56		118km	S90W	50.08
17.	A012	El Centro,Imperial Valley	2. 9.56		118km	SE	11.82
18.	A012	El Centro,Imperial Valley	2. 9.56		118km	S90W	15.44
19.	A013	San Francisco S.P.Bldg.	3.22.57	5.3	17km	N45E	45.86
20.	A013	San Francisco S.P.Bldg.	3.22.57	5.3	17km	N45W	44.88
21.	A018	Hollister City Hall	4. 8.61	5.6	21km	S01W	63.41
22.	A018	Hollister City Hall	4. 8.61	5.6	21km	N89W	175.68
23.	A019	El Centro,Imperial Valley	4. 8.68	6.5	64km	SW	127.76
24.	A019	El Centro,Imperial Valley	4. 8.68	6.5	64km	S90W	56.26
25.	A020	San Diego Light & Power	4. 8.68	6.5	96km	SW	20.52
26.	A020	San Diego Light & Power	4. 8.68	6.5	96km	N90E	28.88
27.	B021	Vernon CMD Bldg.	3.10.33	6.3	53km	S08W	130.63
28.	B021	Vernon CMD Bldg.	3.10.33	6.3	53km	N82W	151.52
29.	B023	Hollywood Storage Bldg. Basement,Los Angeles	10. 2.33	5.4	38km	N90W	26.35
30.	B023	Hollywood Storage Bldg. Basement,Los Angeles	10. 2.33	5.4	38km	NE	32.13
31.	B024	El Centro,Imperial Valley	12.30.34	6.5	64km	SW	156.82
32.	B024	El Centro,Imperial Valley	12.30.34	6.5	64km	S90W	179.14
33.	B028	Seattle,Wash.(Army Base)	4.13.49	7.1	55km	S02W	66.51
34.	B028	Seattle,Wash.(Army Base)	4.13.49	7.1	55km	N88W	65.86
35.	B029	Olympia,Wash.Hwy.Test Lab.	4.13.49	7.1	16km	N04W	161.63
36.	B029	Olympia,Wash.Hwy.Test Lab.	4.13.49	7.1	16km	N86E	274.63
37.	B031	Taft,Lincoln School	1.12.54	5.9	43km	N21E	63.87
38.	B031	Taft,Lincoln School	1.12.54	5.9	43km	S69E	66.81
39.	B032	Olympia,Wash.Hwy.Test Lab.	4.29.65	6.5	50km	S04E	134.23
40.	B032	Olympia,Wash.Hwy.Test Lab.	4.29.65	6.5	50km	S86W	194.33
41.	B035	Cholame-Shandon #8	6.27.66	5.6	38km	N50E	232.63
42.	B035	Cholame-Shandon #8	6.27.66	5.6	38km	N40W	269.60
43.	B036	Cholame-Shandon #12	6.27.66	5.6	38km	N50E	52.14
44.	B036	Cholame-Shandon #12	6.27.66	5.6	38km	N40W	63.17
45.	C048	8244 Orion Blvd,Los Angeles	2. 9.71	6.6	20km	NW	249.95
46.	C048	8244 Orion Blvd,Los Angeles	2. 9.71	6.6	20km	S90W	131.71
47.	C051	250 East First St.,L.A.	2. 9.71	6.6	41km	N36E	97.81
48.	C051	250 East First St.,L.A.	2. 9.71	6.6	41km	N54W	122.73
49.	C054	445 S.Figueroa St.,L.A.	2. 9.71	6.6	41km	N52W	144.10
50.	C054	445 S.Figueroa St.,L.A.	2. 9.71	6.6	41km	S38W	116.96
51.	D054	Hollywood Storage Bldg., Basement, Los Angeles	2. 9.71	6.6	35km	SW	103.78
52.	D054	Hollywood Storage Bldg., Basement, Los Angeles	2. 9.71	6.6	35km	W90E	148.24
53.	D058	Hollywood Storage Bldg., P.E. Lot, Los Angeles	2. 9.71	6.6	35km	SW	167.26
54.	D058	Hollywood Storage Bldg., P.E. Lot, Los Angeles	2. 9.71	6.6	35km	N90E	206.99
55.	D059	1901 Ave, of the Stars,L.A.	2. 9.71	6.6	38km	N46W	133.83
56.	D059	1901 Ave, of the Stars,L.A.	2. 9.71	6.6	38km	S44W	147.10
57.	D062	1640 S. Marrengo,L.A.	2. 9.71	6.6	42km	N38W	117.98
58.	D062	1640 S. Marrengo,L.A.	2. 9.71	6.6	42km	S53W	130.31
59.	D068	7080 Hollywood Blvd.,L.A.	2. 9.71	6.6	34km	NE	81.21
60.	D068	7080 Hollywood Blvd.,L.A.	2. 9.71	6.6	34km	N90E	98.01
61.	E071	Wheeler Ridge	2. 9.71	6.6	89km	SW	26.53
62.	E071	Wheeler Ridge	2. 9.71	6.6	89km	N90E	25.28
63.	E075	3470 Wilshire Blvd.,L.A.	2. 9.71	6.6	39km	NE	133.81
64.	E075	3470 Wilshire Blvd.,L.A.	2. 9.71	6.6	39km	S90W	111.84
65.	E083	3407 W. Sixth St.,L.A.	2. 9.71	6.6	39km	SW	158.18
66.	E083	3407 W. Sixth St.,L.A.	2. 9.71	6.6	39km	N90E	161.95
67.	F086	Vernon CMD Bldg.	2. 9.71	6.6	46km	N83W	104.56
68.	F086	Vernon CMD Bldg.	2. 9.71	6.6	46km	S07W	80.46
69.	F087	Orange Co.Engr.Bldg., Santa Ana	2. 9.71	6.6	86km	S04E	26.76
70.	F087	Orange Co.Engr.Bldg., Santa Ana	2. 9.71	6.6	86km	S86W	28.24
71.	F089	808 S.Olive,Los Angeles	2. 9.71	6.6	42km	S53E	131.87
72.	F089	808 S.Olive,Los Angeles	2. 9.71	6.6	42km	S37W	139.00
73.	F095	120 N.Robertson,L.A.	2. 9.71	6.6	36km	S88E	96.23
74.	F095	120 N.Robertson,L.A.	2. 9.71	6.6	36km	S02W	83.85
75.	F098	646 S. Olive, L.A.	2. 9.71	6.6	42km	S53E	236.42
76.	F098	646 S. Olive, L.A.	2. 9.71	6.6	42km	S37W	192.01
77.	F101	Southern Calif.Edison, Colton	2. 9.71	6.6	104km	SW	37.46
78.	F101	Southern Calif.Edison, Colton	2.9.71	6.6	104km	N90E	29.96
79.	F103	Pumping Plant,Pearblossom	2. 9.71	6.6	46km	NE	91.48
80.	F103	Pumping Plant,Pearblossom	2. 9.71	6.6	46km	N90W	120.52
81.	F105	UCLA,(Bontlel Hall),L.A.	2. 9.71	6.6	38km	SW	83.15
82.	F105	UCLA,(Boetlel Hall),L.A.	2. 9.71	6.6	38km	N90E	77.63
83.	G107	Atheneum,CIT,Pasadena	2. 9.71	6.6	37km	NE	93.50

TABLE 2 (Cont.)

Strong Motion Earthquake Records for Soil Class 0

NO.	EERL NO.	LOCATION	DATE	RM	DIST. FROM EPI	DIRECTION	PGA CM/SEC^2
84.	G107	Atheneum,CIT,Pasadena	2. 9.71	6.6	37km	N90E	107.25
85.	G108	Millivan Lib.,CIT,Pasadena	2. 9.71	6.6	37km	NE	197.99
86.	G108	Millivan Lib.,CIT,Pasadena	2. 9.71	6.6	37km	N90E	181.56
87.	G112	611 W. Sixth St.,L.A.	2. 9.71	6.6	41km	N38E	101.92
88.	G112	611 W. Sixth St.,L.A.	2. 9.71	6.6	41km	N52W	78.54
89.	G114	Fire Sta.,Palmdale	2. 9.71	6.6	33km	S60E	110.81
90.	G114	Fire Sta.,Palmdale	2. 9.71	6.6	33km	S30W	136.25
91.	H115	15250 Ventura Blvd.,L.A.	2. 9.71	6.6	28km	N11E	220.57
92.	H115	15250 Ventura Blvd.,L.A.	2. 9.71	6.6	28km	N79W	146.04
93.	H118	8639 Lincoln,Los Angeles	2. 9.71	6.6	48km	S45E	33.75
94.	H118	8639 Lincoln,Los Angeles	2. 9.71	6.6	48km	S45W	32.72
95.	H121	900 S. Fremont Ave. Alhambra	2. 9.71	6.6	41km	S90W	119.41
96.	H121	900 S. Fremont Ave. Alhambra	2. 9.71	6.6	41km	SW	112.29
97.	H124	2600 Nutwood,Fullerton	2. 9.71	6.6	74km	S90W	34.94
98.	H124	2600 Nutwood,Fullerton	2. 9.71	6.6	74km	SW	34.51
99.	I128	435 N. Oakhurst,Beverly Hills	2. 9.71	6.6	36km	NE	60.87
100.	I128	435 N. Oakhurst,Beverly Hills	2. 9.71	6.6	36km	S90W	91.58
101.	I131	450 N. Roxbury, Beverly Hills	2. 9.71	6.6	37km	N50E	184.28
102.	I131	450 N. Roxbury, Beverly Hills	2. 9.71	6.6	37km	N40W	160.63
103.	I134	1800 Century East Los Angeles	2. 9.71	6.6	38km	N54E	97.92
104.	I134	1800 Century East Los Angeles	2. 9.71	6.6	38km	S36E	82.33
105.	I137	15910 Ventura Blvd., Los Angeles	2. 9.71	6.6	28km	S81E	140.16
106.	I137	15910 Ventura Blvd., Los Angeles	2. 9.71	6.6	28km	S09W	128.95
107.	J145	15107 Van Owen Street Los Angeles	2. 9.71	6.6	24km	SW	113.93
108.	J145	15107 Van Owen Street Los Angeles	2. 9.71	6.6	24km	S90W	103.40
109.	M176	1150 S.Hill,Los Angeles	2. 9.71	6.6	42km	N37E	83.41
110.	M176	1150 S.Hill,Los Angeles	2. 9.71	6.6	42km	S53E	116.03
111.	M180	4000 W.Chapmat Ave.,Orange	2. 9.71	6.6	83km	SW	23.90
112.	M180	4000 W.Chapmat Ave.,Orange	2. 9.71	6.6	83km	S90W	29.87
113.	N186	Whittier Narrows Dam, Whittier	2. 9.71	6.6	52km	S37E	95.72
114.	N186	Whittier Narrows Dam, Whittier	2. 9.71	6.6	52km	S53W	96.68
115.	N187	San Antonio Dam,Upland	2. 9.71	6.6	71km	N15E	55.74
116.	N187	San Antonio Dam,Upland	2. 9.71	6.6	71km	N75W	75.87
117.	N188	1880 Century East Los Angeles	2. 9.71	6.6	38km	N54E	114.44
118.	N188	1880 Century East Los Angeles	2. 9.71	6.6	38km	N36W	126.53
119.	N195	San Juan Capistrano	2. 9.71	6.6	120km	N33E	40.90
120.	N195	San Juan Capistrano	2. 9.71	6.6	120km	N57W	30.98
121.	N196	Long Beach State College	2. 9.71	6.6	73km	N76W	35.05
122.	N196	Long Beach State College	2. 9.71	6.6	73km	S14W	31.21
123.	O199	1625 Olympic Blvd.,L.A.	2. 9.71	6.6	41km	N28E	137.86
124.	O199	1625 Olympic Blvd.,L.A.	2. 9.71	6.6	41km	N62W	238.83
125.	O204	205 W. Broadway,Long Beach	2. 9.71	6.6	73km	NE	26.00
126.	O204	205 W. Broadway,Long Beach	2. 9.71	6.6	73km	N90E	20.78
127.	O205	Terminal Island,Long Beach	2. 9.71	6.6	71km	N21W	28.42
128.	O205	Terminal Island,Long Beach	2. 9.71	6.6	71km	S69W	28.13
129.	O206	Hall of Records,San Bernardino	2. 9.71	6.6	104km	NE	37.44
130.	O206	Hall of Records,San Bernardino	2. 9.71	6.6	104km	N90E	43.93
131.	O210	Fire Station,Hemet	2. 9.71	6.6	140km	S45E	34.93
132.	O210	Fire Station,Hemet	2. 9.71	6.6	140km	S45W	38.44
133.	P217	3345 Wilshire Blvd.,L.A.	2. 9.71	6.6	39km	SW	108.28
134.	P217	3345 Wilshire Blvd.,L.A.	2. 9.71	6.6	39km	N90E	88.17
135.	P222	Navy Lab.,Port Hueneme	2. 9.71	6.6	78km	SW	25.91
136.	P222	Navy Lab.,Port Hueneme	2. 9.71	6.6	78km	S90W	25.22
137.	P231	9841 Airport Blvd.,L.A.	2. 9.71	6.6	49km	NE	41.33
138.	P231	9841 Airport Blvd.,L.A.	2. 9.71	6.6	49km	S90W	37.76
139.	Q233	14724 Ventura Blvd,L.A.	2. 9.71	6.6	28km	S12W	243.28
140.	Q233	14724 Ventura Blvd,L.A.	2. 9.71	6.6	28km	N78W	197.05
141.	Q236	1760 N. Orchid Ave,L.A.	2. 9.71	6.6	34km	South	167.29
142.	Q236	1760 N. Orchid Ave,L.A.	2. 9.71	6.6	34km	East	122.43
143.	Q239	9100 Wilshire Blvd, Beverly Hills	2. 9.71	6.6	37km	South	119.17
144.	Q239	9100 Wilshire Blvd, Beverly Hills	2. 9.71	6.6	37km	East	161.76
145.	R246	6464 Sunset Blvd,L.A.	2. 9.71	6.6	34km	South	115.97
146.	R246	6464 Sunset Blvd,L.A.	2. 9.71	6.6	34km	East	106.99
147.	R248	6430 Sunset Blvd,L.A.	2. 9.71	6.6	34km	South	184.03
148.	R249	6430 Sunset Blvd,L.A.	2. 9.71	6.6	34km	East	174.35
149.	R249	1900 Avenue of the Stars,LA	2. 9.71	6.6	38km	N44E	79.89
150.	R249	1900 Avenue of the Stars,LA	2. 9.71	6.6	38km	S46E	84.18
151.	R253	533 S.Fremont Avenue,L.A.	2. 9.71	6.6	41km	N30W	242.00
152.	R253	533 S.Fremont Avenue,L.A.	2. 9.71	6.6	41km	S60W	220.69
153.	S258	3440 University Ave.,L.A.	2. 9.71	6.6	42km	N29E	56.36
154.	S258	3440 University Ave.,L.A.	2. 9.71	6.6	42km	S61E	83.39

TABLE 2 (Cont.)

Strong Motion Earthquake Records for Soil Class 0

NO.	EERL NO.	LOCATION	DATE	RM	DIST. FROM EPI	DIRECTION	PGA CM/SEC^2
155.	S261	1177 Beverly Drive,L.A.	2. 9.71	6.6	39km	N59E	97.76
156.	S261	1177 Beverly Drive,L.A.	2. 9.71	6.6	39km	N31W	107.75
157.	S266	3550 Wilshire Blvd.,L.A.	2. 9.71	6.6	39km	North	153.56
158.	S266	3550 Wilshire Blvd.,L.A.	2. 9.71	6.6	39km	West	129.68
159.	S267	5260 Century Blvd.,L.A.	2. 9.71	6.6	49km	North	55.54
160.	S267	5260 Century Blvd.,L.A.	2. 9.71	6.6	49km	East	61.52
161.	T274	El Centro,Imperial Valley Irrigation District	4.12.38	3.0	13km	North	28.22
162.	T274	El Centro,Imperial Valley Irrigation District	4.12.38	3.0	13km	East	48.79
163.	T275	El Centro,Imperial Valley Irrigation District	6. 5.38	5.0	13km	North	33.29
164.	T275	El Centro,Imperial Valley Irrigation District	6. 5.38	5.0	13km	East	26.03
165.	T277	El Centro,Imperial Valley Irrigation District	5.18.40	6.7	13km	North	22.50
166.	T277	El Centro,Imperial Valley Irrigation District	5.18.40	6.7	13km	East	24.13
167.	T278	El Centro,Imperial Valley Irrigation District	5.18.40	6.7	18km	North	11.91
168.	T278	El Centro,Imperial Valley Irrigation District	5.18.40	6.7	18km	East	14.43
169.	T279	El Centro,Imperial Valley Irrigation District	5.18.40	6.7	13km	North	11.37
170.	T279	El Centro,Imperial Valley Irrigation District	5.18.40	6.7	13km	East	18.46
171.	T280	El Centro,Imperial Valley Irrigation District	5.18.40	6.7	13km	North	22.36
172.	T280	El Centro,Imperial Valley Irrigation District	5.18.40	6.7	13km	East	9.51
173.	T281	El Centro	5.18.40	6.7		North	6.49
174.	T281	El Centro	5.18.40	6.7		East	10.51
175.	T282	El Centro	5.18.40	6.7		North	3.28
176.	T282	El Centro	5.18.40	6.7		East	3.93
177.	T283	El Centro	5.18.40	6.7		North	63.97
178.	T283	El Centro	5.18.40	6.7		East	77.20
179.	T284	El Centro	5.18.40	6.7		NORTH	11.42
180.	T284	El Centro	5.18.40	6.7		East	16.05
181.	T285	El Centro	5.18.40	6.7		North	50.96
182.	T285	El Centro	5.18.40	6.7		East	70.92
183.	T286	El Centro	10.21.42	6.5		North	58.49
184.	T286	El Centro	10.21.42	6.5		East	46.54
185.	T287	El Centro	1.23.51	5.6		North	30.35
186.	T287	El Centro	1.23.51	5.6		East	27.56
187.	T288	El Centro	6.13.53	5.5		North	7.21
188.	T288	El Centro	6.13.53	5.5		East	35.85
189.	T289	El Centro	11.12.54	6.3		North	24.18
190.	T289	El Centro	11.12.54	6.3		East	27.02
191.	T290	El Centro	12.16.55	4.3		North	30.42
192.	T290	El Centro	12.16.55	4.3		East	15.87
193.	T291	El Centro	12.16.55	3.9		North	6.39
194.	T291	El Centro	12.16.55	3.9		East	7.19
195.	T292	El Centro	12.16.55	5.4		North	62.52
196.	T292	El Centro	12.16.55	5.4		East	71.06
197.	T293	El Centro	8.7.66	6.3		North	13.51
198.	T294	El Centro	8.7.66	6.3		East	14.78
199.	U299	S.B. Court House	6.30.41	5.9	16km	N45E	233.78
200.	U299	S.B. Court House	6.30.41	5.9	16km	S45E	172.31
201.	U301	Hollister Public Library	3. 9.49	3.5	20km	S01W	119.44
202.	U301	Hollister Public Library	3. 9.49	3.5	20km	N89W	193.61
203.	U305	Hollister Public Library	3. 9.49	5.3	32km	N89W	52.02
204.	U305	Hollister Public Library	3. 9.49	5.3	32km	S01W	48.94
205.	U307	Hollister Public Library	1.19.60	5.0		N89W	55.52
206.	U307	Hollister Public Library	1.19.60	5.0		S01W	35.34
207.	U309	Hollister Public Library	4. 8.61	5.5	21km	N89W	168.56
208.	U309	Hollister Public Library	4. 8.61	5.5	21km	S01W	74.94
209.	U310	Seattle,Washington	4.29.65	6.5	22km	S32E	52.19
210.	U310	Seattle,Washington	4.29.65	6.5	22km	S58W	77.57
211.	U311	Lincoln School Tunnel,Taft	6.27.66	5.6	179km	N21E	8.11
212.	U311	Lincoln School Tunnel,Taft	6.27.66	5.6	179km	S69E	11.24
213.	U313	Hollister Public Library	12.18.67	5.2	45km	N89W	13.10
214.	U313	Hollister Public Library	12.18.67	5.2	45km	S01W	16.30
215.	V314	L.A.Subway Terminal Sub-Basement,L.A.	3.10.33	6.3	59km	N39E	62.33
216.	V314	L.A.Subway Terminal Sub-Basement,L.A.	3.10.33	6.3	59km	N51W	95.63
217.	V315	Long Beach Utilities Bldg.	3.10.33	6.3	27km	South	192.73
218.	V315	Long Beach Utilities Bldg.	3.10.33	6.3	27km	West	155.00
219.	V316	Long Beach Utilities Bldg.	11.14.41	5.4	4km	North	39.73
220.	V316	Long Beach Utilities Bldg.	11.14.41	5.4	4km	East	53.69
221.	V317	Chamber of Commerce Basement, L.A.	11.14.41	5.4	26km	S50E	14.94
222.	V317	Chamber of Commerce Basement, L.A.	11.14.41	5.4	26km	S40W	11.25
223.	V320	Southern Pacific Bldg. Basement, San Fran.	3.22.57	3.8	16km	N45E	2.02
224.	V320	Southern Pacific Bldg. Basement, San Fran.	3.22.57	3.8	16km	N45W	2.42
225.	V322	Southern Pacific Bldg. Basement, San Fran.	3.22.57	5.3	17km	N45E	8.56
226.	V322	Southern Pacific Bldg. Basement, San Fran.	3.22.57	5.3	17km	N45W	24.59
227.	V328	Southern Pacific Bldg. Basement, San Fran.	3.22.57	4.4	17km	N45E	2.07
228.	V328	Southern Pacfic Bldg. Basement, San Fran.	3.22.57	4.4	17km	N45W	9.00

TABLE 2 (Cont.)

Strong Motion Earthquake Records for Soil Class 0

NO.	EERL	LOCATION	DATE	RM	DIST. FROM EPI	DIRECTION	PGA CM/SEC^2
229.	V329	Navy Res.& Eval.Lab, Port Hueneme	3.18.57	4.7	7km	South	163.64
230.	V329	Navy Res. & Eval.Lab, Port Hueneme	3.18.57	4.7	7km	West	86.86
231.	V332	Pacific Tel & Tel Bldg. Basement,Sacremento	9.12.66	6.3	178km	South	14.49
232.	V332	Pacific Tel & Tel Bldg. Basement,Sacremento	9.12.66	6.3	178km	East	12.49
233.	W338	Hall of Records, San Bernardino	9.12.70	5.4	33km	North	113.83
234.	W338	Hall of Records, San Bernardino	9.12.70	5.4	33km	East	57.53
235.	W339	Southern Calif.Edison Colton	9.12.70	5.4	34km	South	40.20
236.	W339	Southern Calif.Edison Colton	9.12.70	5.4	34km	East	35.38
237.	W342	Millikan Lib.CIT,Pasadena	9.12.70	6.4	48km	North	19.38
238.	W342	Millikan Lib.CIT,Pasadena	9.12.70	6.4	48km	East	18.71
239.	Y370	Southern Calif.Edison Colton	4. 8.68	6.4	161km	South	21.49
240.	Y370	Southern Calif.Edison Colton	4. 8.68	6.4	161km	East	28.14
241.	Y371	Orange County Engr.Bldg. Santa Ana	4. 8.68	6.4	200km	S04E	13.19
242.	Y371	Orange County Engr.Bldg. Santa Ana	4. 8.68	6.4	200km	S86W	11.73
243.	Y372	Southern Calif. Edison Term.Isl.,Long Beach	4. 8.68	6.4	239km	N21W	8.73
244.	Y372	Southern Calif. Edison Term.Isl.,Long Beach	4. 8.68	6.4	239km	S69W	9.51
245.	Y375	Millikan,CIT,Pasadena	4. 8.68	6.4	242km	North	9.82
246.	Y375	Millikan,CIT,Pasadena	4. 8.68	6.4	242km	East	10.32
247.	Y376	Atheneum,CIT,Pasadena	4. 8.68	6.4	242km	South	7.00
278.	Y376	Atheneum,CIT,Pasadena	4. 8.68	6.4	242km	West	10.07
279.	Y377	Southern Calif.Edison 601 W. 5th St.,L.A.	4. 8.68	6.4	253km	N52W	7.67
280.	Y377	Southern Calif.Edison 601 W. 5th St.,L.A.	4. 8.68	6.4	253km	S38W	11.92
281.	Y378	Subway Terminal,Basement Los Angeles	4. 8.68	6.4	253km	S52E	6.97
282.	Y378	Subway Terminal,Basement Los Angeles	4. 8.68	6.4	253km	S38W	11.47
283.	Y379	CMD Building, Vernon	4. 8.68	6.4	245km	N83W	18.45
284.	Y379	CMD Building, Vernon	4. 8.68	6.4	245km	S07W	18.51
285.	Y380	Hollywood Storage Bldg, Basement, Los Angeles	4. 8.68	6.4	262km	South	10.93
286	Y380	Hollywood Storage Bldg, Basement, Los Angeles	4. 8.68	6.4	262km	East	12.39

TABLE 3

Strong Motion Earhtquake Records for Soil Class 1

NO.	EERL NO	LOCATION	DATE	RM	DIST. FROM EPI	DIRECTION	PGA CM/SEC^2
1.	A002	Ferndale City Hall	10.7.51	5.8	53km	S44W	102.03
2.	A002	Ferndale City Hall	10.7.51	5.8	53km	N46W	109.51
3.	A008	Eureka Fed.Building	12.21.54	6.5	24km	N11W	164.53
4.	A008	Eureka Fed.Building	12.21.54	6.5	24km	N79E	252.72
5.	A009	Ferndale City Hall	12.21.54	6.5	40km	N44E	155.73
6.	A009	Ferndale City Hall	12.21.54	6.5	40km	N46W	197.25
7.	A014	Alex.Bldg.,Basement San Francisco	3.22.57	5.3	16km	N09W	41.79
8.	A014	Alex.Bldg.,Basement San Francisco	3.22.57	5.3	16km	N81W	45.40
9.	A015	G.G.Pane, San Francisco	3.22.57	5.3	11km	N10E	81.79
10.	A015	G.G.Pane, San Francisco	3.22.57	5.3	11km	S80E	102.80
11.	A016	State Building San Francisco	3.22.57	5.3	17km	S09E	83.81
12.	A016	State Building San Francisco	3.22.57	5.3	17km	S81W	55.07
13.	A017	Oakland City Hall	3.22.57	5.3	24km	N26E	38.97
14.	A017	Oakland City Hall	3.22.57	5.3	24km	S64E	23.75
15.	B026	Ferndale City Hall	9.11.38	5.5	56km	N45E	140.89
16.	B026	Ferndale City Hall	9.11.38	5.5	56km	S45E	87.14
17.	B027	Ferndale City Hall	2. 9.41	6.6	104km	N45E	61.30
18.	B027	Ferndale City Hall	2. 9.41	6.6	104km	S45E	38.40
19.	B030	Ferndale City Hall	9.22.52	5.4	43km	N44E	53.11
20.	B030	Ferndale City Hall	9.22.52	5.4	43km	S46E	74.14
21.	B038	San Luis Obispo Recreation Bldg.	6.27.66		72km	N36W	14.21
22.	B038	San Luis Obispo Recreation Bldg.	6.27.66		72km	S54W	11.44
23.	B039	Eureka City Hall	12.10.67		59km	S11E	20.42
24.	B039	Eureka City Hall	12.10.67		59km	N79E	19.49
25.	B040	San Onofre SCE Power Plant	4. 8.68		158km	N33E	40.03
26.	B040	San Onofre SCE Power Plant	4. 8.68		158km	N57W	45.54
27.	D056	Castaic	2. 9.71	6.6	29km	N21E	309.40
28.	D056	Castaic	2. 9.71	6.6	29km	N69W	265.45
29.	D065	3710 Wilshire Blvd., Los Angeles, Ca.	2. 9.71	6.6	39km	SW	146.74
30.	D065	3710 Wilshire Blvd., Los Angeles, Ca.	2. 9.71	6.6	39km	S90W	155.73
31.	E072	4680 Wilshire Blvd., Los Angeles, Ca.	2. 9.71	6.6	38km	N75W	82.24
32.	E072	4680 Wilshire Blvd., Los Angeles, Ca.	2. 9.71	6.6	38km	N15E	114.98
33.	E078	Los Angeles Water & Power	2. 9.71		41km	N50W	126.46
34.	E078	Los Angeles Water & Power	2. 9.71		41km	S40W	169.16
35.	E081	Santa Felicia Dam, Piru	2. 9.71		33km	S08E	213.00
36.	E081	Santa Felicia Dam, Piru	2. 9.71		33km	S82W	198.25
37.	F088	633 E.Broadway, Glendale	2. 9.71		32km	S70E	265.68
38.	F088	633 E. Broadway,Glendale	2. 9.71		32km	S20W	209.11
39.	F092	2011 Zonal, Los Angeles	2. 9.71		42km	S62E	64.22
40.	F092	2011 Zonal, Los Angeles	2. 9.71		42km	S28W	79.15
41.	F104	Oso Pumping Plant, Gorman	2. 9.71		55km	NE	85.20
42.	F104	Oso Pumping Plant, Gorman	2. 9.71		55km	N90W	103.06
43.	G110	JPL, Pasadena	2. 9.71		29km	S82E	207.77
44.	G110	JPL, Pasadena	2. 9.71		29km	S08W	138.98
45.	J144	ArrayStation # 12, Lance Houghes	2. 9.71		25km	N21E	346.17
46.	J144	Array Station # 12, Lance Houghes	2. 9.71		25km	N69W	277.90
47.	J148	616 S. Normandie Avenue Los Angeles	2. 9.71		39km	NE	107.63
48.	J148	616 S. Normandie Avenue Los Angeles	2. 9.71		39km	S90E	111.99
49.	L166	3838 Larkenshire Blvd. Los Angeles	2. 9.71		30km	NE	164.24
50.	L166	3838 Larkenshire Blvd. Los Angeles	2. 9.71		30km	S90W	147.65
51.	L171	Southern Calif. Edison San Onofre	2. 9.71		135km	N33E	11.95
52.	L171	Southern Calif. Edison San Onofre	2. 9.71		135km	N57W	15.87
53.	M178	Tehachapi Pumping Plant, Grapevine	2. 9.71		73km	N37E	117.28
54.	M178	Tehachapi Pumping Plant, Grapevine	2. 9.71		73km	S53E	139.04
55.	M183	6074 Pa Drive Wrightwood	2. 9.71		70km	N65E	42.40
56.	M183	6074 Pa Drive Wrightwood	2. 9.71		70km	N25E	55.71
57.	M184	6074 Pa Drive Wrightwood	2. 9.71		70km	S65E	43.10
58.	M184	6074 Pa Drive Wrightwood	2. 9.71		70km	S25W	57.19
59.	N185	Carbon Canyon Dam, Brea	2. 9.71	6.6	74km	S50E	67.33
60.	N185	Carbon Canyon Dam, Brea	2. 9.71	6.6	74km	S40W	67.28
61.	N191	2516 Via Tejon, Palos Verdes Estates	2. 9.71	6.6	67km	N65E	24.74
62.	N191	2516 Via Tejon, Palos Verdes Estates	2. 9.71	6.6	67km	S25E	40.07

TABLE 3 (Cont.)

Strong Motion Earthquake Records for Soil Class 1

NO.	EERL NO.	LOCATION	DATE	RM	DIST. FROM EPI	DIRECTION	PGA CM/SEC^2
		Palos Verdes Estates	2. 9.71	6.6	67km	S25E	40.07
63.	N192	2500 Wilshire Blvd., Los Angeles	2. 9.71	6.6	40km	N29E	96.75
64.	N192	2500 Wilshire Blvd., Los Angeles	2. 9.71	6.6	40km	N61W	98.88
65.	O208	University of Calif. Santa Barbara	2. 9.71	6.6	133km	N42E	16.50
66.	O208	University of Calif. Santa Barbara	2. 9.71	6.6	133km	S48E	17.05
67.	P214	4867 Sunset Blvd., Los Angeles.Calif.	2. 9.71	6.6	35km	S89W	154.10
68.	P214	4867 Sunset Blvd., Los Angeles, Calif.	2. 9.71	6.6	35km	S01E	156.35
69.	P220	666 West 19th Street Costa Messa	2. 9.71	6.6	96km	SW	24.17
70.	P220	666 West 19th Street Costa Messa	2. 9.71	6.6	96km	N90E	34.34
71.	Q241	800 West First Street Los Angeles	2. 9.71	6.6	41km	N37E	86.80
72.	Q241	800 West First Street Los Angeles	2. 9.71	6.6	41km	N53W	138.02
73.	R244	222 Figueroa Street Los Angeles	2. 9.71	6.6	41km	N53W	149.35
74.	R244	222 Figueroa Street Los Angeles	2. 9.71	6.6	41km	S37W	126.79
75.	R251	234 S. Figueroa Street Los Angeles	2. 9.71	6.6	41km	N37E	195.61
76.	R251	234 S. Figueroa Street Los Angeles	2. 9.71	6.6	41km	S53E	188.27
77.	S255	6200 Wilshire Blvd., Los Angeles	2. 9.71	6.6	38km	N08E	123.80
78.	S255	6200 Wilshire Blvd., Los Angeles	2. 9.71	6.6	38km	N82W	128.41
79.	S262	5900 Wilshire Blvd., Los Angeles	2. 9.71	6.6	38km	N83W	68.39
80.	S262	5900 Wilshire Blvd., Los Angeles	2. 9.71	6.6	38km	S07W	93.69
81.	S265	3411 Wilshire Blvd., Los Angeles	2. 9.71	6.6	39km	South	104.17
82.	S265	3411 Wilshire Blvd., Los Angeles	2. 9.71	6.6	39km	West	125.22
83.	U294	Ferndale City Hall	7. 6.34	5MMI	110km	N45W	14.50
84.	U294	Ferndale City Hall	7. 6.34	5MMI	110km	S45W	14.65
85.	U298	Ferndale City Hall	2. 6.37	5MMI	87km	N45W	38.45
86.	U298	Ferndale City Hall	2. 6.37	5MMI	87km	S45W	35.91
87.	U300	Ferndale City Hall	10. 3.41	6.4	76km	N45W	118.64
88.	U300	Ferndale City Hall	10. 3.41	6.4	76km	S45W	113.62
89.	U302	Tehachapi,Calif.Firehse	7.23.52	7.6		N10E	63.72
90.	U302	Tehachapi,Calif.Firehse	7.23.52	7.6		S80E	61.81
91.	U303	Tehachapi,Calif.Firehse	7.23.52	7.6		N10E	47.51
92.	U303	Tehachapi,Calif.Firehse	7.23.52	7.6		S80E	57.28
93.	U304	Tehachapi,Calif.Firehse	7.23.52	7.6		N10E	11.21
94.	U304	Tehachapi,Calif.Firehse	7.23.52	7.6		S80E	18.22
95.	U308	Ferndale City Hall	6. 5.60	5.7	67km	N46W	57.58
96.	U308	Ferndale City Hall	6. 5.60	5.7	67km	S44W	73.58
97.	U312	Ferndale City Hall	12.10.67	5.8	41km	N46W	103.07
98.	U312	Ferndale City Hall	12.10.67	5.8	41km	S44W	232.07
99.	V319	City Recreation Bldg. San Louis Obispo	11.21.52	6.0	73km	N36W	52.92
100.	V319	City Recreation Bldg., San Louis Obispo	11.21.52	6.0	73km	S54W	35.41
101.	V323	Alexander Building San Francisco	3.22.57	4.4	14km	N81E	15.69
102.	V323	Alexander Building San Francisco	3.22.57	4.4	14km	N09W	18.60
103.	V326	Oakland City Hall	3.22.57	4.4	20km	N26E	2.87
104.	V326	Oakland City Hall	3.22.57	4.4	20km	S64E	3.53
105.	V330	Eureka Federal Bldg.	9. 4.62	5.0		N79E	45.31
106.	V330	Eureka Federal Bldg.	9. 4.62	5.0		S11E	47.34
107.	V331	Old Ridge Route,Castaic	7.15.65	4.0	18km	South	40.45
108.	V331	Old Ridge Route,Castaic	7.15.65	4.0	18km	East	35.93
109.	W334	6074 Pa Drive Wrightwood	9.12.70	5.4	32km	S65E	139.04
110.	W334	6074 Pa Drive Wrightwood	9.12.70	5.4	32km	S25W	194.41
111.	W336	CWR Site, Cedar Springs,Calif.	9.12.70	5.4	25km	S54E	55.95
112.	W336	CWR Site, Cedar Springs,Calif.	9.12.70	5.4	25km	S36W	69.42
113.	W344	JPL, CIT, Pasadena, Calif.	9.12.70	5.4	62km	S82E	14.46
114.	W344	JPL, CIT Pasadena, Calif.	9.12.70	5.4	62km	S08W	24.14
115.	Y373	JPL, CIT, Pasadena, Calif.	4. 8.68	6.4	223km	S82E	7.36
116.	Y373	JPL, CIT Pasadena, Calif.	4. 8.68	6.4	223km	S08W	7.03

TABLE 4

Strong Motion Earthquake Records for Soil Class 2

NO.	EERL NO.	LOCATION	DATE	RM	DIST. FROM EPI	DIRECTION	PGA CM/SEC^2
1.	B025	Helena, Montana	10.31.35	6.0	8km	SW	143.47
2.	B025	Helena, Montana	10.31.35	6.0	8km	S90W	142.50
3.	B037	Temblor, Cal. No. 2	6.27.66	5.6	7km	N65W	264.35
4.	B037	Temblor, Cal. No. 2	6.27.66	5.6	7km	S25W	340.81
5.	C041	Pacoimadam, Pacioma	2.9.71	6.6	8km	S16E	1148.06
6.	C041	Pacoimadam, Pacioma	2.9.71	6.6	8km	S74W	1054.95
7.	C042	Pacoimadam, Pacoima	2.9.71	6.6	8km	S74W	27.07
8.	C042	Pacoimadam, Pacoima	2.9.71	6.6	8km	S16E	20.73
9.	C043	Pacoimadam, Pacoima	2.9.71	6.6	8km	S74W	45.47
10.	C043	Pacoimadam, Pacoima	2.9.71	6.6	8km	S16E	51.36
11.	C044	Pacoimadam, Pacoima	2.9.71	6.6	8km	S74W	109.94
12.	C044	Pacoimadam, Pacoima	2.9.71	6.6	8km	S16E	113.21
13.	C045	Pacoimadam, Pacoima	2.9.71	6.6	8km	S74W	47.53
14.	C045	Pacoimadam, Pacoima	2.9.71	6.6	8km	S16E	31.39
15.	C046	Pacoimadam, Pacoima	2.9.71	6.6	8km	S74W	23.60
16.	C046	Pacoimadam, Pacoima	2.9.71	6.6	8km	S16E	30.94
17.	C047	Pacoimadam, Pacoima	2.9.71	6.6	8km	S74W	18.25
18.	C047	Pacoimadam, Pacoima	2.9.71	6.6	8km	S16E	27.51
19.	F102	Fort Tejon, Tejon	2.9.71	6.6	71km	NE	24.65
20.	F102	Fort Tejon, Tejon	2.9.71	6.6	71km	N90E	20.64
21.	G106	Seism. Lab, C.I.T., Pasadena	2.9.71	6.6	37km	SW	87.48
22.	G106	Seism. Lab, C.I.T., Pasadena	2.9.71	6.6	37km	S90W	188.59
23.	J141	Array Sta. #1, Lake Hughes, Cal.	2.9.71	6.8	31km	N21E	145.52
24.	J141	Array Sta. #1, Lake Hughes, Cal.	2.9.71	6.8	31km	S69E	108.88
25.	J142	Array Sta. #4, Lake Hughes, Cal.	2.9.71	6.8	29km	S69E	168.25
26.	J142	Array Sta. #4, Lake Hughes, Cal.	2.9.71	6.8	29km	S21W	143.52
27.	J143	Array Sta. #9, Lake Hughes, Cal.	2.9.71	6.8	29km	N21E	119.26
28.	J143	Array Sta. #9, Lake Hughes, Cal.	2.9.71	6.8	29km	N69W	109.45
29.	0198	Griffith Park Obser., L.A.	2.9.71	6.8	33km	SW	176.90
30.	0198	Griffith Park Obser., L.A.	2.9.71	6.8	33km	S90W	167.38
31.	0207	Fairmont Reservoir, Fairmont	2.9.71	6.6	36km	N56E	64.70
32.	0207	Fairmont Reservoir, Fairmont	2.9.71	6.6	36km	N34W	97.09
33.	P221	Santa Anita Reserv., Arcadia	2.9.71	6.6	42km	N03E	137.68
34.	P221	Santa Anita Reserv., Arcadia	2.9.71	6.6	42km	N87W	165.75
35.	P223	Puddingstone Reserv., San Dimas	2.9.71	6.6	62km	N55E	69.70
36.	P223	Puddingstone Reserv., San Dimas	2.9.71	6.6	62km	N35W	53.25
37.	U296	Helena, Montana	11.21.35	6(MMI)		North	7.30
38.	U296	Helena, Montana	11.21.35	6(MMI)	62km	East	11.05
39.	U297	Helena, Montana	11.28.35	6(MMI)	62km	North	74.85
40.	U297	Helena, Montana	11.28.35	6(MMI)	62km	East	83.06
41.	W335	Allen Ranch, CWR Site, Sedar Springs	9.12.70	5.4	20km	S85E	69.88
42.	W335	Allen Ranch, CWR Site, Sedar Springs	9.12.70	5.4	20km	S05W	54.91

been recorded on soil type of Class 2. It should be noted that the accelerograms used are the horizontal components of motion only.

The records from each soil class are identified in Tables 2 to 4. The soil description for the recording sites were obtained from References (5), (8), (14), (17). In Tables 2 to 4, the Richter magnitude of the earthquake, the epicentral distance in km and the peak ground acceleration value in units of cm/sec^2 are also listed.

On the model described by Kiremidjian (11) the peak ground acceleration value obtained at a given site was derived by convolving the largest acceleration values from all nearby seismic sources and attenuating them to the site. Thus, the resulting peak ground acceleration value is governed by the nearest point on the closest source. An approach for obtaining k_0 and k_1 will be to consider accelerograms that are recorded at different epicentral distances. Because of the sparsity of the data, records are selected from each soil type for only two epicentral distances. Their ranges are from 0 km to 25 km, and from 26 km to 50 km. It would be desirable to consider different magnitude ranges for this analysis, however such data is not available at the present.

An interesting feature of the soil modification factors k_i in Tables 5a and 5b is their deamplification for distances between 26 km and 50 km. The value of $k_0 = 0.62$ for distances from 0 km to 25 km is very close to the value of $k^0 = 0.6$ suggested by Seed, et al (14) for sites located at 8 km from the source. The value of $k_1 = 0.75$, however, is 25% lower than the value of k_1 used by Seed, et al (14).

The amplification of peak ground acceleration for sites between 26 km and 50 km from the epicenter confirms the observations made by

TABLE 5a

Soil Modification Factors
(Distance From 0 km to 25 km, 5.5 < M < 6.5)

Soil Class	No. of Rec.	Mean PGA	k_i
Class 0	32	127.05	0.62
Class 1	10	155.38	0.75
Class 2	18	206.67	1.00

TABLE 5b

Soil Modification Factors
(Distance From 26 km to 50 km, 5.5 < M < 6.5)

Soil Class	No. of Rec.	Mean PGA	k_i
Class 0	80	135.25	1.09
Class 1	40	144.77	1.16
Class 2	14	124.48	1.00

Seed, et al (14). For example, k_0 for this distance range obtained through this study is approximately 1.1. The corresponding value suggested by Seed, et al (14) at 32 km distance is about 1.3. Similarly, k_1 value from this study is approximately 1.2. At 32 km, Seed, et al (14) used a value of 1.5.

For any subsequent analysis the following factors will be used:

TABLE 6

Soil Modification Factors
($5.5 \leq M \leq 6.5$)

Distance	k_0	k_1
0 km - 25 km	0.6	0.75
26 km - 50 km	1.1	1.2

The usefulness of k_0 and k_1 is best illustrated by an example. Since most of the original data is from Southern California and primarily from the February 9, 1971 San Fernando earthquake, a site in that area will be used for their application. Figure 1 shows the cumulative probability distribution of peak ground acceleration at a firm ground site (soil Class 2) in the Los Angeles area. Using Equation (3) and the soil modification values for epicentral distance up to 25 km, the cumulative probability distributions of peak ground acceleration are computed for soil Class 0 and 1. Figure 3 shows the acceleration zone graphs for each soil type. From these figures, the peak ground acceleration value at Los Angeles for the next 50 years and 10% chance of exceedence changes from 0.3g for firm ground to 0.22g for Class 1 soils to 0.18g for alluvial soils.

As a second example, it is hypothesized that the k_i values obtained in this study for the epicentral distance of 0 km to 25 km are valid in the San Francisco area. The cumulative probability distributions on peak ground acceleration for 50 years future time period are computed for the three soil classes and are shown in Figure 2. The peak ground acceleration value for 10% chance of exceedence decreases

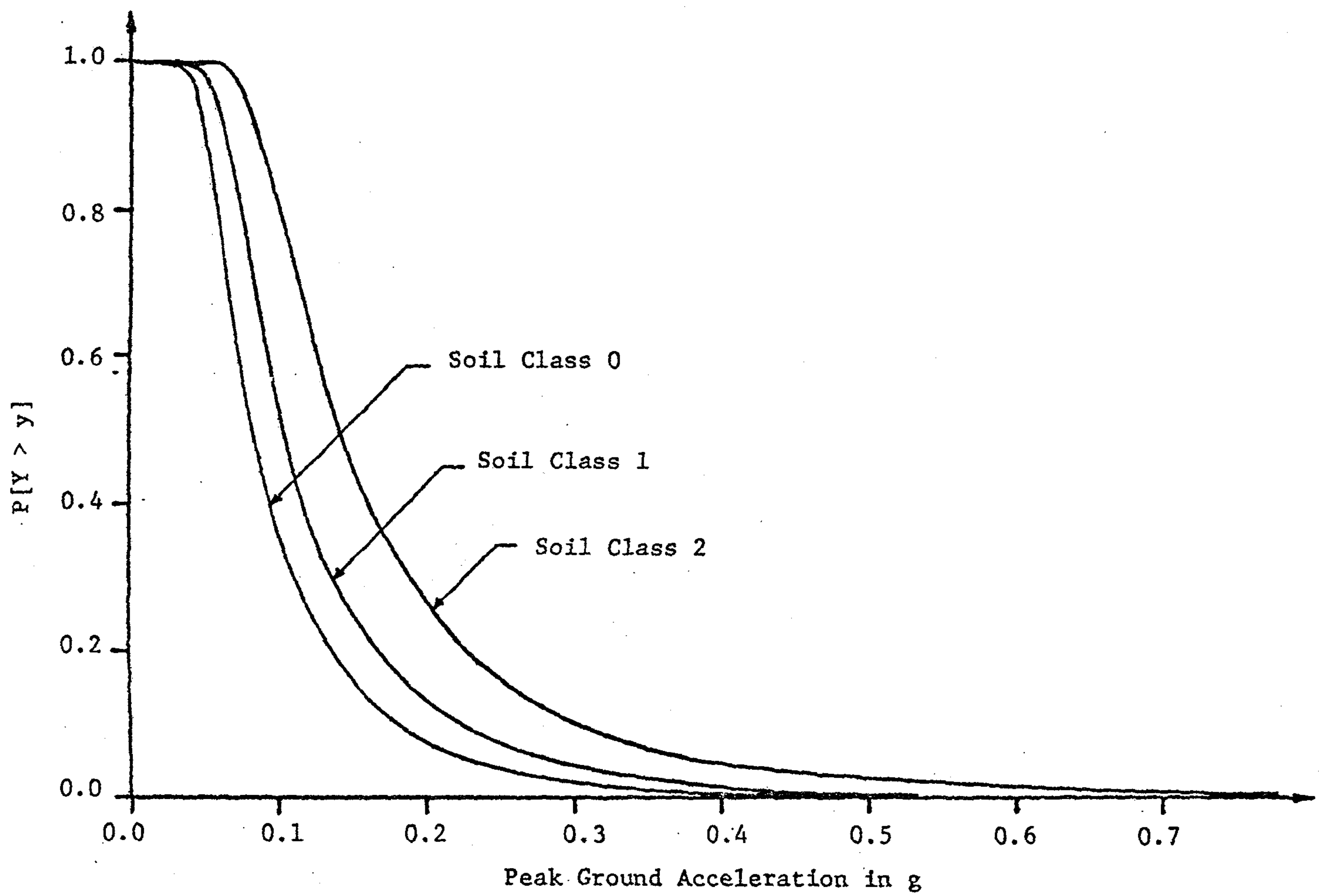

FIGURE 1 1.-CDF(PGA) for Three Soil Types at Los Angeles, Time = 50 years

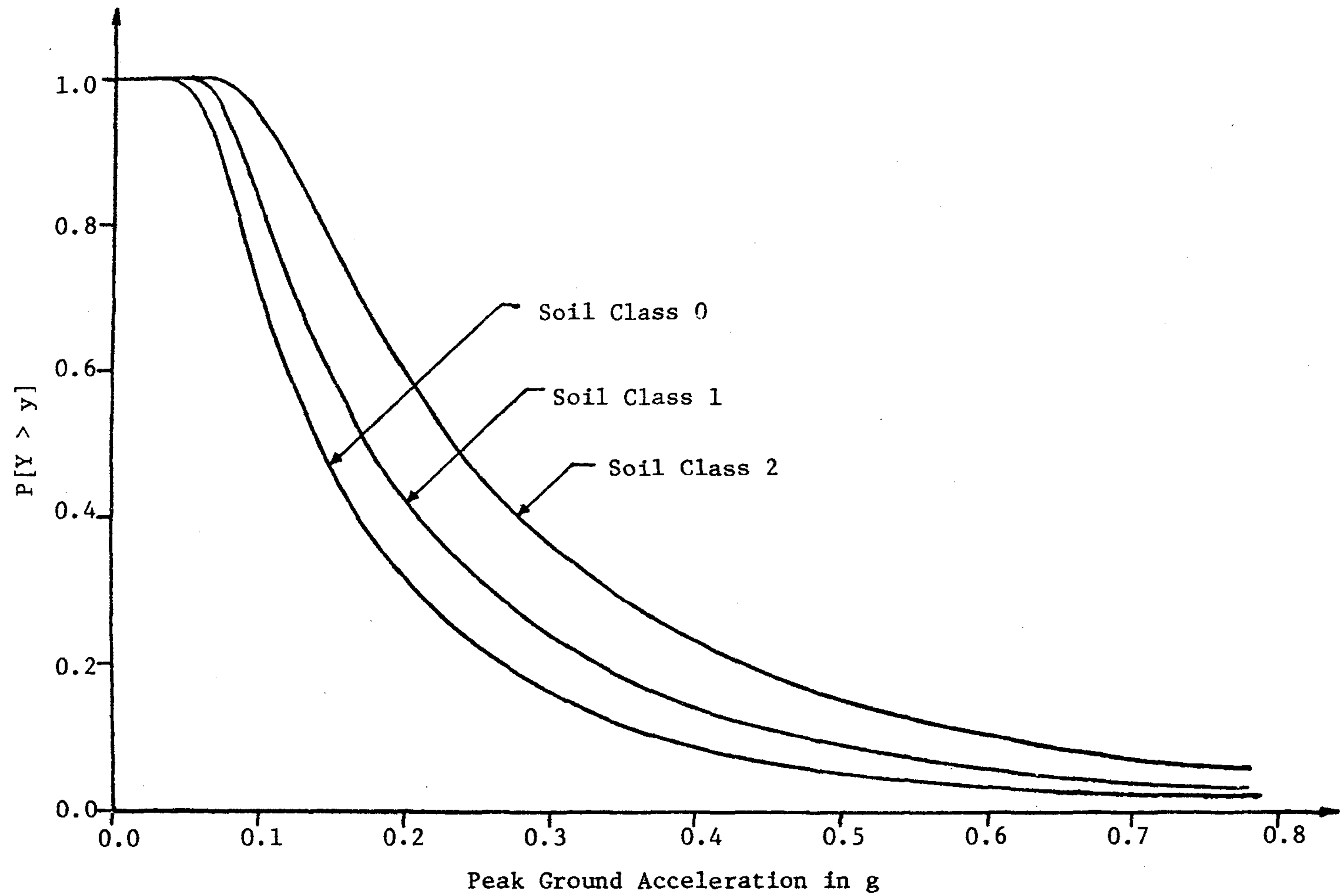

FIGURE 2 1.-CDF(PGA) for Three Soil Types at San Francisco, Time = 50 years

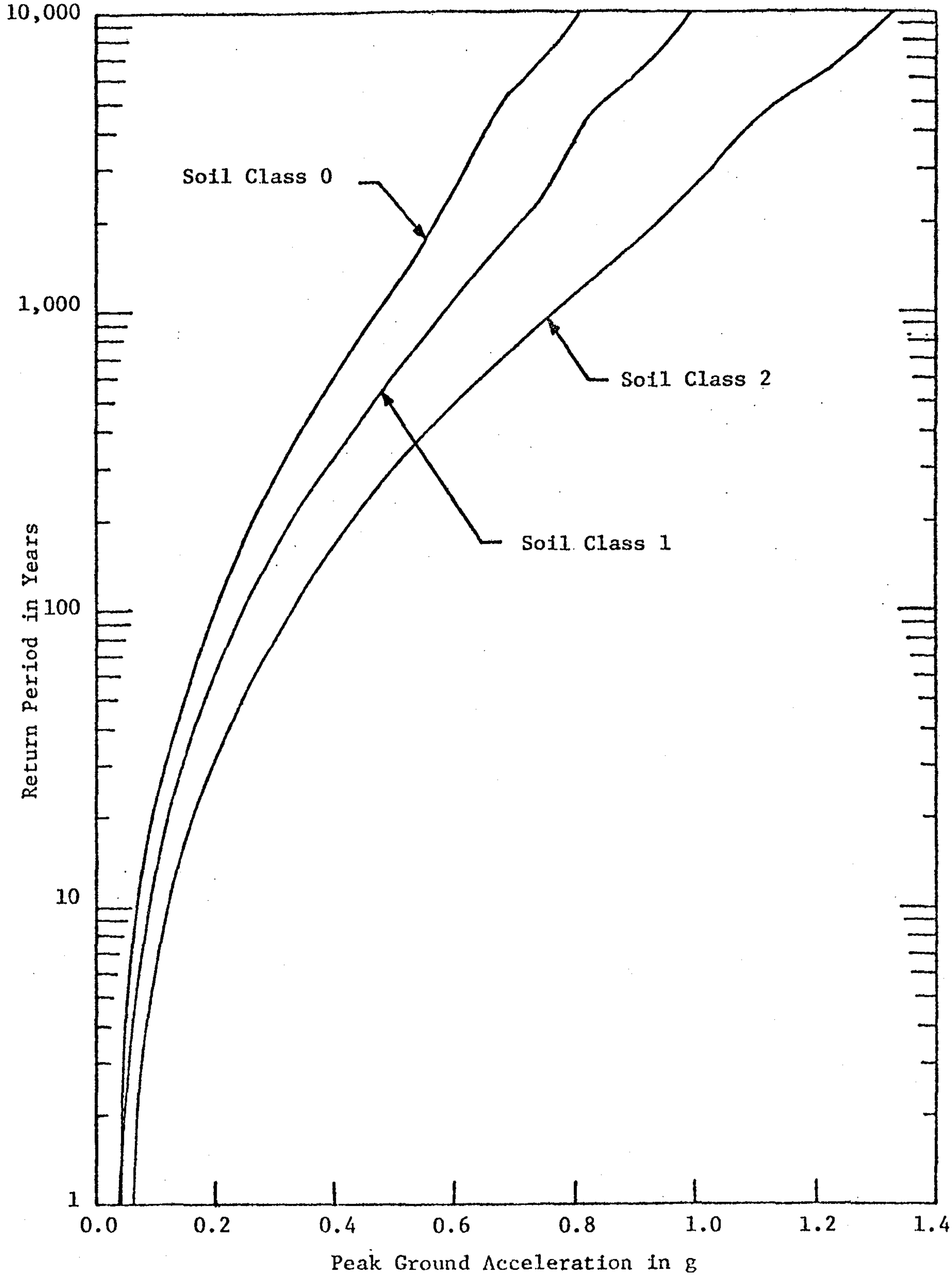

FIGURE 3 Acceleration Zone Graphs for Three Soil Types, Los Angeles Site.

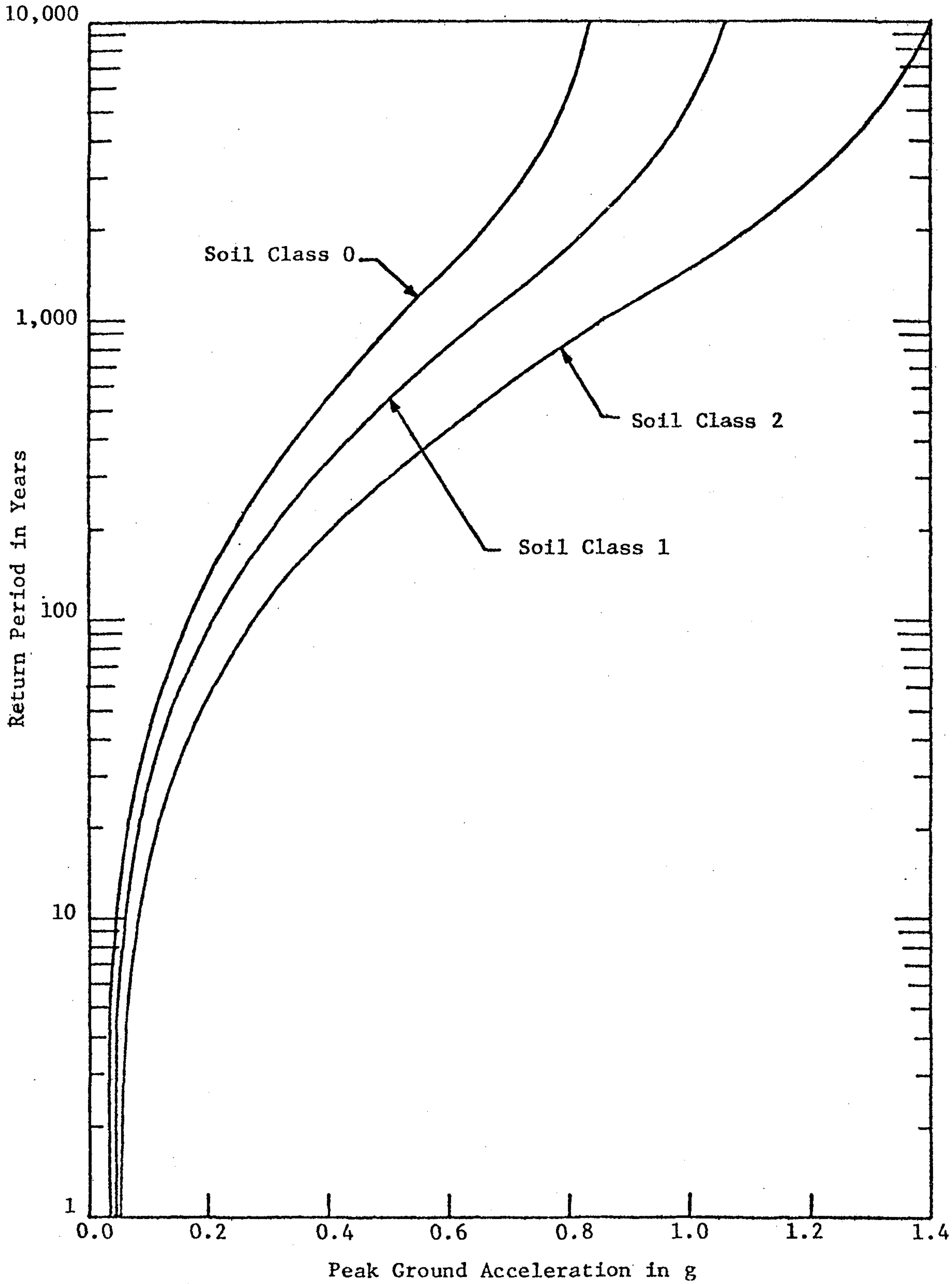

FIGURE 4 Acceleration Zone Graphs for Three Soil Types, San Francisco Site

from 0.60g for firm ground sites to 0.45g for intermediate sites to 0.36g for alluvial sites. The acceleration zone graphs for each soil type are also computed and are shown on Figure 4.

In the above examples, it should be noted that the CDF's for soil Classes 0 and 1 represent the lower bounds of acceleration at a given risk level. A more precise analysis for the evaluation of these CDF's will require the application of the soil factors to each seismic source. Then the contribution from all sources is combined by integration. This integration could not be done at the present time since soil correction factors for epicentral distances larger than 50 km are not available.

CHAPTER 3

SITE DEPENDENT RESPONSE SPECTRA

Structural response to ground motion depends on various parameters amongst which the amplitude of the input motion, its frequency content and its duration are important. The motion is amplified or deamplified depending on the predominant natural frequencies and damping of the structure. Fourier amplitude spectra and response spectra are the measures most commonly used for representing the frequency content and the amplitudes of the ground motions. In this chapter, probability distributions will be developed for response spectra depending on the soil conditions of the site of interest. Such response spectra are extremely useful in design and analysis of structures.

3.1 Definition of Response Spectrum

In general a response spectrum is defined as the relationship between the maximum value of a response parameter to the natural period or frequency of a linear single degree of freedom system (Figure 5) with a specified damping. For clarity, the equation of vibratory motion of a single degree of freedom system is stated below:

$$m\ddot{x} + c\dot{x} + kx = F(t) \tag{5}$$

where
- m = mass of the single degree of freedom system
- c = constant of viscous damping
- k = stiffness (or spring constant) of the single degree of freedom system
- x = displacement relative to the ground
- $\dot{x}$ = velocity relative to the ground
- $\ddot{x}$ = acceleration relative to the ground
- $F(t)$ = time dependent forcing function

Alternatively Equation (5) can be written as:

$$\ddot{x} + 2\beta\omega\dot{x} + \omega^2 x = \frac{F(t)}{m} \qquad (6)$$

where

$\omega = \frac{k}{m}$ = natural frequency of the system in radians

$\beta = \frac{c}{2\omega m}$ = percent of critical damping of the system

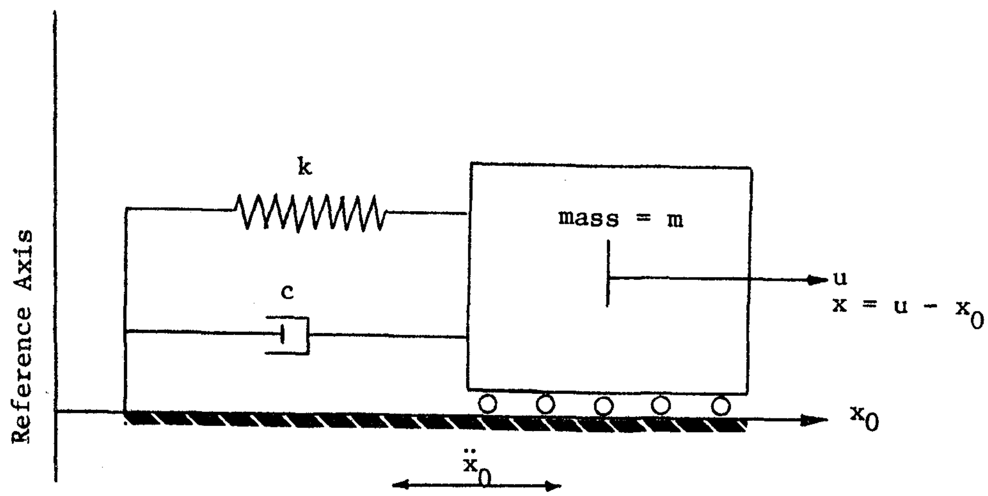

FIGURE 5. Vibration of a Single Degree of Freedom System

It should be noted that for ground motion the forcing function can be written as

$$F(t) = -m\ddot{x}_0 \quad \text{or} \quad \frac{F(t)}{m} = -\ddot{x}_0 \qquad (7)$$

in which $\ddot{x}_0$ = is the ground acceleration relative to a fixed reference frame.

The relative displacement response spectrum is defined as follows:

$$s_d = \max |x(t)| \qquad (8)$$

Two other quantities used extensively in structural engineering are the pseudo-relative velocity response spectrum (Equation 9) and the pseudo-absolute acceleration response spectrum (Equation 10).

$$s_v = \omega s_d = \omega \max|x(t)| \qquad (9)$$

$$s_a = \omega^2 s_d = \omega^2 \max|x(t)| \qquad (10)$$

The product of the pseudo-absolute acceleration with the mass of the vibrating system gives the spring force on the system. Thus, s_a is very often directly applied in earthquake resistant design. It should be noted that s_a approaches the value of peak ground acceleration as the period of the oscillatory system approaches zero (1).

The accelerograms from 57 major past earthquakes discussed in Section 2.2 will be used to develop statistics for site dependent response spectra. The response spectra values for each one of these strong motion records were made available by the Earthquake Engineering Research Laboratory of the California Institute of Technology (7). The response spectra are divided in three soil categories in the same way as the accelerograms.

In order to compare the response spectra from the different earthquakes, it is necessary to normalize them to some parameter, that will relate the data to a common measure. Dalal (1) defines a dynamic amplification factor or spectral shape, which is nothing more than the pseudo-absolute acceleration response spectrum normalized with respect to the peak ground acceleration from the corresponding accelerogram. Other normalization factors that can be used are the root-mean-square value of the response and area under the acceleration curve. Peak ground acceleration has been used throughout the first development of this work, and it is felt that its use for normalization of the response spectra will provide a link between the two parts of the study, thus it is adopted here.

The dynamic amplification factor is defined as:

$$D(T,\beta) = \frac{s_a(T,\beta)}{y} \tag{11}$$

where:

$D(T,\beta)$ = dynamic amplification (DAF) for period T and damping β

$s_a(T,\beta)$ = pseudo-absolute acceleration response spectrum for period T and damping β

y = peak ground acceleration value

The mean value and standard deviation of a sample of DAF's are given by Equations (12) to (14) below:

$$m_D(T,\beta) = \frac{1}{n}\sum_{i=1}^{n} D_i(T,\beta) = \text{mean DAF} \tag{12}$$

$$v_D(T,\beta) = \frac{1}{n}\sum_{i=1}^{n} [D_i(T,\beta) - m_D(T,\beta)]^2 = \text{variance} \tag{13}$$

$$\sigma_D(T,\beta) = \sqrt{v_D} = \text{standard deviation} \tag{14}$$

To obtain the median of the sample, the elements in the sample have to be ordered in either ascending or descending order and if n is odd then:

$$\bar{m}_D(T,\beta) = D_{\frac{n+1}{2}}(T,\beta) \tag{15}$$

and when n is even

$$\bar{m}_D(T,\beta) = \frac{1}{2}\left[D_{\frac{n}{2}}(T,\beta) + D_{\frac{n}{2}+1}(T,\beta)\right] \tag{16}$$

The central values defined here will be used in the next section to develop the probability distribution on response spectra.

3.2 Probability Distribution of Response Spectra

Peak ground acceleration depends neither on the frequency content, the general distribution of peaks, nor the duration of the ground motion. However, the dynamic amplification factor is both frequency dependent and amplitude dependent, thus it is assumed that these two quantities are statistically independent. This assumption was proven to be valid for 33 accelerograms used by Dalal (1) and it will be confirmed for the records used in this study in the following section.

At this time Equation (11) is recalled and is rewritten in the form:

$$S_a(T,\beta) = Y\,D(T,\beta) \tag{17}$$

in which $S_a(T,\beta)$, Y, and $D(T,\beta)$ denote random variables corresponding to pseudo-absolute acceleration response spectra, the peak ground acceleration, and the dynamic amplification respectively. Then the probability distribution function on response spectra can be obtained as follows:

$$F_{S_a}(s_a) = P[S_a \leq s_a] = P[YD \leq s_a] = \int_0^{\infty} \int_0^{s_a/\eta} f_{Y,D}(\xi,\eta)\,d\xi\,d\eta \tag{18}$$

where $f_{Y,D}(y,d)$ = joint probability distribution of PGA and DAF. From the independence of Y and D, the joint distribution can be written as:

$$f_{Y,D}(y,d) = f_Y(y) f_D(d) \tag{19}$$

Substituting back into Equation (18)

$$F_{S_a}(s_a) = P[S_a \leq s_a] = \int_0^{\infty} \int_0^{s_a/\eta} f_Y(\xi) f_D(\eta) d\xi d\eta$$

$$= \int_0^{\infty} f_D(\eta) F_Y \frac{s_a}{\eta} d\eta \tag{20}$$

where

$$F_Y \frac{s_a}{\eta} = \int_0^{s_a/\eta} f_Y(\xi) d\xi \tag{21}$$

In Equation (21), $F_Y(s_a/\eta)$ is the cumulative probability distribution function on peak ground acceleration. For the distribution on dynamic amplification factor $f_D(d)$, Dalal (1) has shown that a log-normal distribution describes its behavior better than a truncated normal distribution. In this study, it is assumed that the dynamic amplification factor D has gamma distribution. The validity of each one will be tested and the results will be shown in the next section.

1. Tuncated Normal DAF

$$f_D(d) = \frac{1}{1 - F_D(0)} \frac{1}{\sqrt{2\pi}\, \sigma_D} \exp\left[- \frac{1}{2}\left(\frac{d - m_D}{\sigma_D}\right)^2\right] \text{for } d \geq 0 \tag{22}$$

where $F_D(0)$ = CDF of DAF when D=0

m_D = mean DAF

σ_D = standard deviation

then the distribution on response spectra becomes:

$$F_{S_a}(s_a) = \frac{1}{1 - F_D(0)} \frac{1}{\sqrt{2\pi}\,\sigma_D} \int_0^{\infty} \exp\left[-\frac{1}{2}\left(\frac{\eta - m_D}{\sigma_D}\right)^2\right] F_Y \frac{s_a}{\eta}\, d\eta \qquad (23)$$

2. <u>Lognormal DAF</u>

$$f_D(d) = \frac{1}{\sqrt{2\pi}\,\sigma_{\ell nD}} \exp\left[-\frac{1}{2}\left(\frac{\ell nd - \ell n\bar{m}_D}{\sigma_{\ell nD}}\right)^2\right] \text{for } d \geq 0 \qquad (24)$$

where $\bar{m}_D$ = median DAF

$\sigma_{\ell nD}$ = standard deviation of the natural logarithm of DAF

the relation between the m_D, σ_D and $\bar{m}_D$, $\sigma_{\ell nD}$ are given by the following equations:

$$V_D = \frac{\sigma_D}{m_D} \qquad (25)$$

$$\bar{m}_D = m_D \exp[-\frac{1}{2}\sigma^2_{\ell nD}] \qquad (26)$$

$$\sigma^2_{\ell nD} = \ell n[V_D^2 + 1] \qquad (27)$$

Thus the parameters of the lognormal distribution can be obtained directly from the sample mean and standard deviation of DAF.

For this case, the response spectrum distribution is:

$$F_{S_a}(s_a) = \frac{1}{\sqrt{2\pi}\,\sigma_{\ell nD}} \int_0^\infty \exp\left[-\frac{1}{2}\left(\frac{\ell n\eta - \ell n\bar{m}_D}{\sigma_{\ell nD}}\right)^2\right] F_Y\left(\frac{s_a}{\eta}\right) d\eta \tag{28}$$

3. <u>Gamma Distributed DAF</u>

$$f_D(d) = \frac{\lambda(\lambda d)^{k-1} e^{-\lambda d}}{\Gamma(k)} \text{ for } d \geq 0 \tag{29}$$

where

$$\Gamma(k) = \int_0^\infty e^{-u}\, u^{k-1}\, du \tag{30}$$

$$m_D = k/\lambda \tag{31}$$

and

$$\sigma_D^2 = k/\lambda^2 \tag{32}$$

The values of k and λ will vary from one soil condition to another. Then

$$F_{S_a}(s_a) = \frac{\lambda}{\Gamma(k)} \int_0^\infty (\lambda\eta)^{k-1} e^{-\lambda\eta} F_Y\left(\frac{s_a}{\eta}\right) d\eta \tag{33}$$

The cumulative distributions on s_a will vary with soil classes 0, 1, and 2. These distributions will depend on the mean and standard deviation of response spectrum shapes computed from each soil data sample.

CHAPTER 4

STATISTICAL ANALYSIS OF RESPONSE SPECTRUM SHAPES

4.1 Correlation of DAF and PGA

To investigate the degree of correlation between peak ground acceleration and the response spectrum, and DAF, response spectrum values for 16 periods and 5 damping values are selected for each of soil classes 0, 1, and 2 described in Tables 2 to 4. The periods range from 0.05 sec to 5.0 sec and the damping values are 0%, 2%, 5%, 10% and 20%. The response spectrum values and the spectrum shape values were plotted against the corresponding value of peak ground acceleration for each soil class. Figures 6 to 29 show the scattergrams for periods 0.05, 0.1, 0.5, and 1 sec, and damping of 2% and 5%. Standard deviations, correlation coefficients and coefficients of variation are computed for all cases. In addition, a least squares fit line is obtained for response spectra versus peak ground acceleration. The following conclusions can be made for all three types of soils.

- There is relatively good correlation between the response values s_a and peak ground accelerations (PGA).
- The correlation coefficients for s_a vs PGA vary from 0.422 to 0.99 for soil class 0, from 0.253 to 0.998 for soil class 1, and from 0.790 to 0.996 for soil class 2.
- The correlation of s_a to PGA is in general higher for lower periods than for higher periods at the same damping.
- The correlation of s_a to PGA increases with higher damping values as is expected.

- The correlation coefficient for s_a vs PGA is highest for soil class 2.
- The correlation coefficients for DAF vs PGA are overall very low and vary from .001 t0 .350 for soil class 0, from 0.005 to .428 for soil class 1, and from .004 to 0.630 for soil class 2. In all these cases the correlation coefficient is much smaller than 1.0 (0.63 in the best case), which implies that the two parameters, DAF and PGA are uncorrelated.
- The scatter of the DAF vs PGA points increases with larger periods.
- There is no noticeable improvement in the correlation between DAF and PGA with increasing damping value.
- The scatter for DAF vs PGA appears to be equally large for all three types of soils.

From the above observations and discussions, the assumption that DAF and PGA are stochastically independent is shown to be reasonable.

4.2 Probability Distribution of DAF

In Section 4.1, three different probability distributions are suggested for the dynamic amplification factor. Equations 22, 24, and 29 are used in this section to find the most appropriate distribution for DAF.

The cumulative distribution functions obtained from Equations 22, 24 and 29 are tested against the cumulative distribution function obtained from the data for the three soil conditions. To obtain the parameters for the truncated normal, lognormal and gamma distributions,

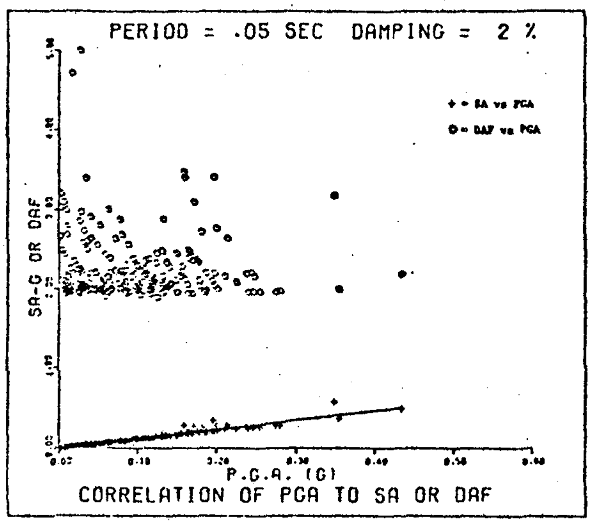

FIGURE 6 Soil Class = 0

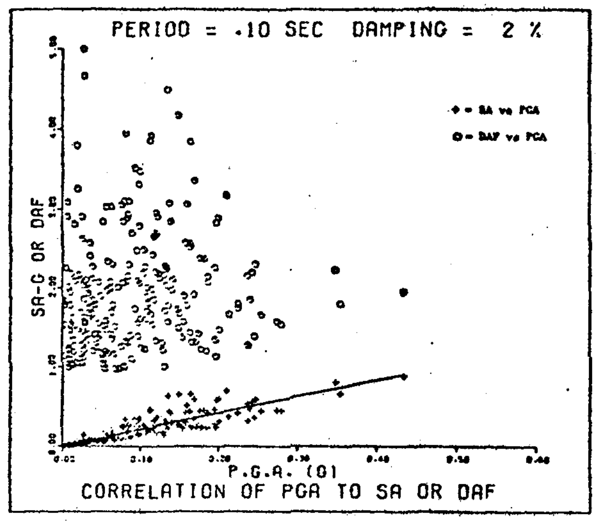

FIGURE 7 Soil Class =0

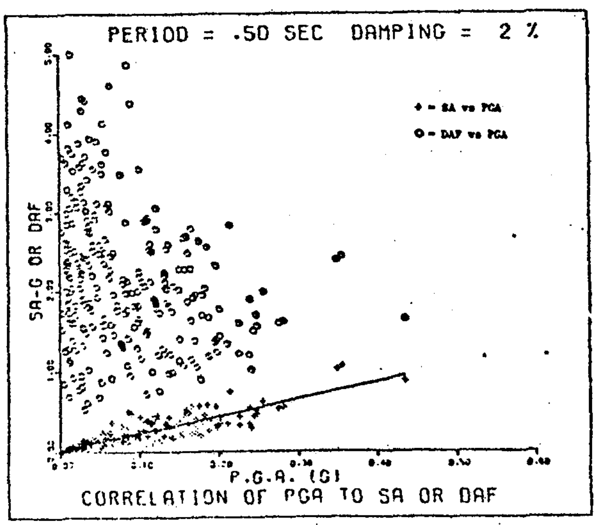

FIGURE 8 Soil Class = 0

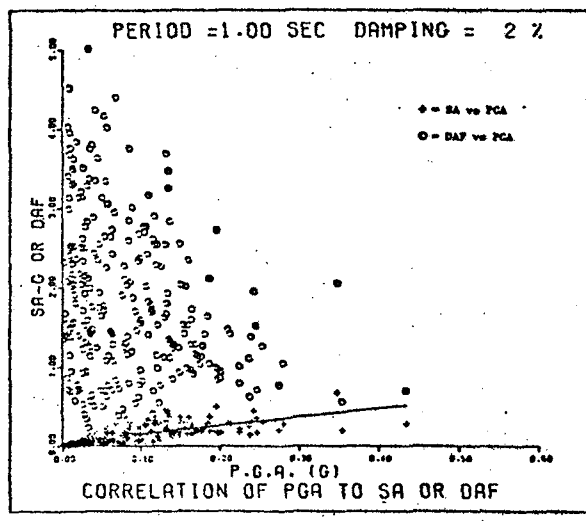

FIGURE 9 Soil Class = 0

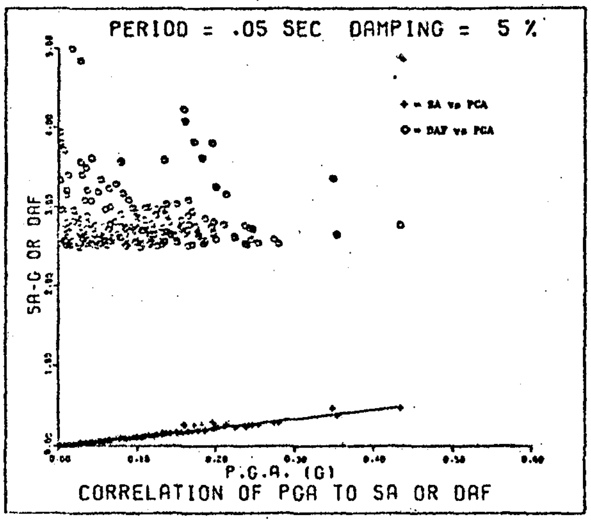

FIGURE 10 Soil Class = 0

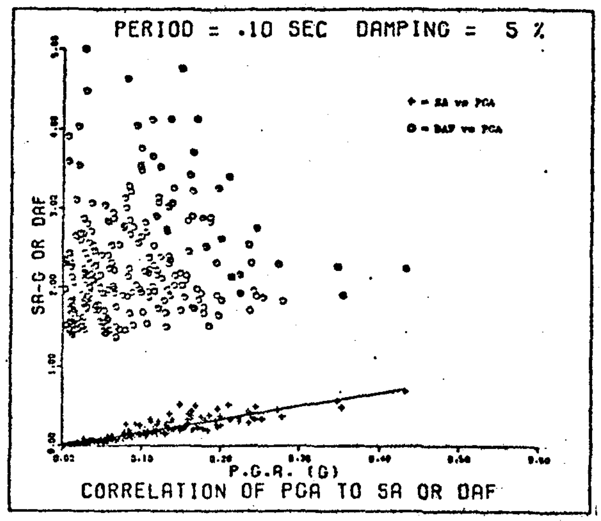

FIGURE 11 Soil Class = 0

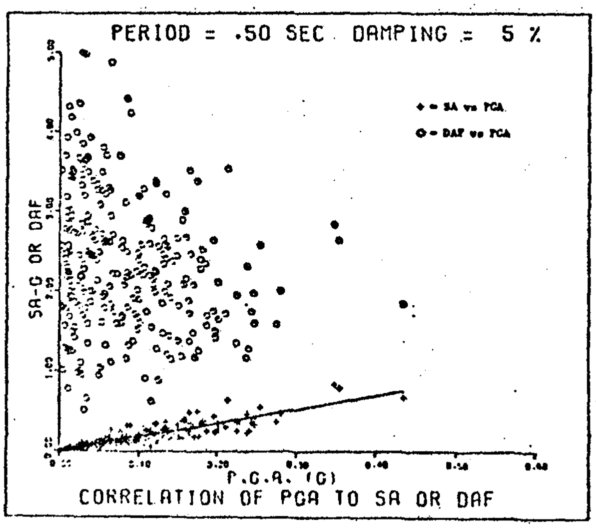

FIGURE 12 Soil Class = 0

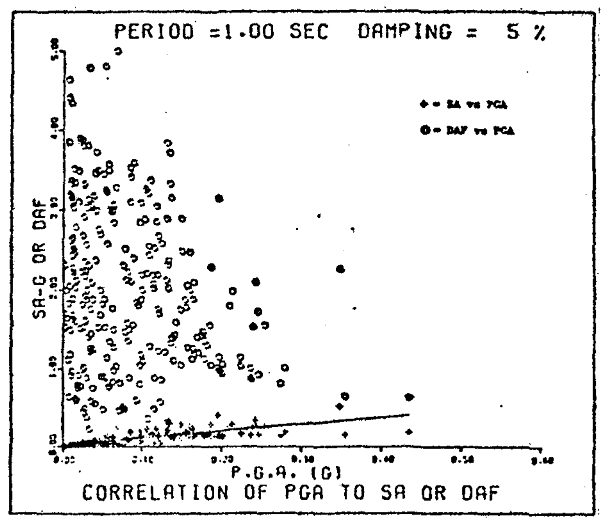

FIGURE 13 Soil Class = 0

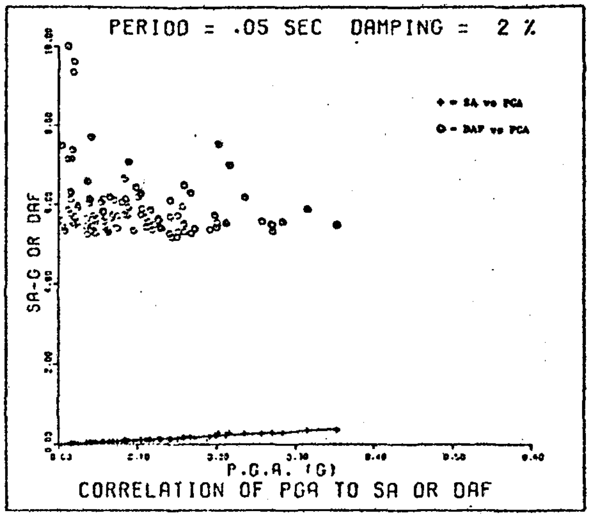

FIGURE 14 Soil Class = 1

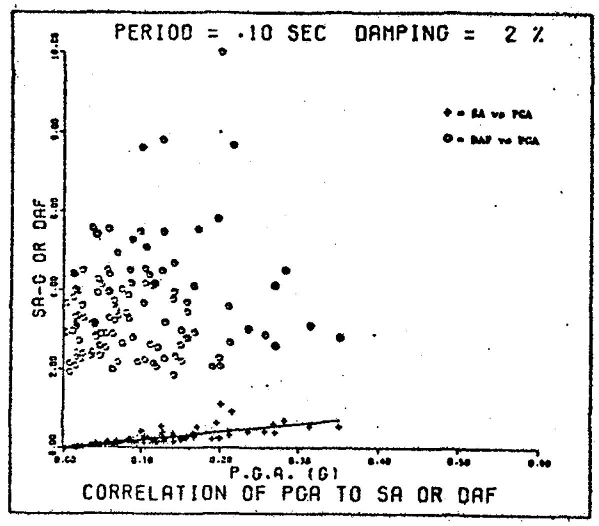

FIGURE 15 Soil Class = 1

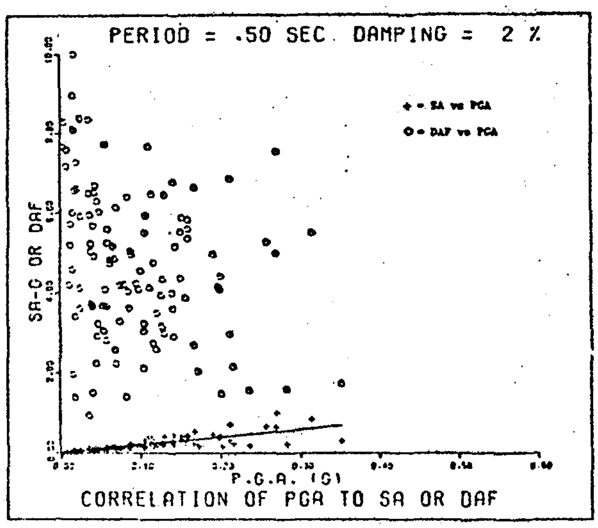

FIGURE 16 Soil Class = 1

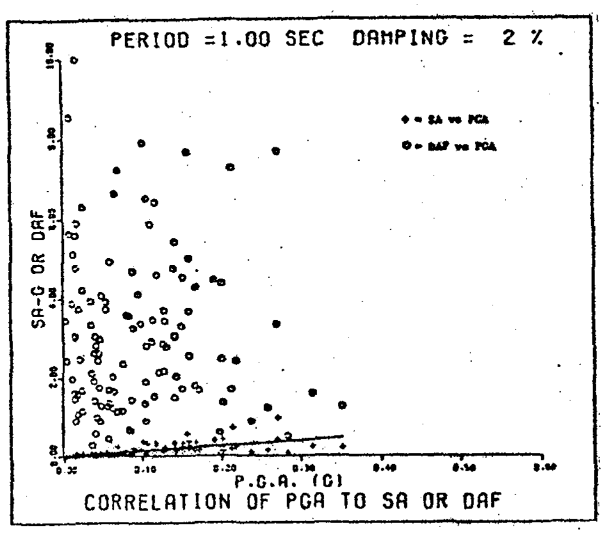

FIGURE 17 Soil Class = 1

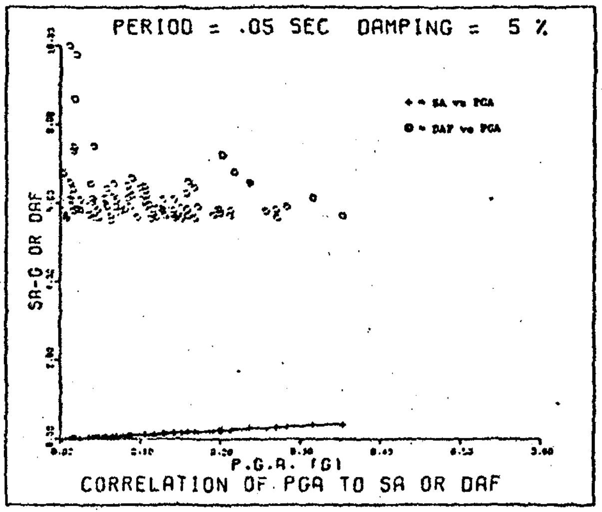

FIGURE 18 Soil Class = 1

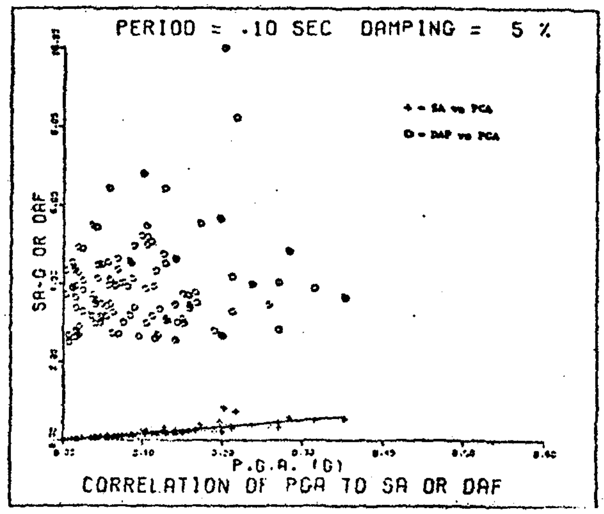

FIGURE 19 Soil Class = 1

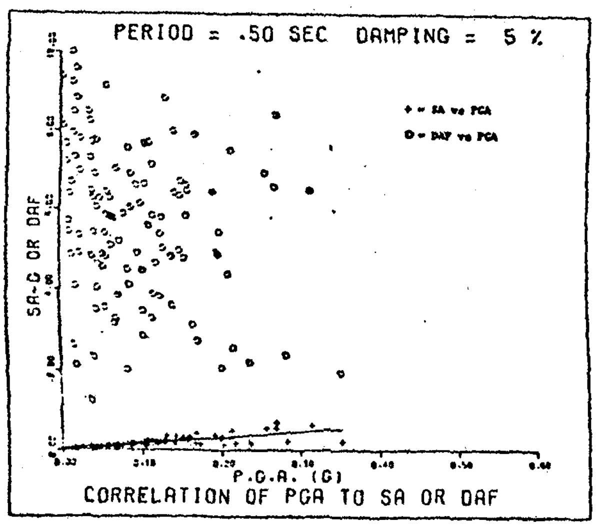

FIGURE 20 Soil Class = 1

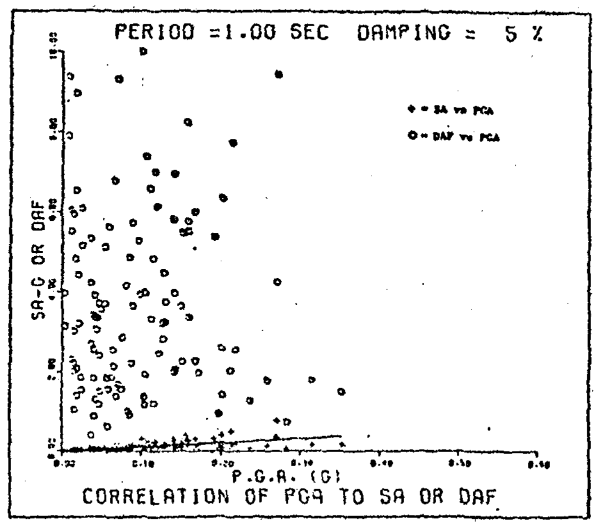

FIGURE 21 Soil Class = 1

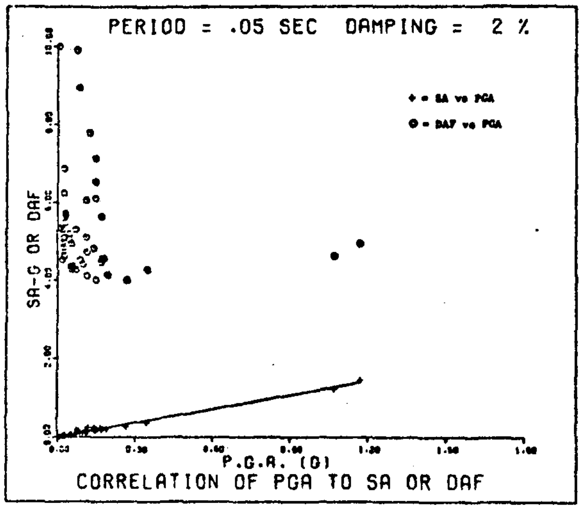

FIGURE 22 Soil Class = 2

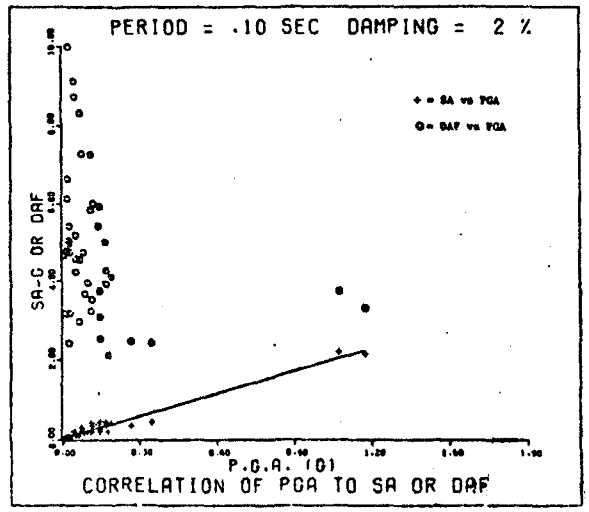

FIGURE 23 Soil Class = 2

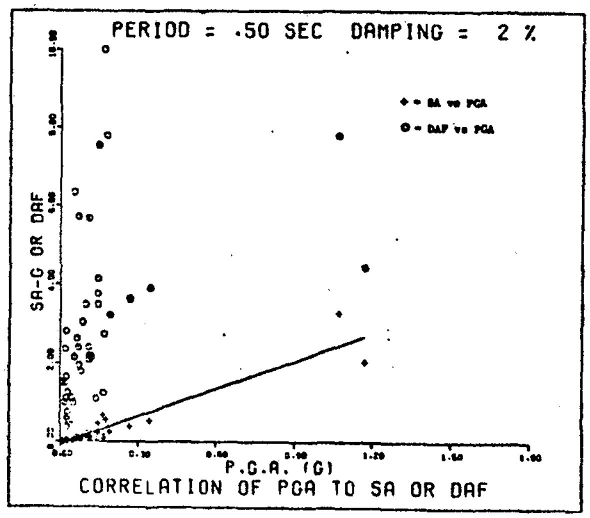

FIGURE 24 Soil Class = 2

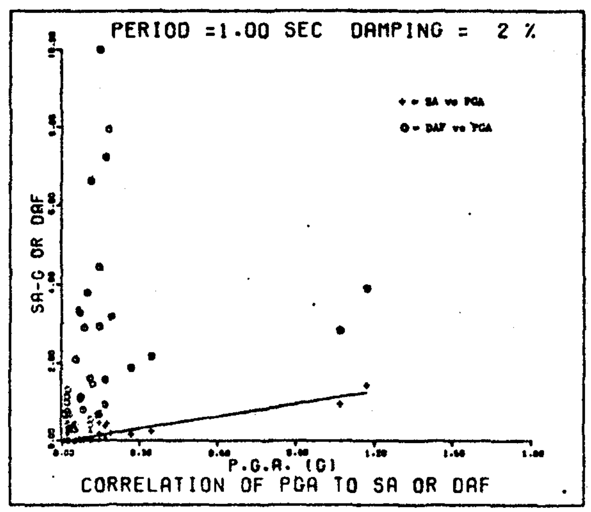

FIGURE 25 Soil Class = 2

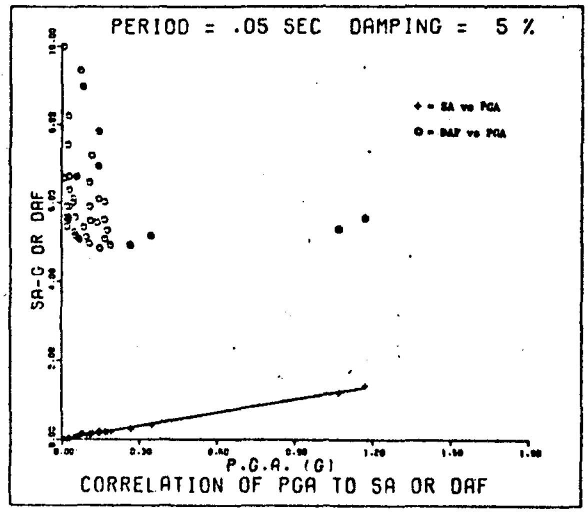

FIGURE 26 Soil Class = 2

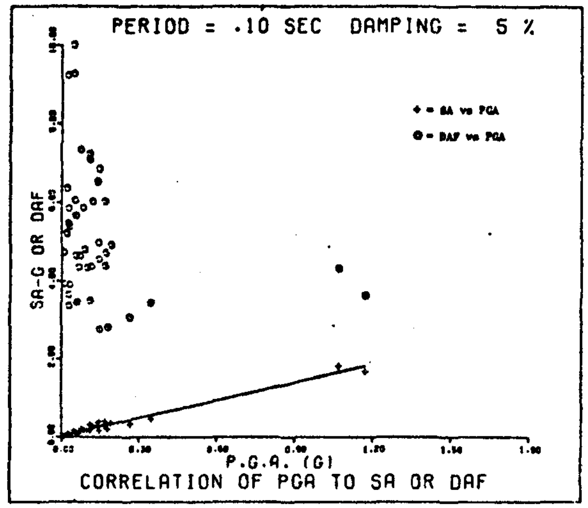

FIGURE 27 Soil Class = 2

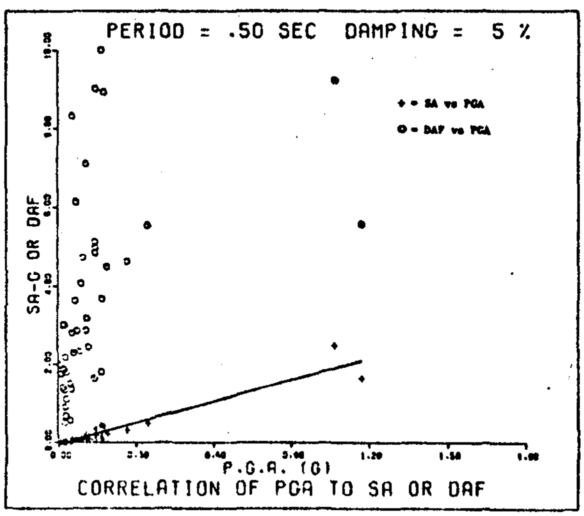

FIGURE 28 Soil Class = 2

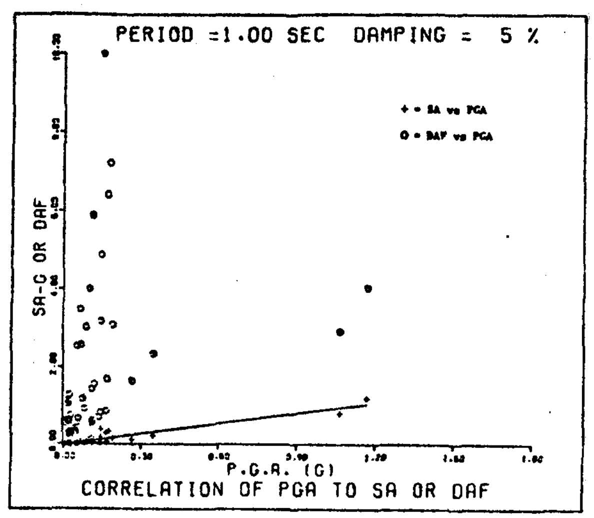

FIGURE 29 Soil Class = 2

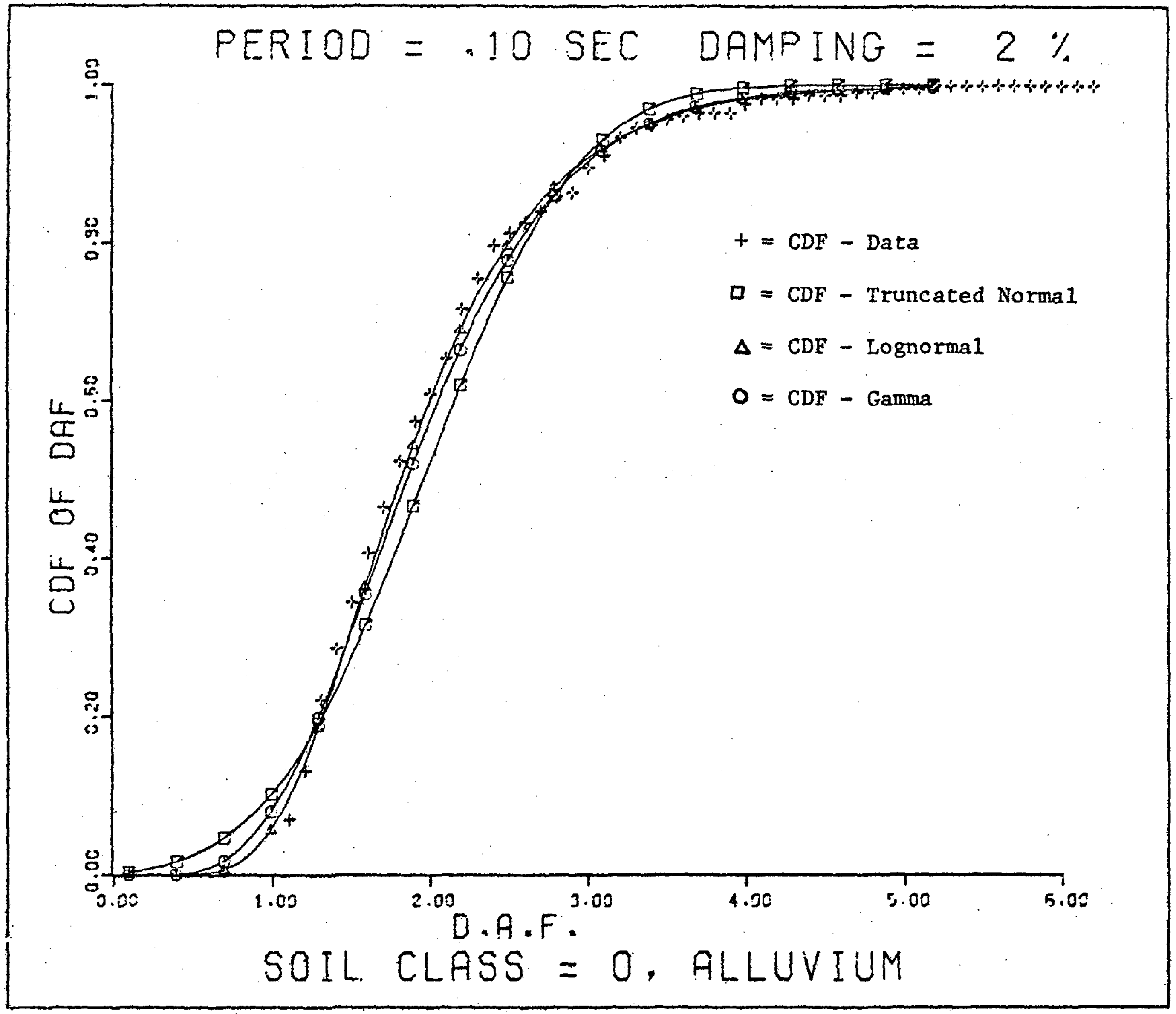

FIGURE 30 Comparison of Three CDF's of DAF

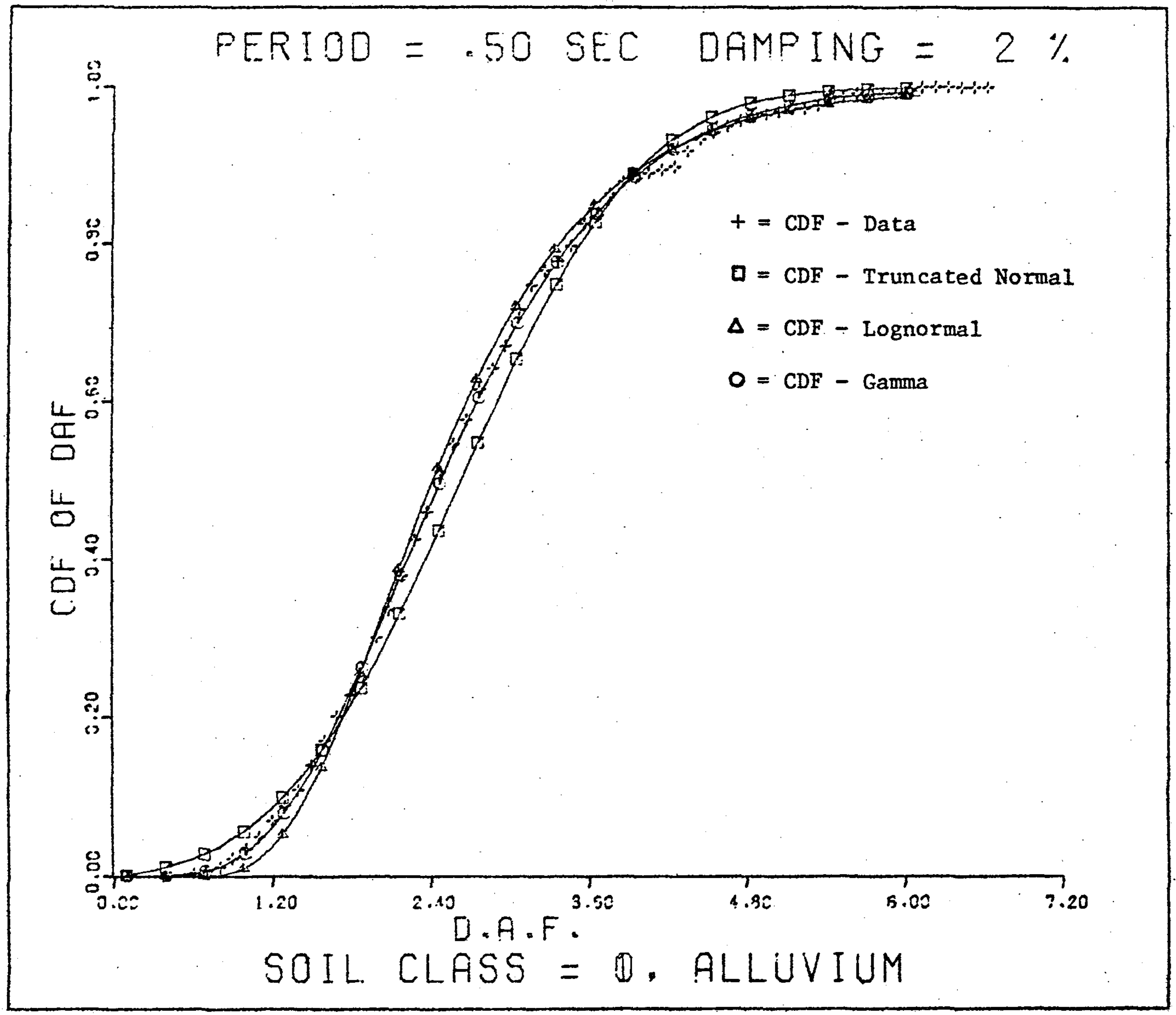

FIGURE 31 Comparison of Three CDF's of DAF

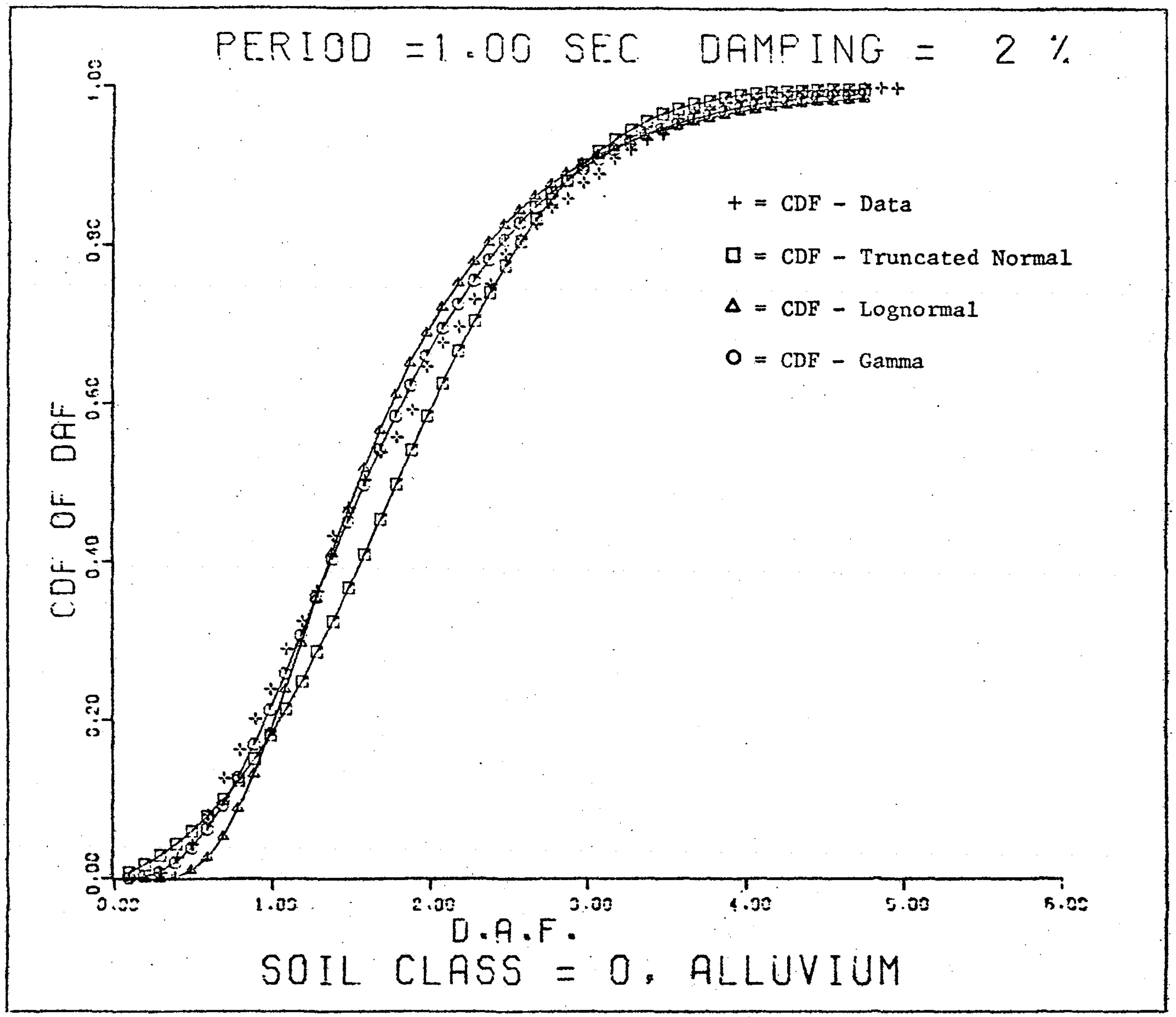

FIGURE 32 Comparison of Three CDF's of DAF

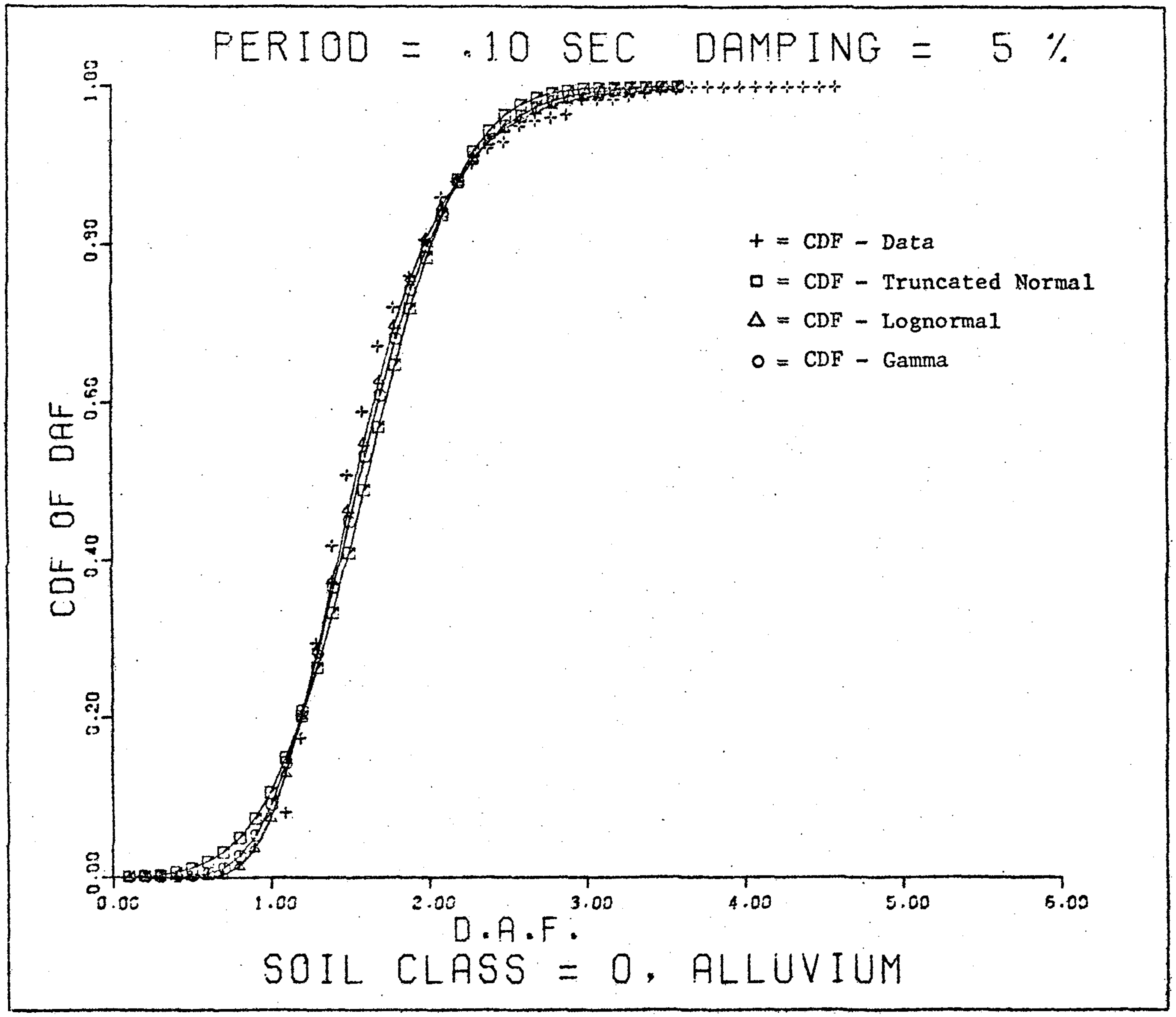

FIGURE 33 Comparison of Three CDF's of DAF

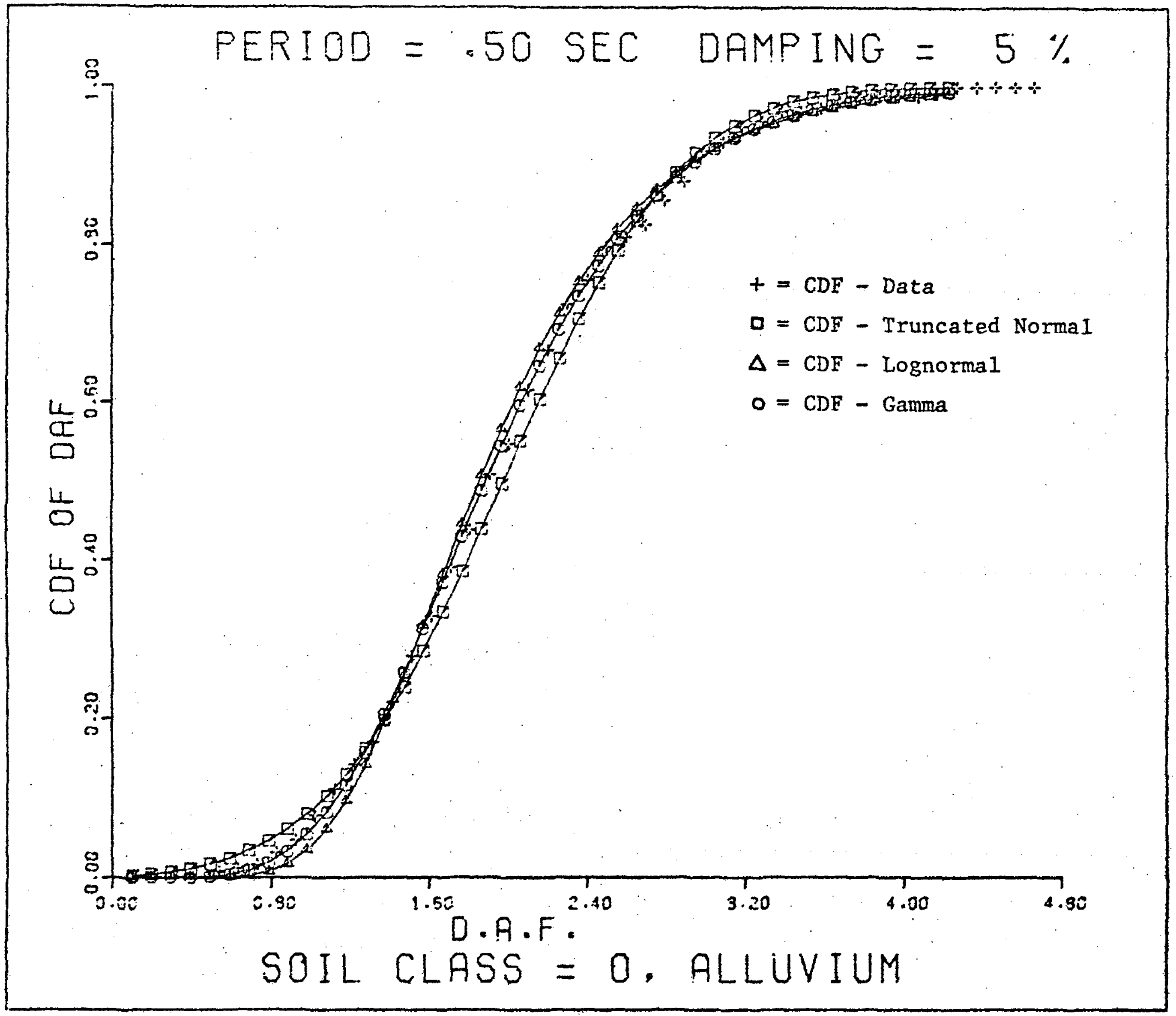

FIGURE 34 Comparison of Three CDF's of DAF

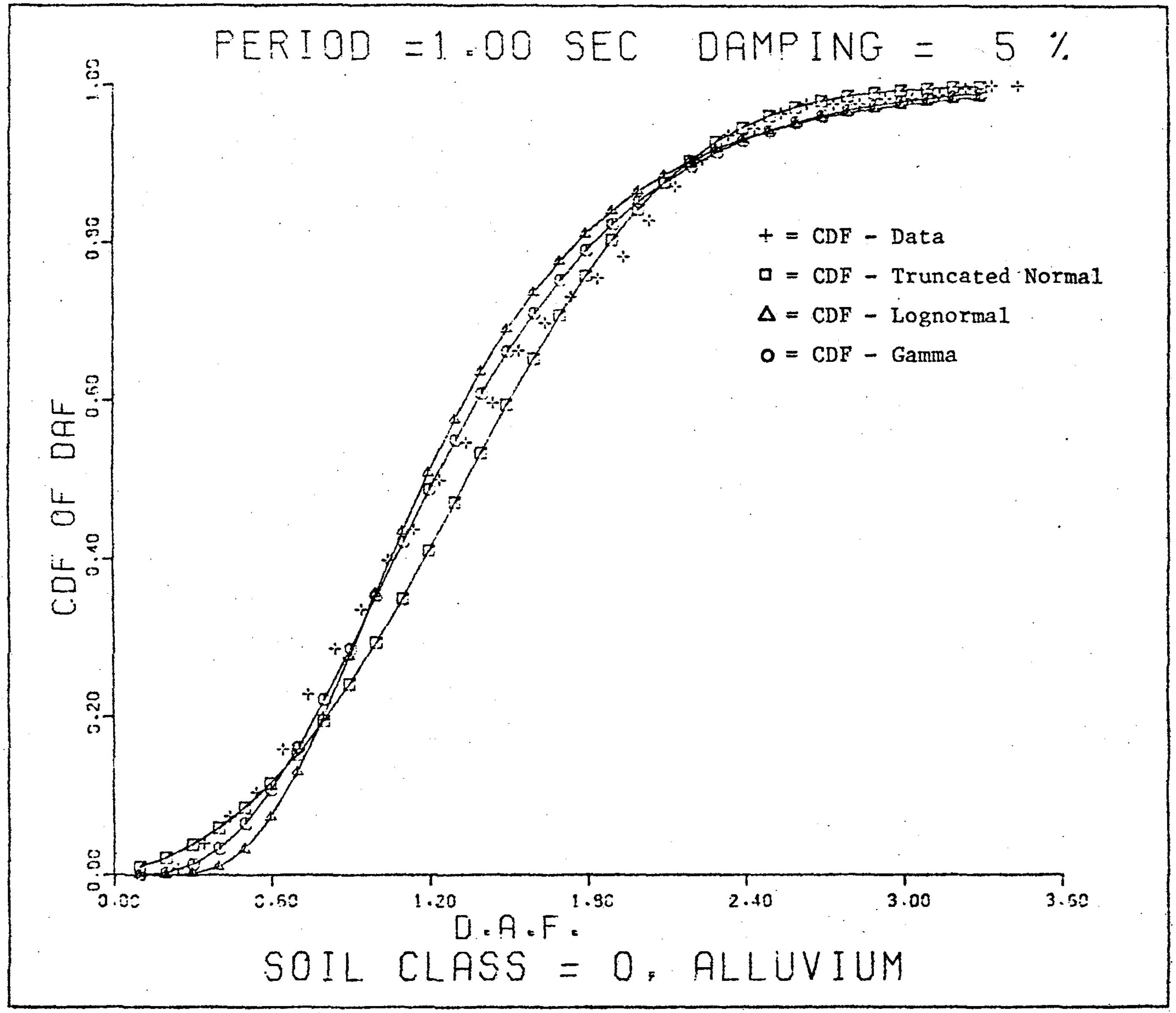

FIGURE 35 Comparison of Three CDF's of DAF

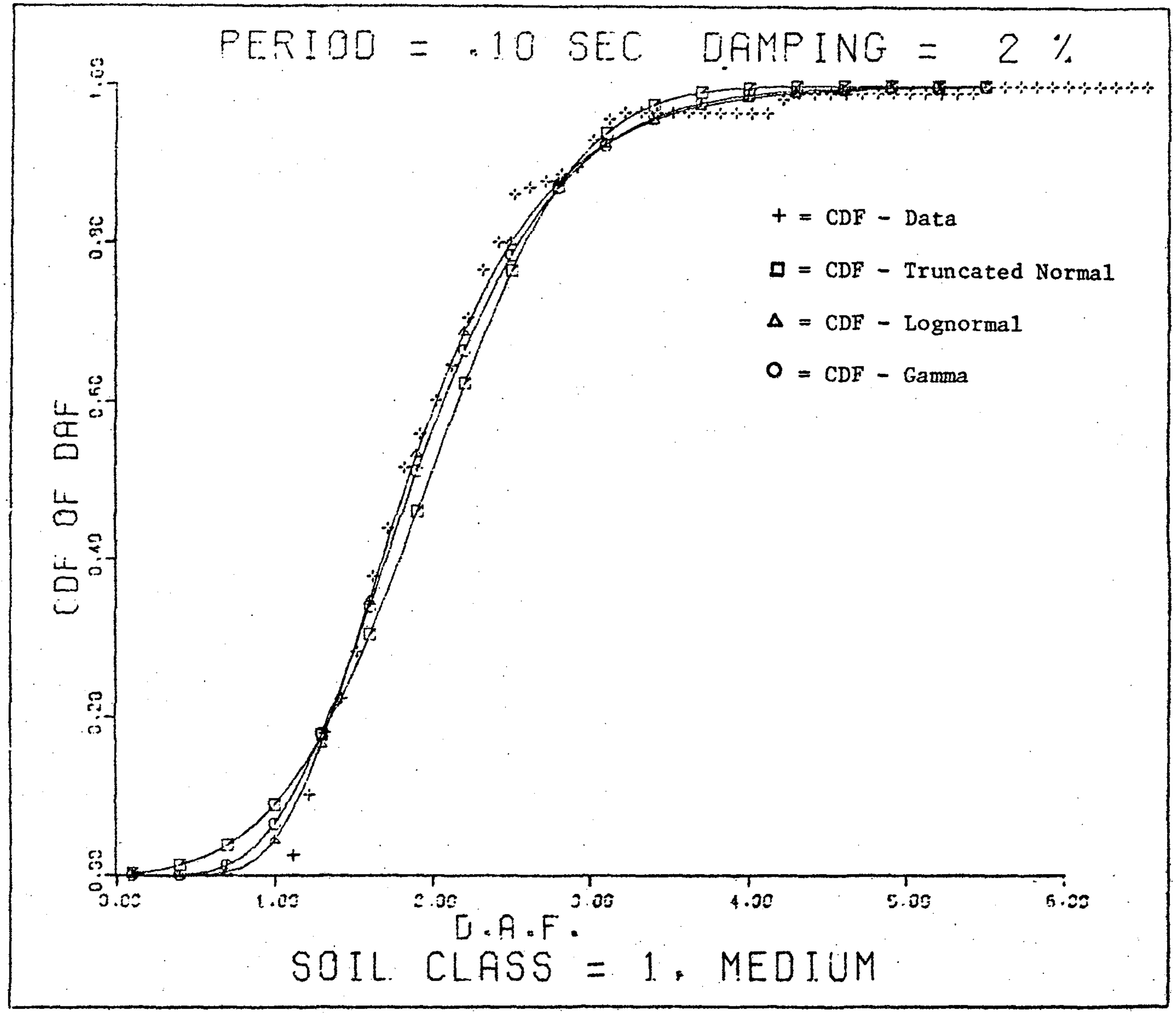

FIGURE 36 Comparison of Three CDF's of DAF

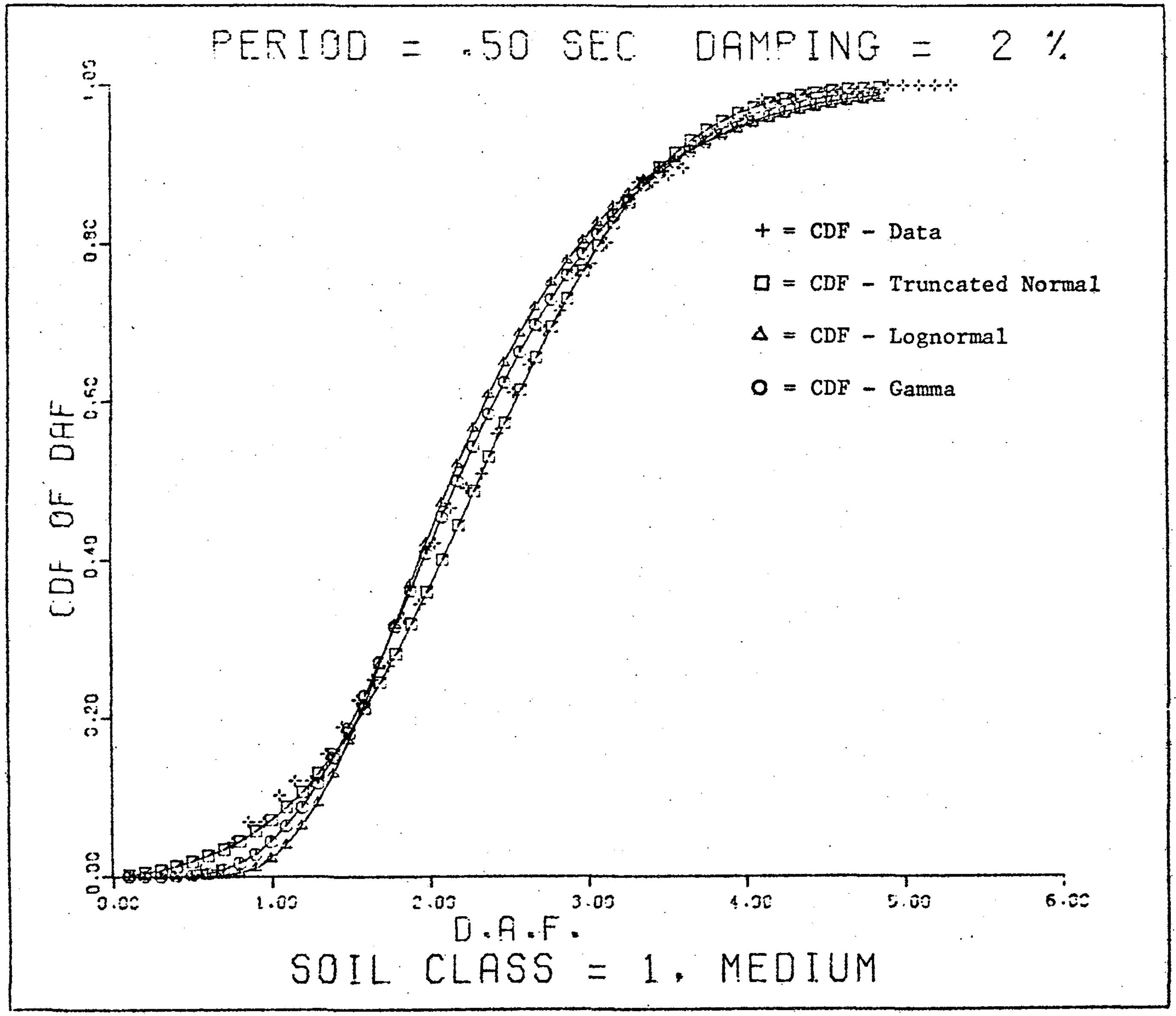

FIGURE 37 Comparison of Three CDF's of DAF

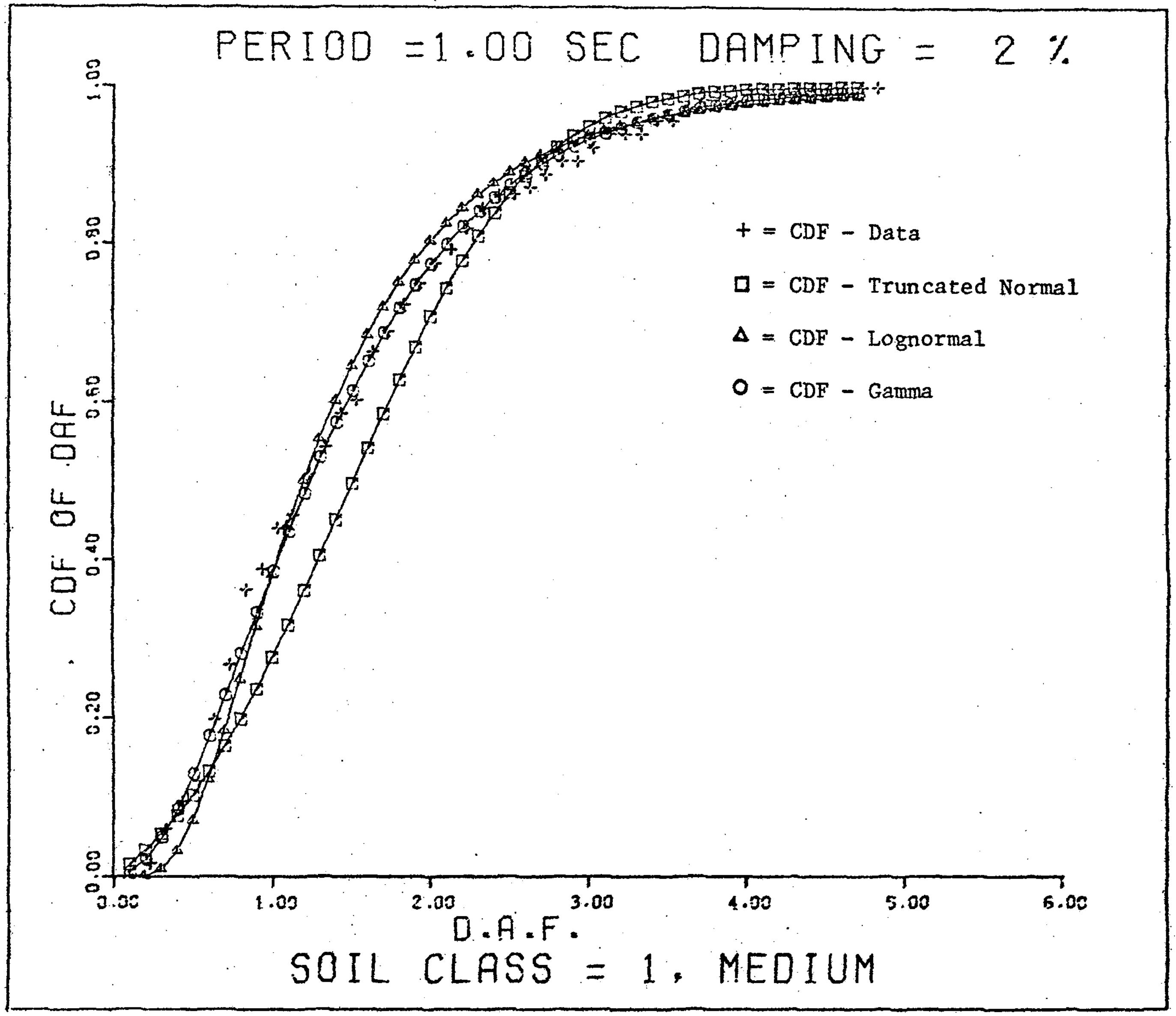

FIGURE 38 Comparison of Three CDF's of DAF

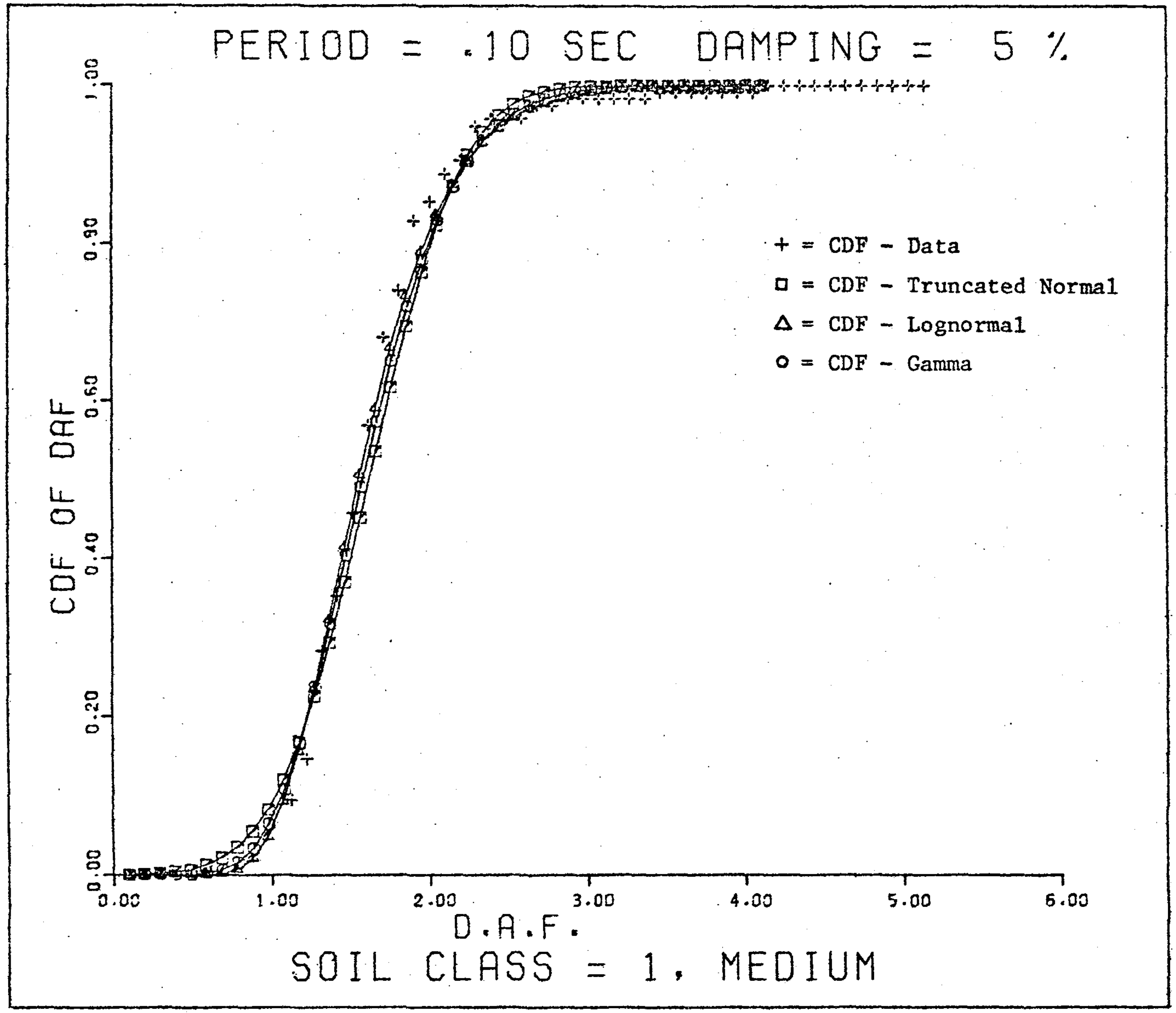

FIGURE 39 Comparison of Three CDF's of DAF

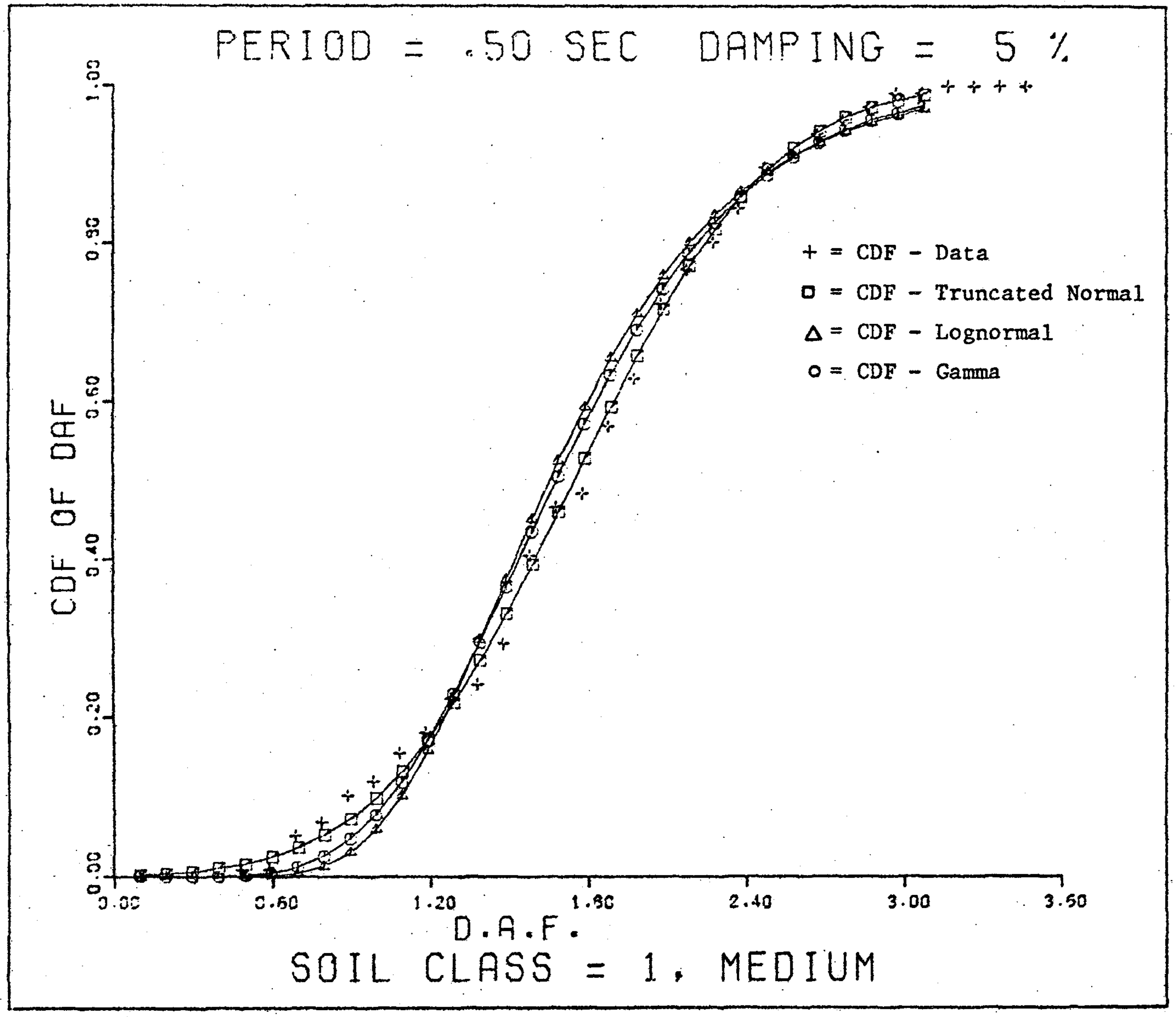

FIGURE 40 Comparison of Three CDF's of DAF

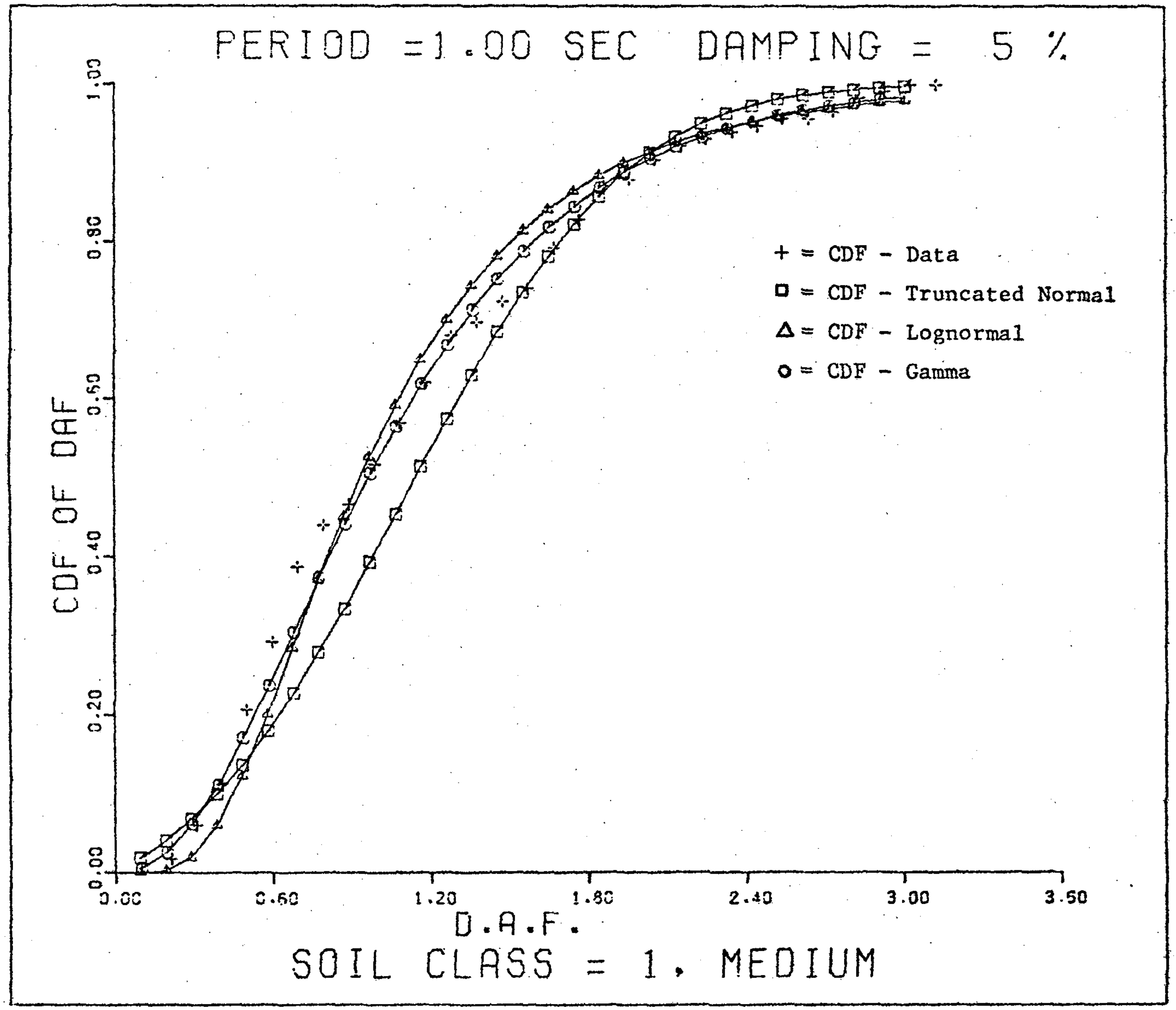

FIGURE 41 Comparison of Three CDF's of DAF

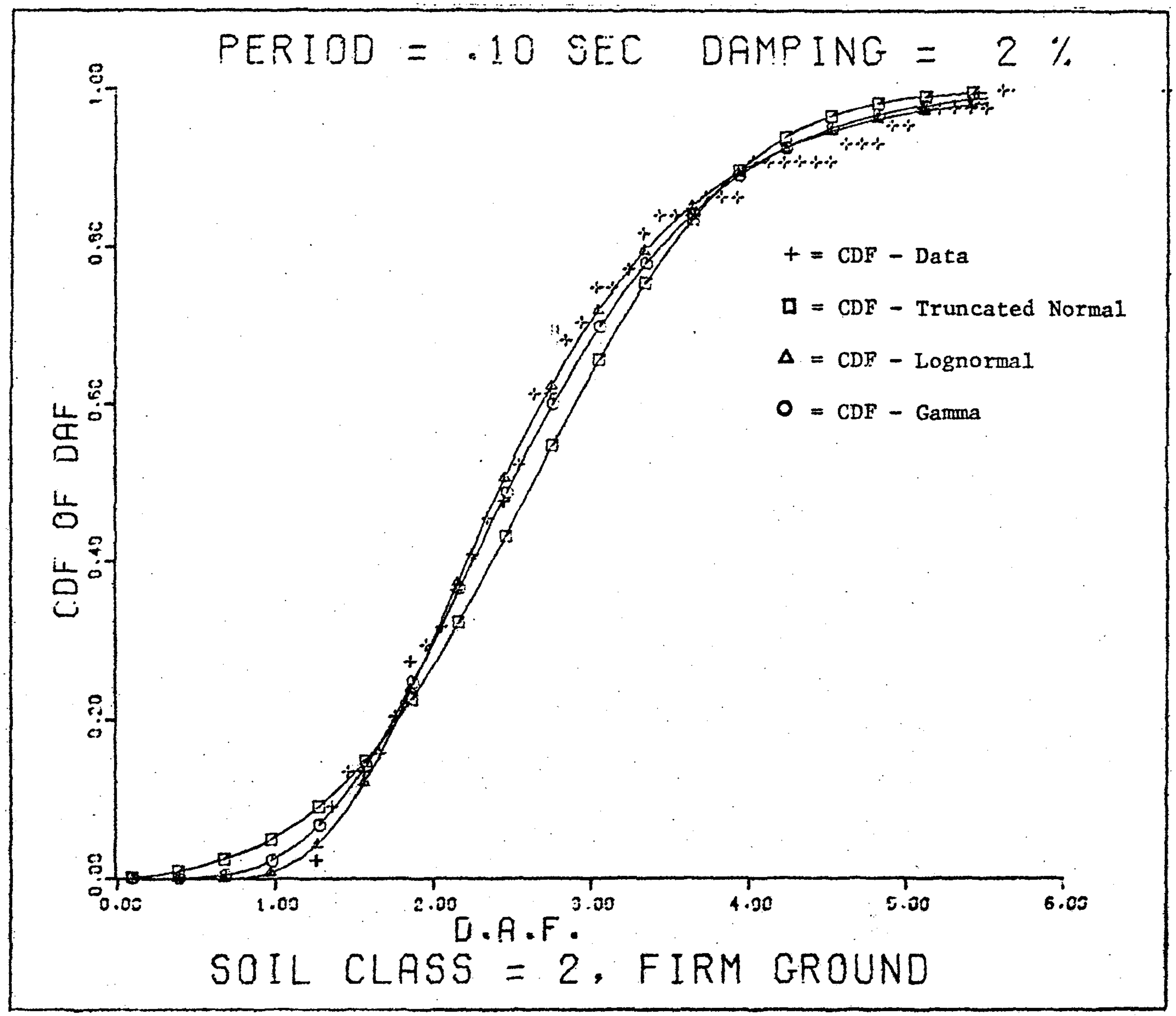

FIGURE 42 Comparison of Three CDF's of DAF

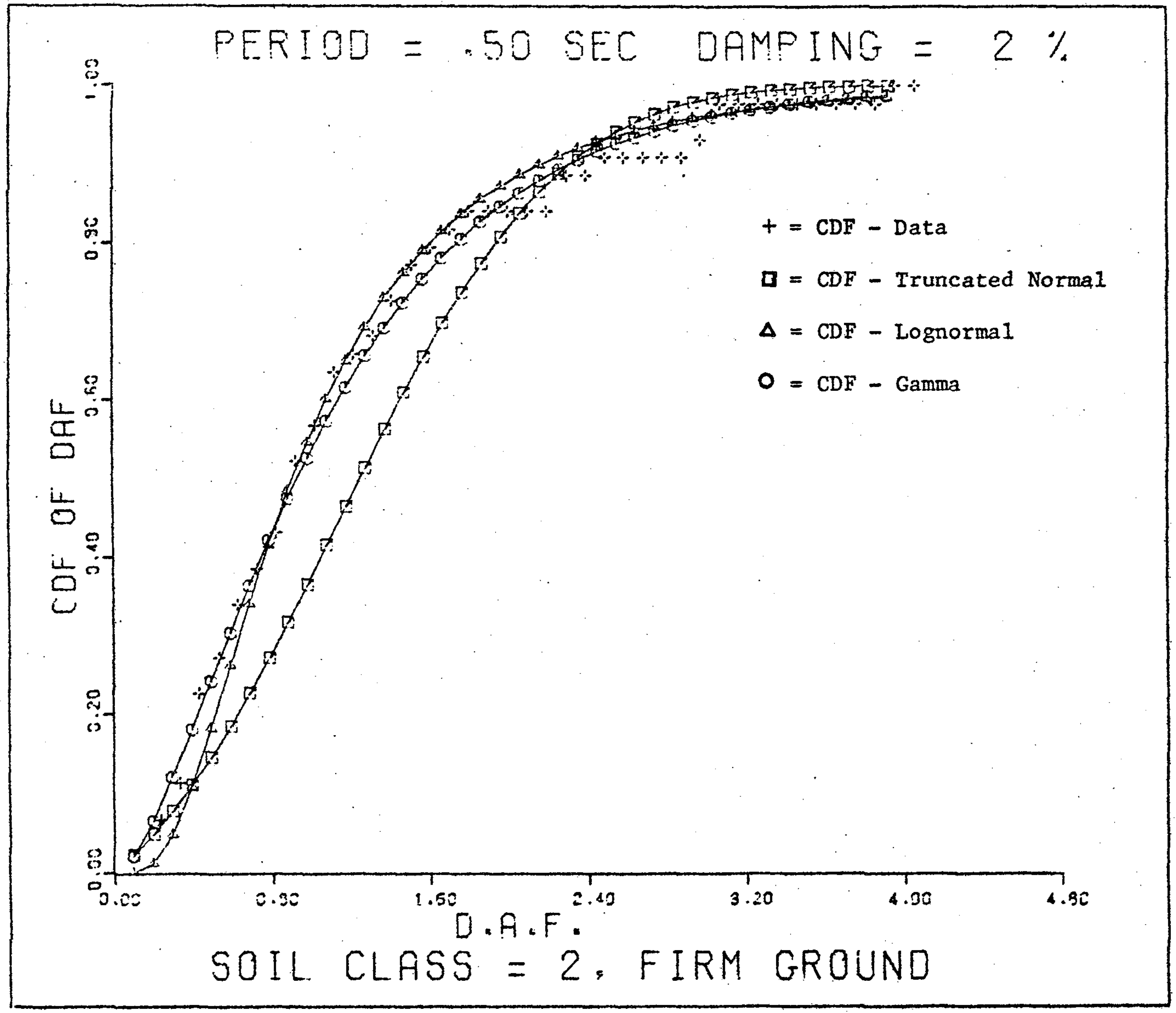

FIGURE 43 Comparison of Three CDF's of DAF

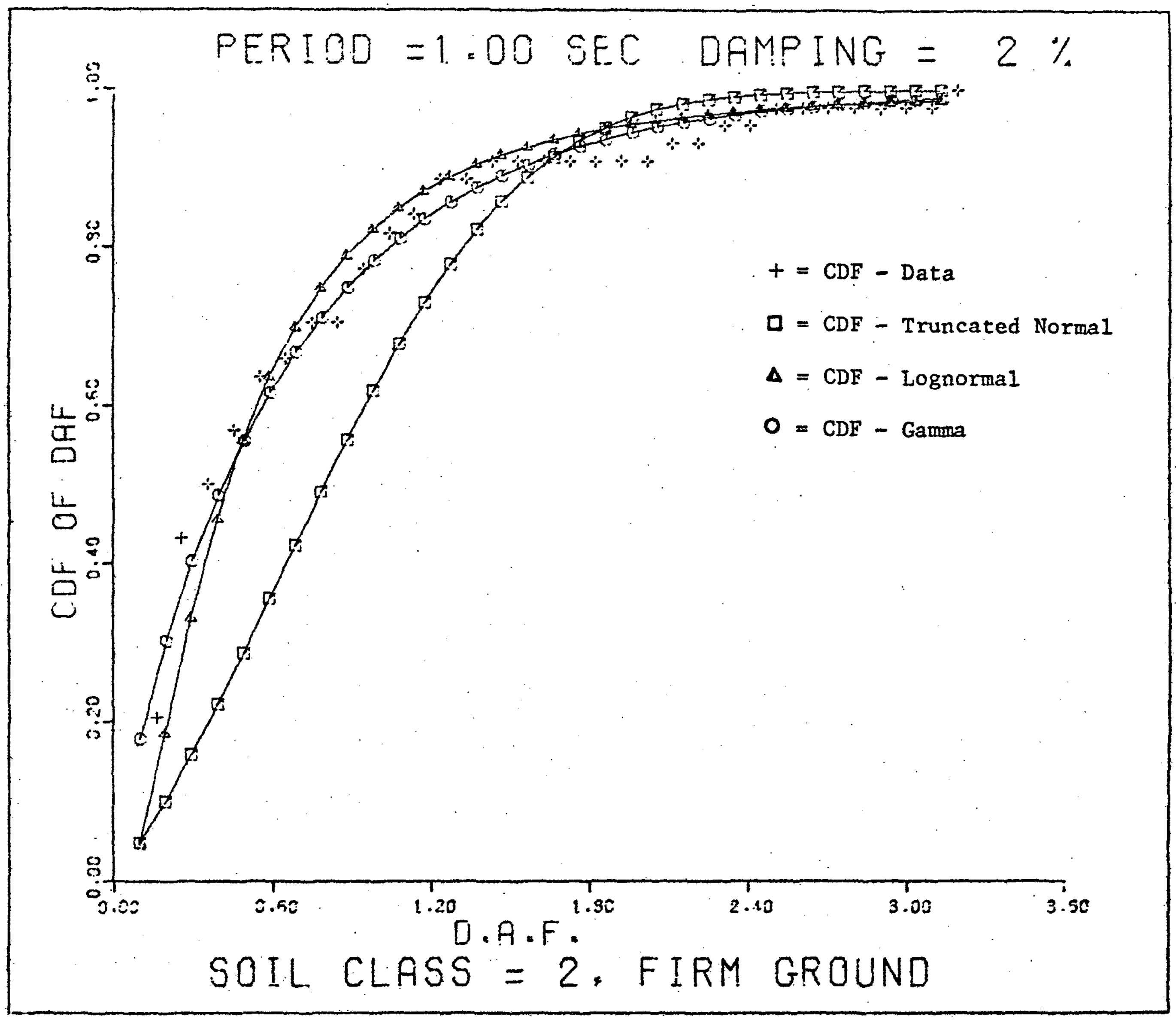

FIGURE 44 Comparison of Three CDF's of DAF

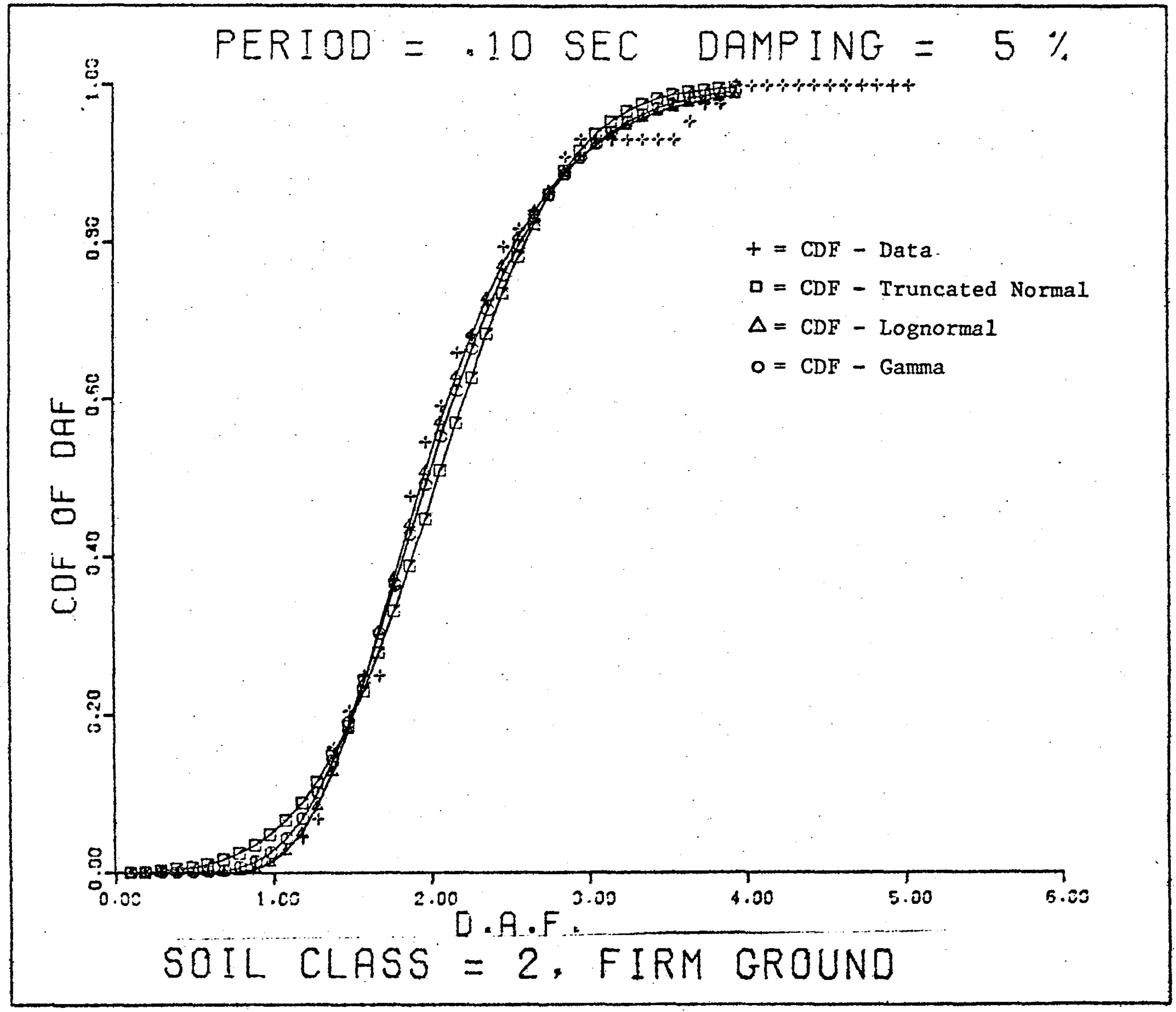

FIGURE 45 Comparison of Three CDF's of DAF

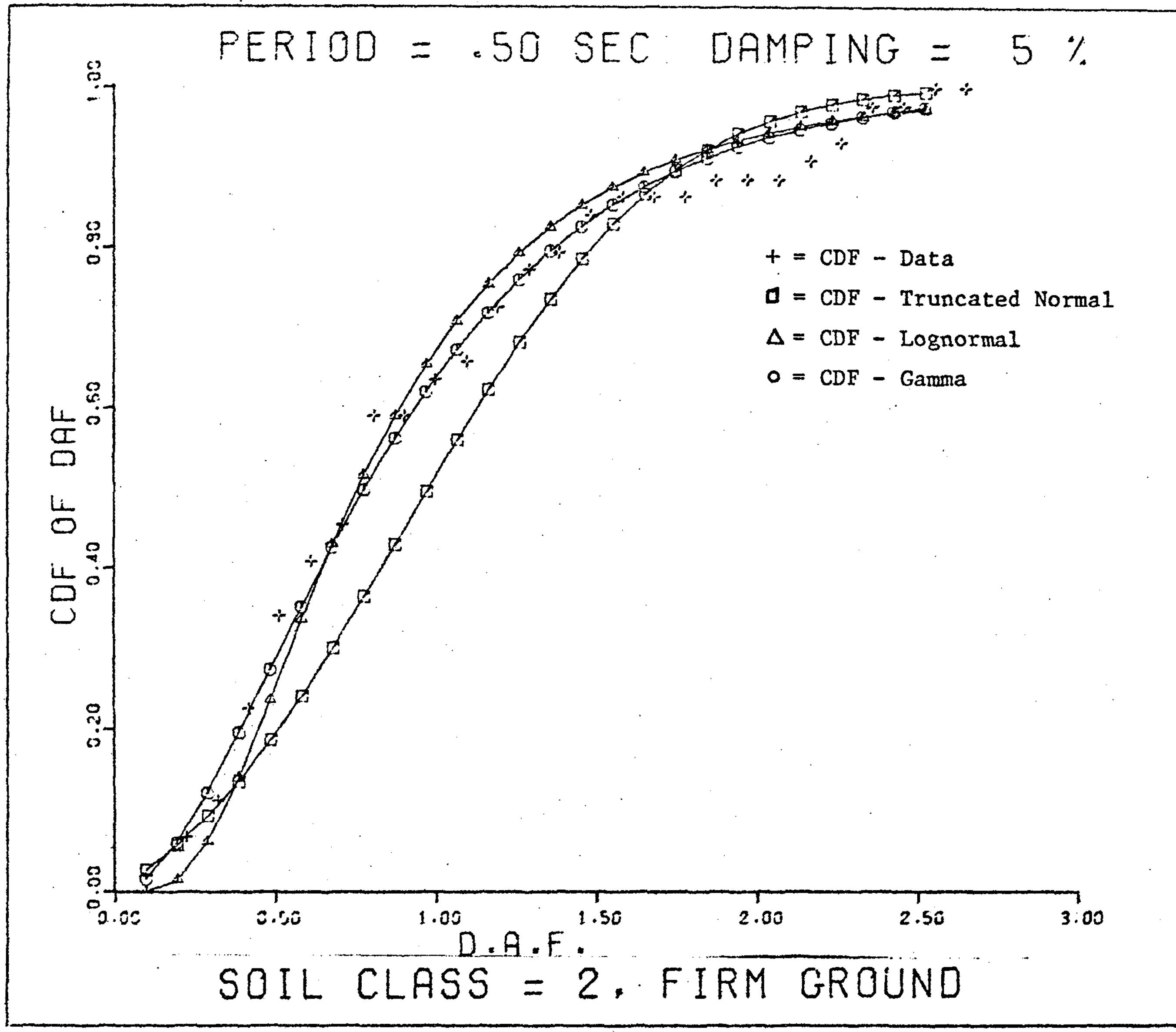

FIGURE 46 Comparison of Three CDF's of DAF

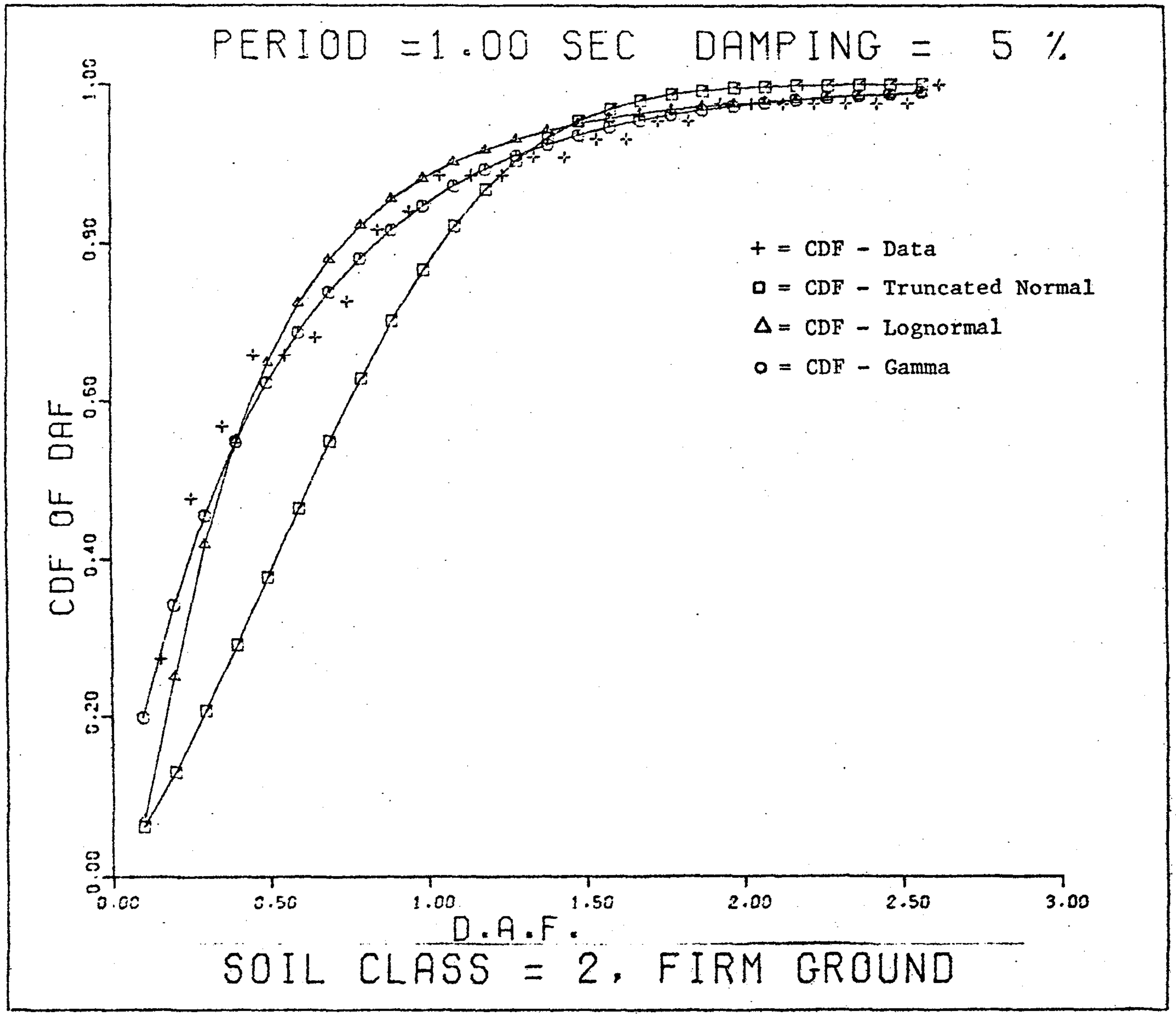

FIGURE 47 Comparison of Three CDF's of DAF

the statistics of the data is computed for each soil type. Equations 12, 13, 26 and 27 are used to evaluate the mean, variance, median, and variance of the logarithm of the parameter and the results are listed in Tables 7 to 12. The statistics for soil class 0 are given in Tables 7 and 8; for soil class 1 are given in Tables 9 and 10; and for soil class 2 are in Tables 11 and 12. The parameters λ and k of the gamma distribution are obtained directly from the mean and the variance as shown by Equations 31 and 32.

Figures 30 to 47 show the three distributions and the data for periods of 0.1, 0.5, 1.0 sec and 2% and 5% damping for soil classes 0, 1 and 2. From the graphs it can be observed that:

- The truncated normal distribution gives the poorest fit to the data.
- The gamma distribution approximates the CDF from the data better than either the truncated normal or the lognormal distributions for all three soil types. This observation is especially true for periods higher than about 0.4 sec. For periods lower than 0.4 sec all three distributions are very close.
- The fit for all three distributions is poorest for soil class 2 and best for soil class 0. The fit improves from soil class 2 to soil class 0 because of the increase in the number of data points in each sample.
- For all three soil conditions the fit to the data is better for low periods of vibration than for high periods.

In the subsequent analysis, the gamma distribution will be used as the representative distribution of DAF.

From the cumulative probability distributions on dynamic amplification factors resulting from the gamma fit, pseudo-acceleration response spectral shapes corresponding to the mean value of the distribution and the 84 percentile (or approximately mean plus one standard deviation) are obtained. The shapes for the three soil conditions are compared to the shapes developed by Seed, et al (14) and are shown on Figures 48 to 50. The spectral shape for very loose sand given by Seed, et al (14) is not compared since there is no counterpart to it in the soil division used in this study.

For all three soil classes, the spectral shapes developed through the above analysis are lower than the spectral shapes shown by Seed, et al (14). For very low periods all the curves are close together giving similar DAF values. The difference in the shapes results primarily because the strong motion data in the two studies is not identical. For example, accelerograms from the Bursa, Turkey, and the Akita, Japan earthquakes used by Seed et al (14) are not included in the data of Table 1.

For high periods, the mean and 84 percentile shapes are almost the same. Only for soil class 1 (intermediate) the DAF values are a little higher than the values given by Seed, et al (14).

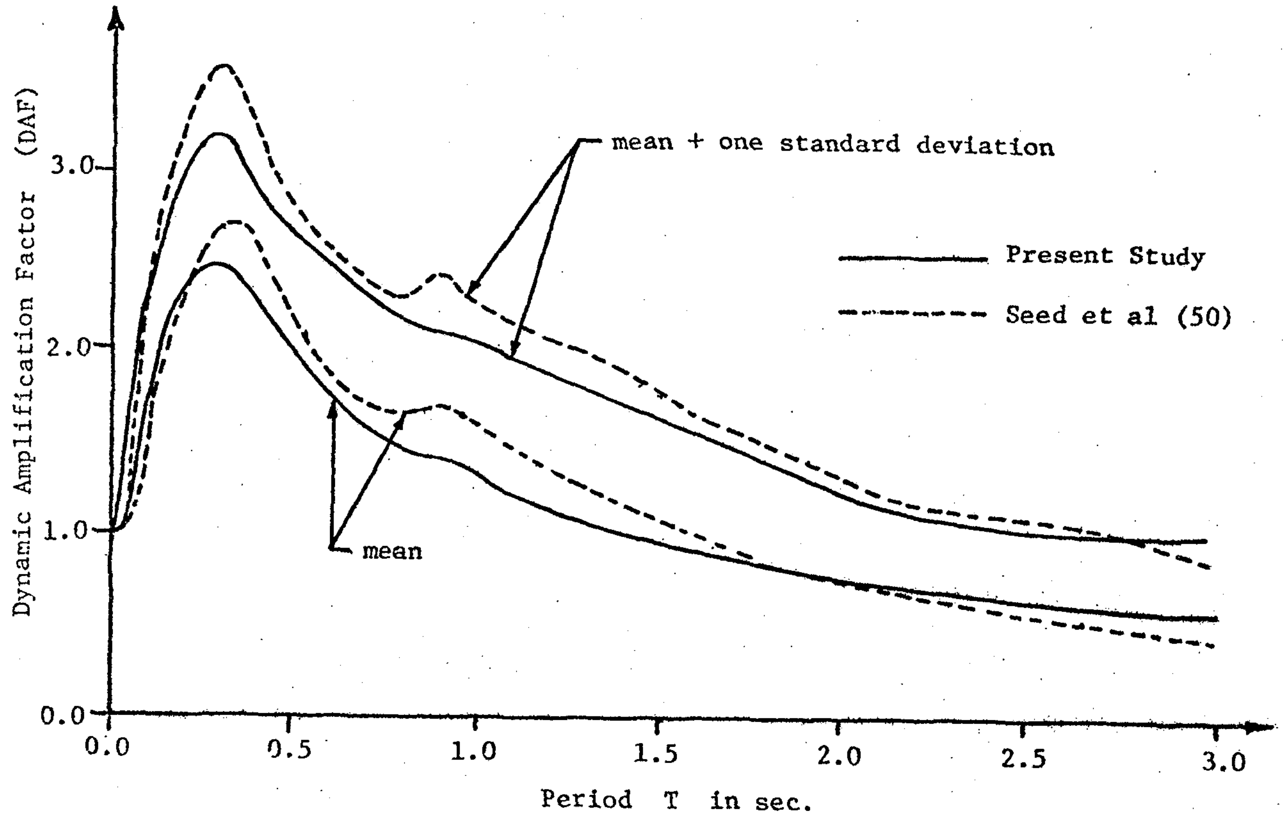

FIGURE 48 Comparison of DAF from Present Study to DAF from Seed et al (50), Soil Class = 0, Damping = 5%.

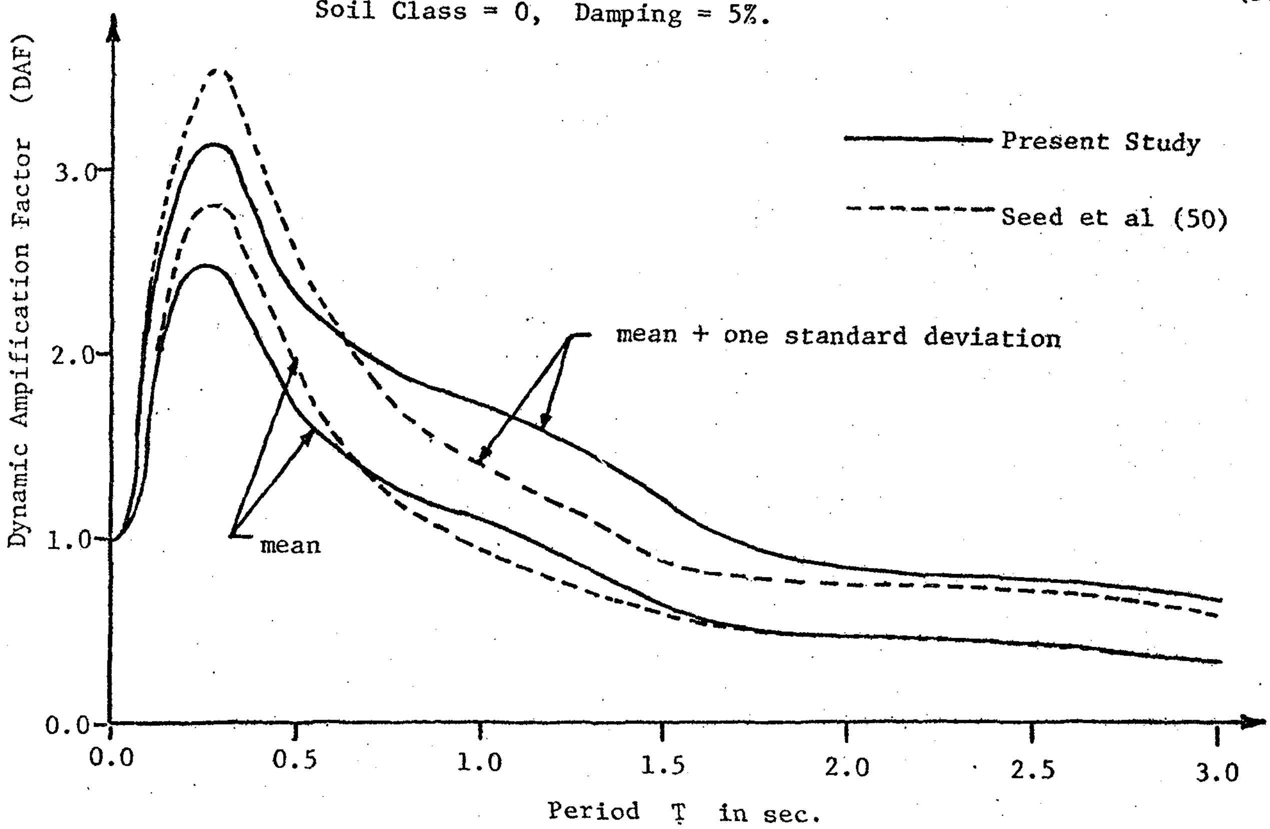

FIGURE 49 Comparison of DAF from Present Study to DAF from Seed et al (50), Soil Class = 1, Damping = 5%.

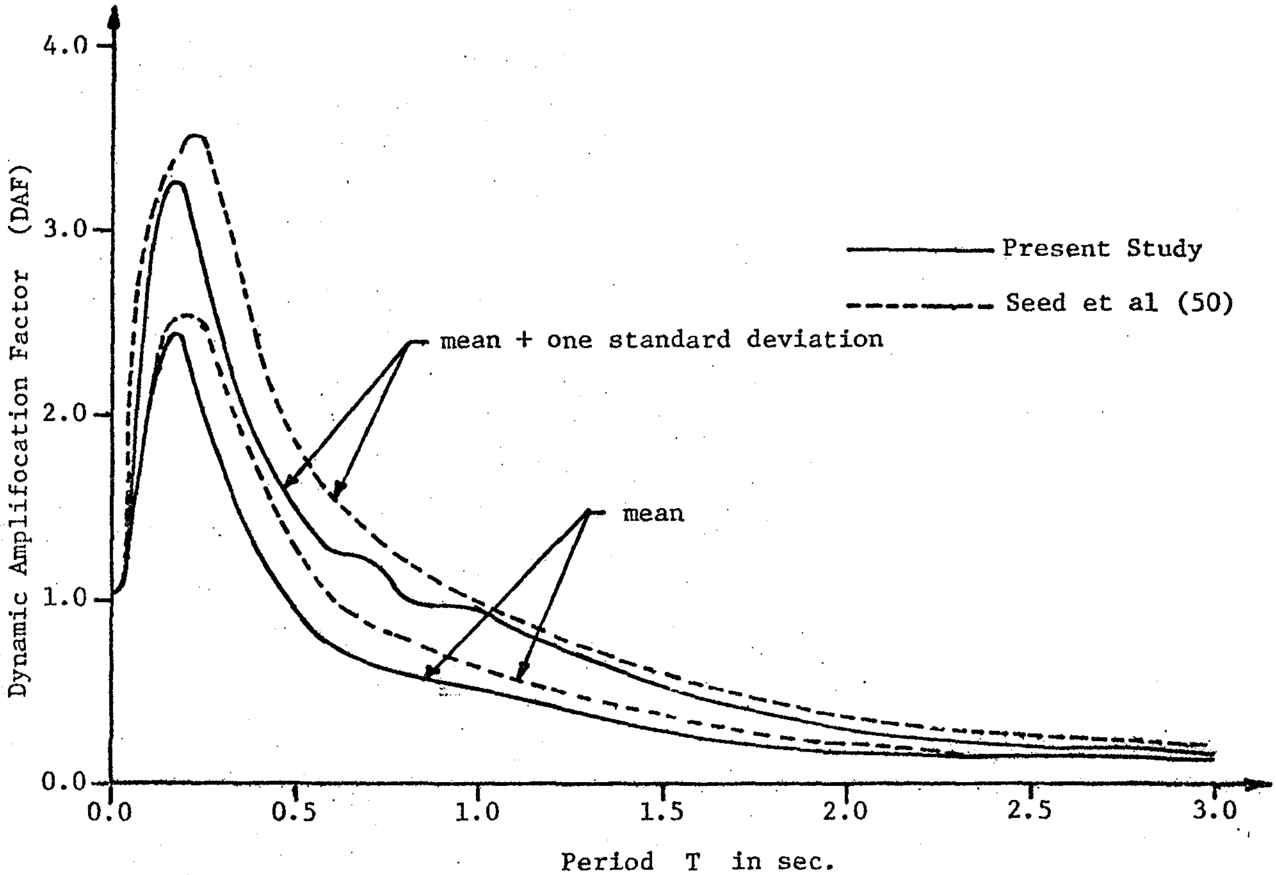

FIGURE 50 Comparison of DAF from Present Study to DAF from Seed et al (50), Soil Class = 2, Damping = 5%.

CHAPTER 5

PROBABILISTIC RESPONSE SPECTRA

The cumulative probability distributions on response spectra, s_a, at Los Angeles for a future time period of 50 years are computed using Equation 33. The cumulative probability distribution on peak ground acceleration for the next 50 years at Los Angeles as obtained by Kiremidjian (11) is used directly in the evaluation of $F_{S_a}(s_a,t)$. Three CDF's of s_a are computed for soil classes 0, 1, and 2. For each of these cases the parameters λ and k are obtained from Tables 7 to 12.

Figures 51 to 74 show the cumulative probability distributions for alluvial soil deposits (class 0), intermediate soils (class 1), and firm soils (class 2), for periods of 0.05, 0.1, 0.5, and 1.0 seconds and dampings of 2% and 5%. These figures give the probability that a structure with one of the natural periods specified above will be excited by an earthquake so that its maximum response acceleration is larger than a given s_a value in the next 50 years in Los Angeles.

For example, a structure with a predominant period of 0.1 second and a critical damping of 5% has 90% chance of being excited in the next 50 years so that its response acceleration will be

0.26g or smaller if it is built on alluvium (class 0)

0.33g or smaller if it is built on intermediate soils (class 1)

0.55g or smaller if it is built on firm ground (class 2)

Similarly, for a structure with a predominant natural period of 1.5 second and 5% damping, there is 90% probability of being excited so that its response acceleration in the next 50 years is 0.18g, 0.19g, and 0.15g for soil classes 0, 1, and 2 respectively, if the structure is located in Los Angeles.

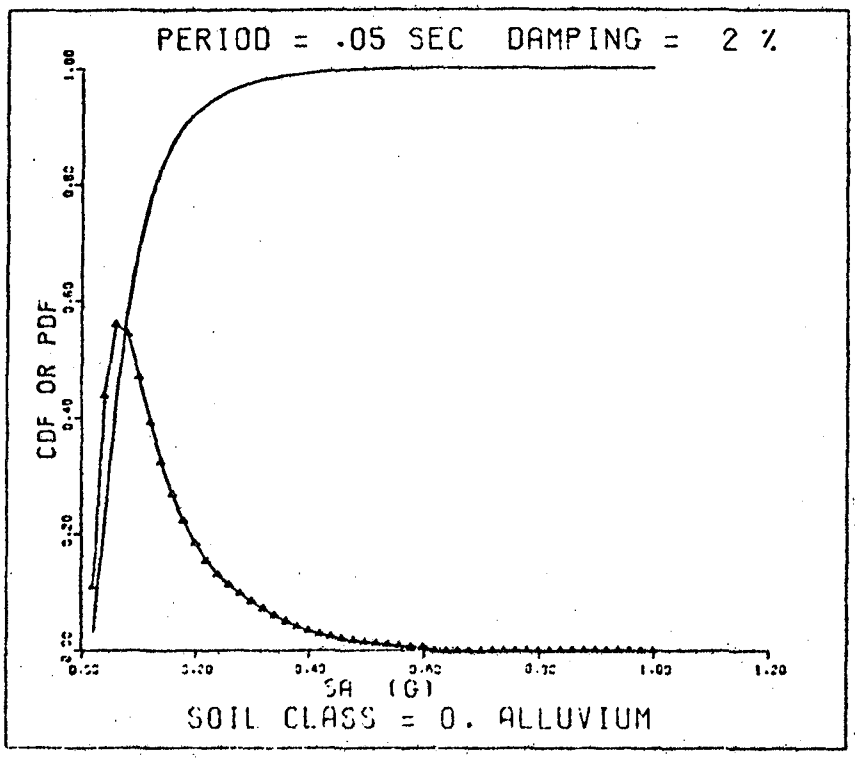

FIGURE 51 CDF(s_a) and PDF(s_a),
Los Angeles Site, Time Period = 50 Yrs.

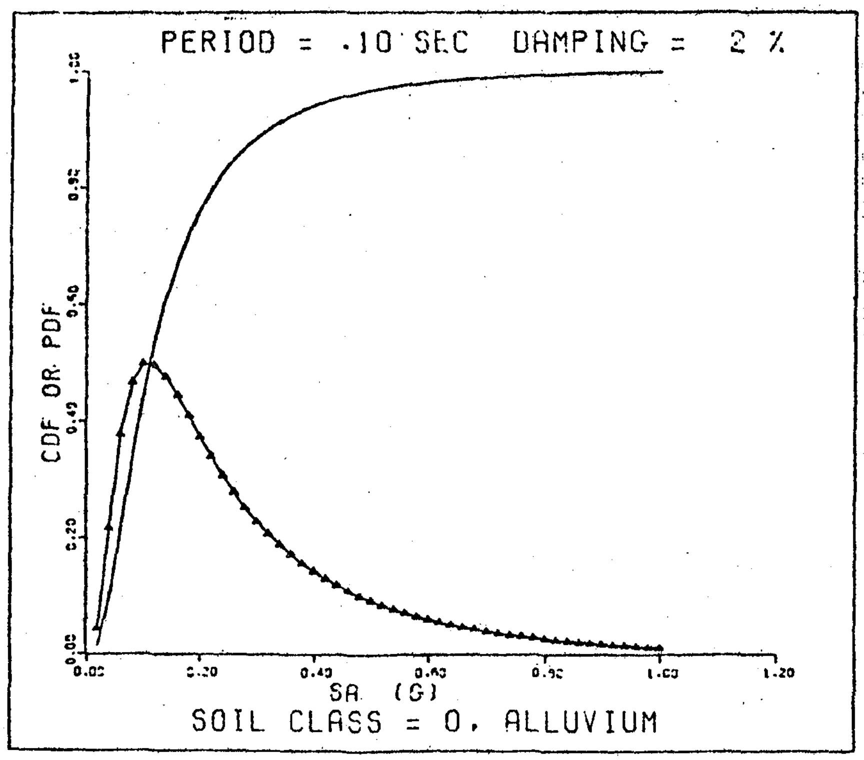

FIGURE 52 CDF(s_a) and PDF(s_a),
Los Angeles Site, Time Period = 50 Yrs.

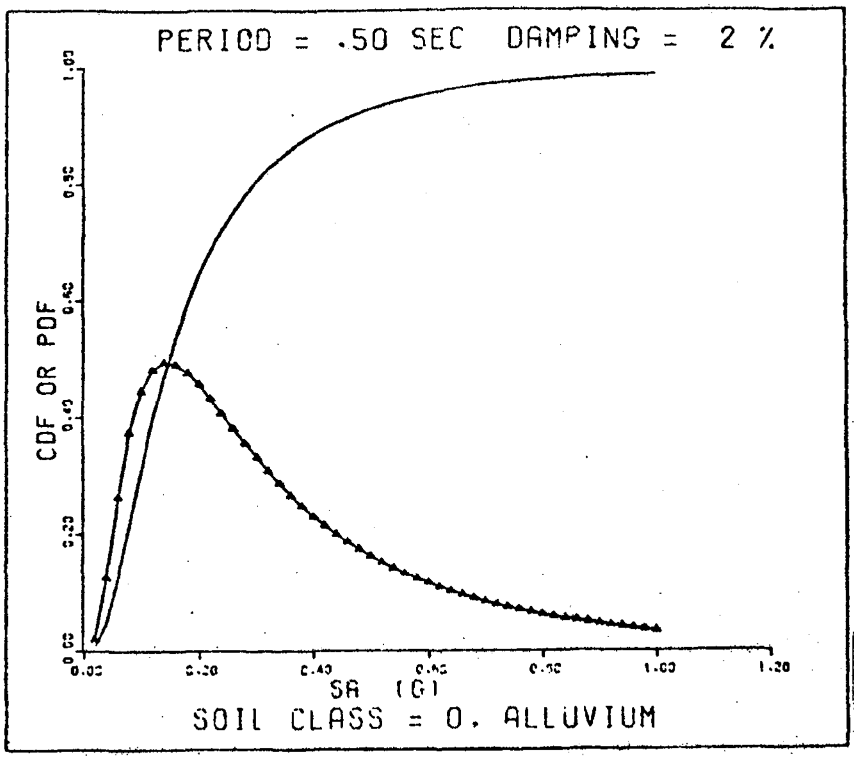

FIGURE 53 CDF(s_a) and PDF(s_a),
Los Angeles Site, Time Period = 50 Yrs.

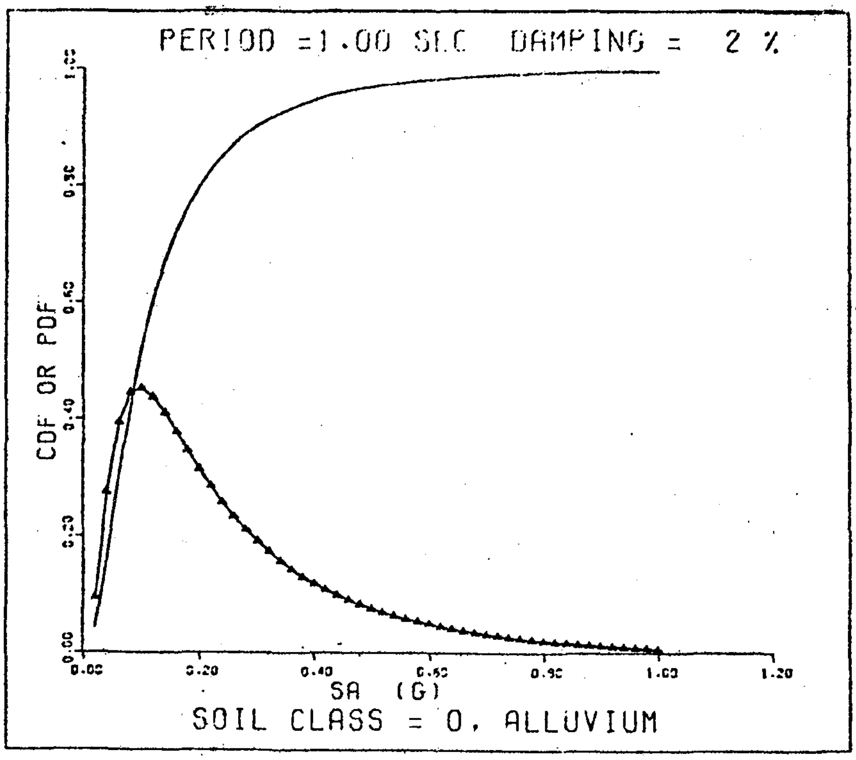

FIGURE 54 CDF(s_a) and PDF(s_a),
Los Angeles Site, Time Period = 50 Yrs.

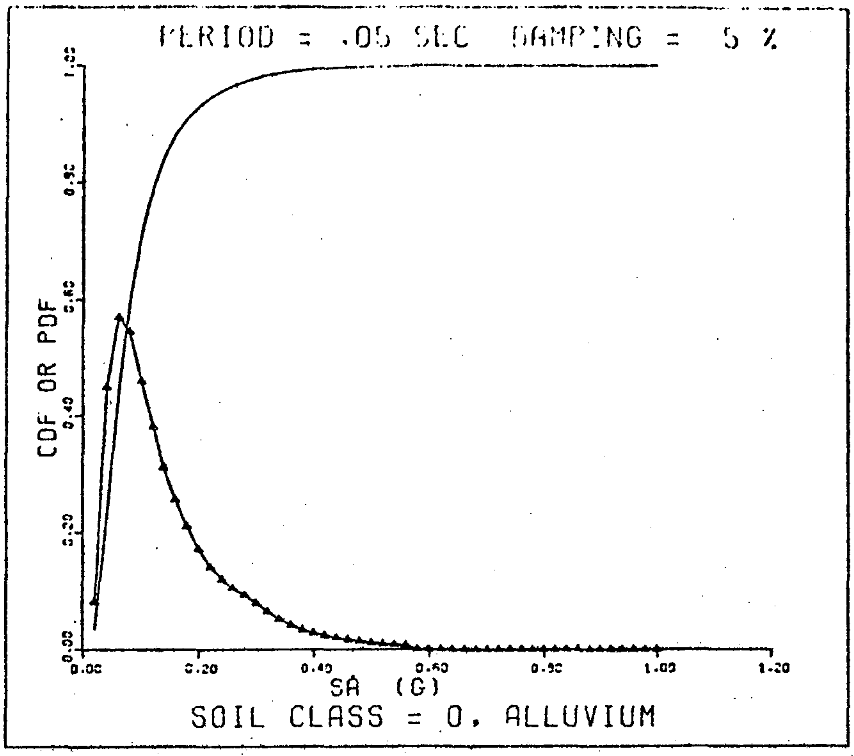

FIGURE 55 CDF(s_a) and PDF(s_a),
Los Angeles Site, Time Period = 50 Yrs.

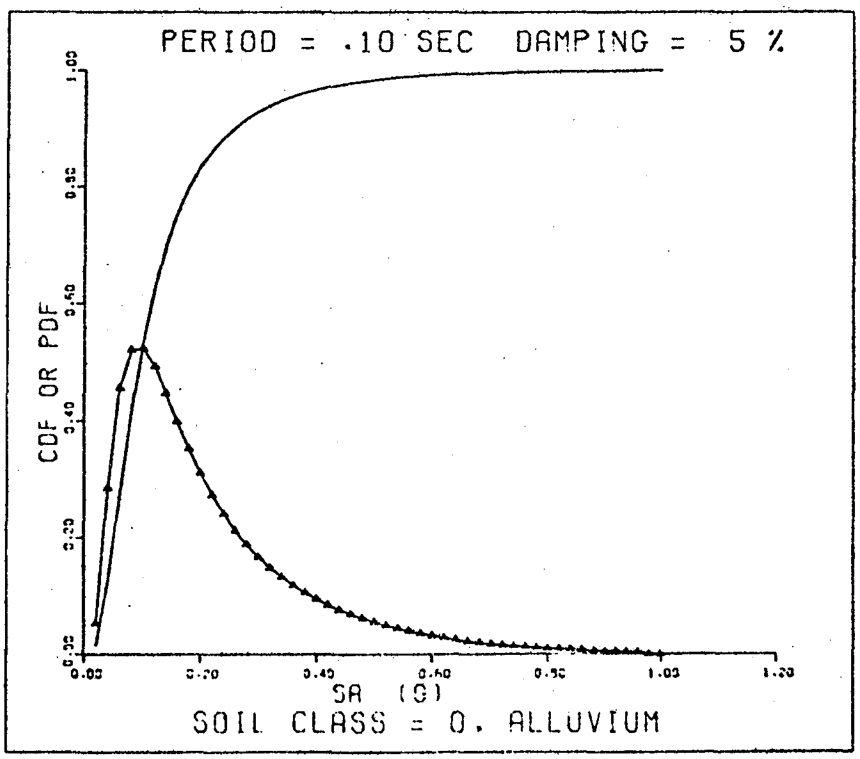

FIGURE 56 CDF(s_a) and PDF(s_a),
Los Angeles Site, Time Period = 50 Yrs.

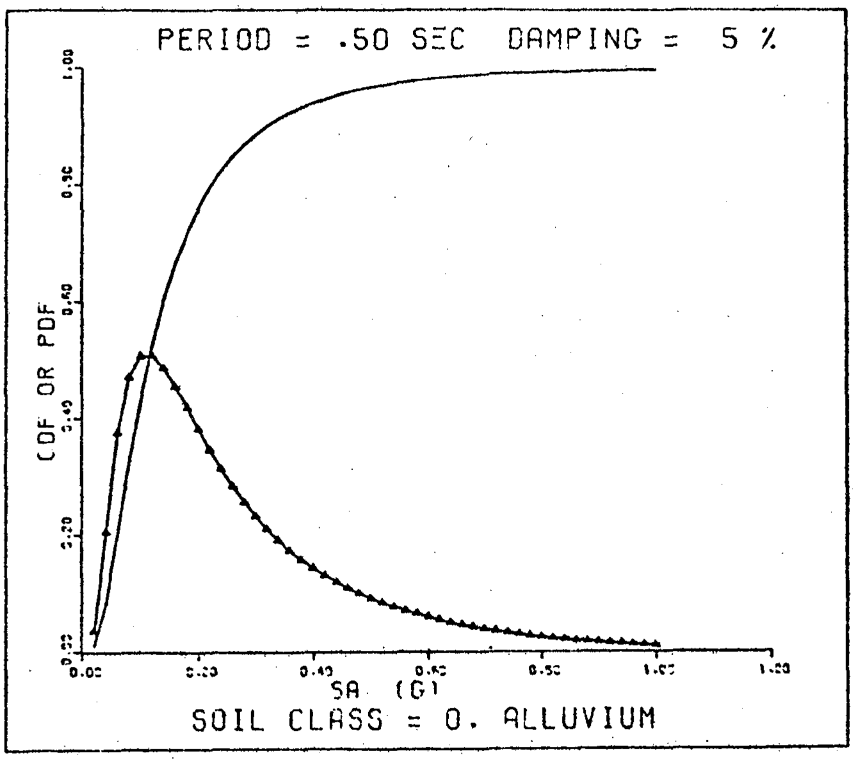

FIGURE 57 CDF(s_a) and PDF(s_a),
Los Angeles Site, Time Period = 50 Yrs.

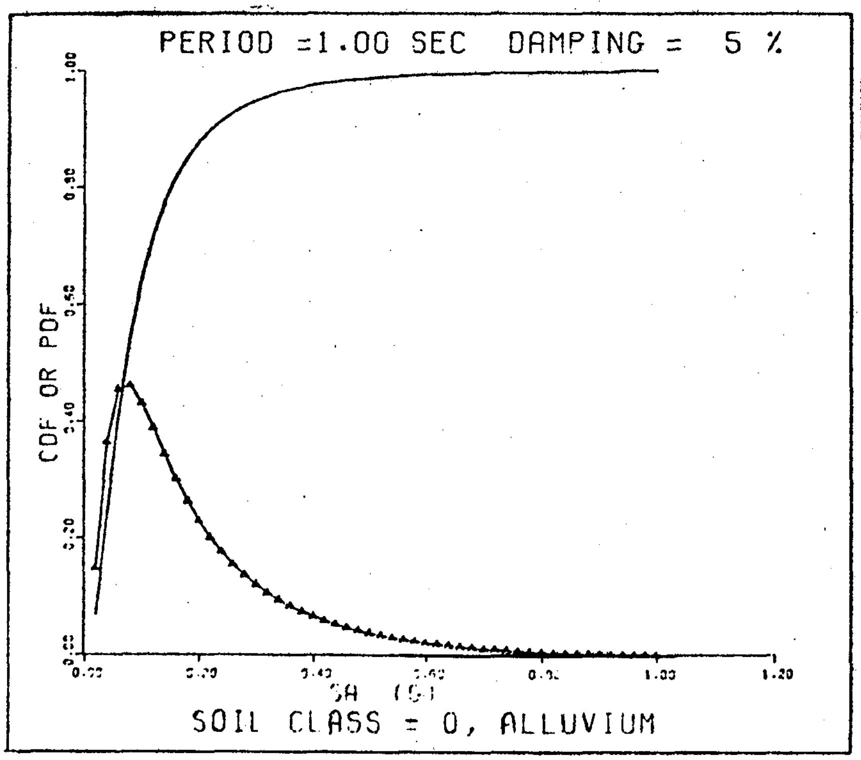

FIGURE 58 CDF(s_a) and PDF(s_a),
Los Angeles Site, Time Period = 50 Yrs.

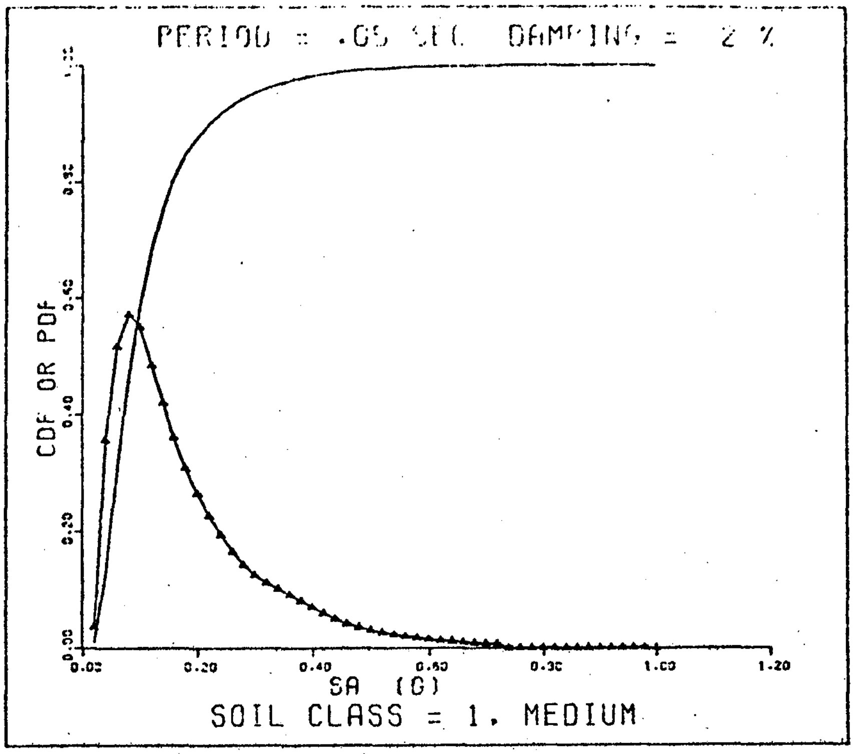

FIGURE 59 CDF(s_a) and PDF(s_a),
Los Angeles Site, Time Period = 50 Yrs.

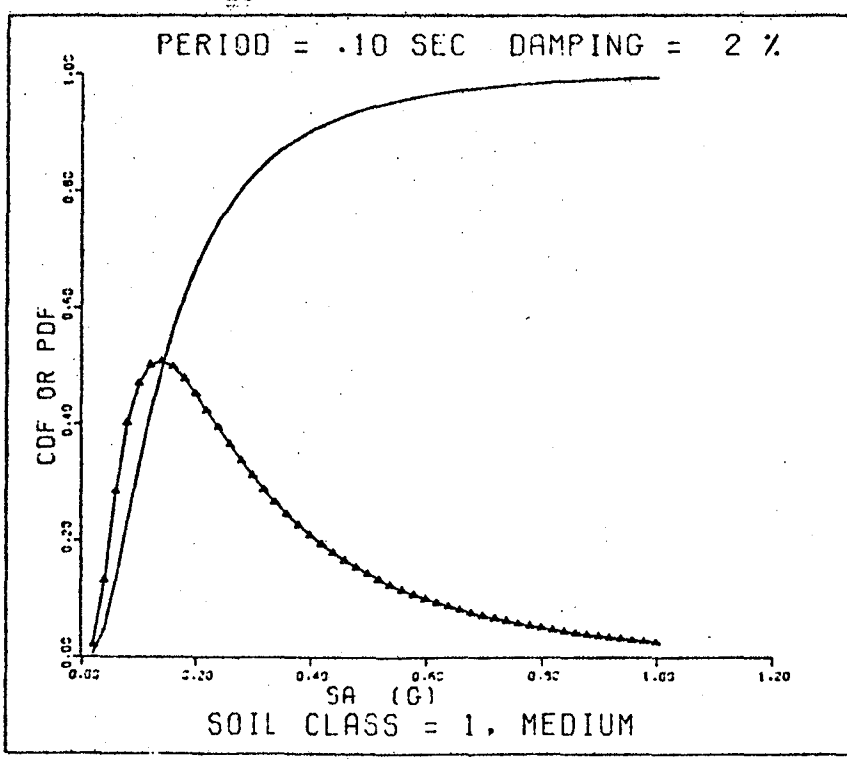

FIGURE 60 CDF(s_a) and PDF(s_a),
Los Angeles Site, Time Period = 50 Yrs.

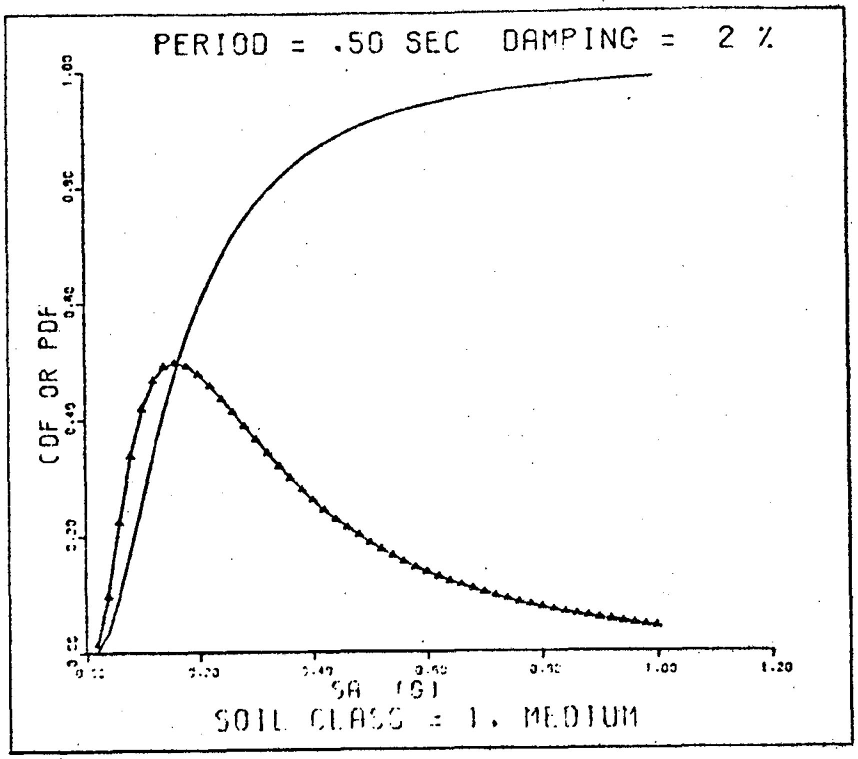

FIGURE 61 CDF(s_a) and PDF(s_a),
Los Angeles Site, Time Period = 50 Yrs.

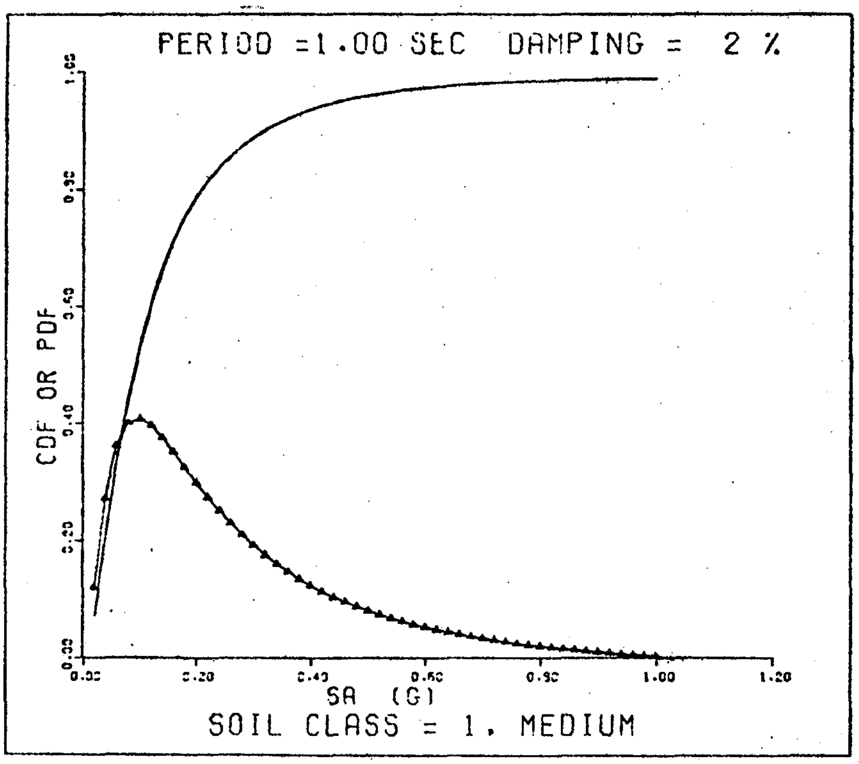

FIGURE 62 CDF(s_a) and PDF(s_a),
Los Angeles Site, Time Period = 50 Yrs.

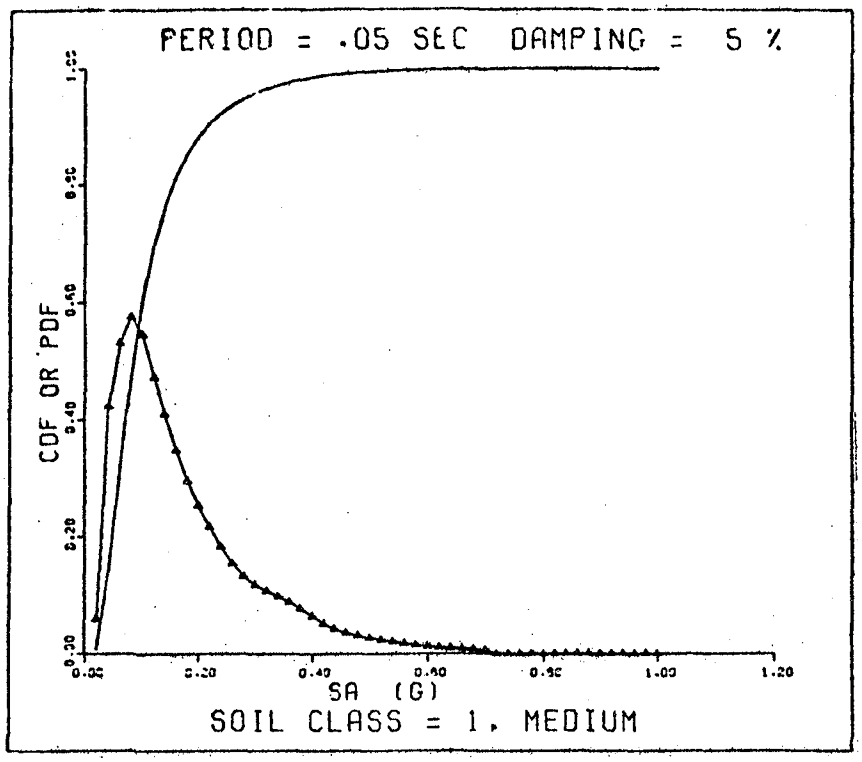

FIGURE 63 CDF(s_a) and PDF(s_a),
Los Angeles Site, Time Period = 50 Yrs.

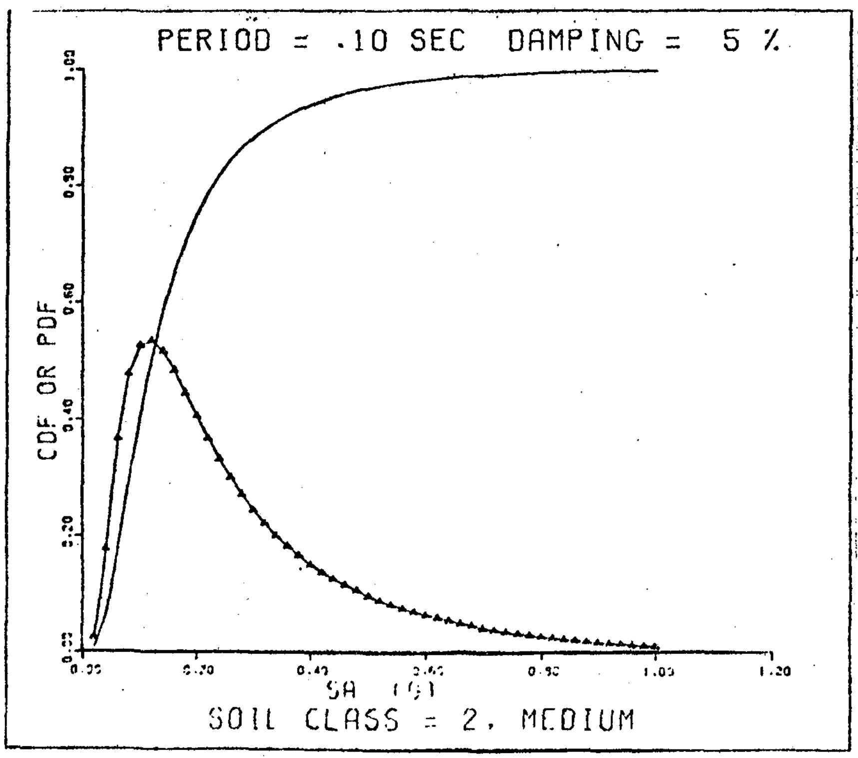

FIGURE 64 CDF(s_a) and PDF(s_a),
Los Angeles Site, Time Period = 50 Yrs.

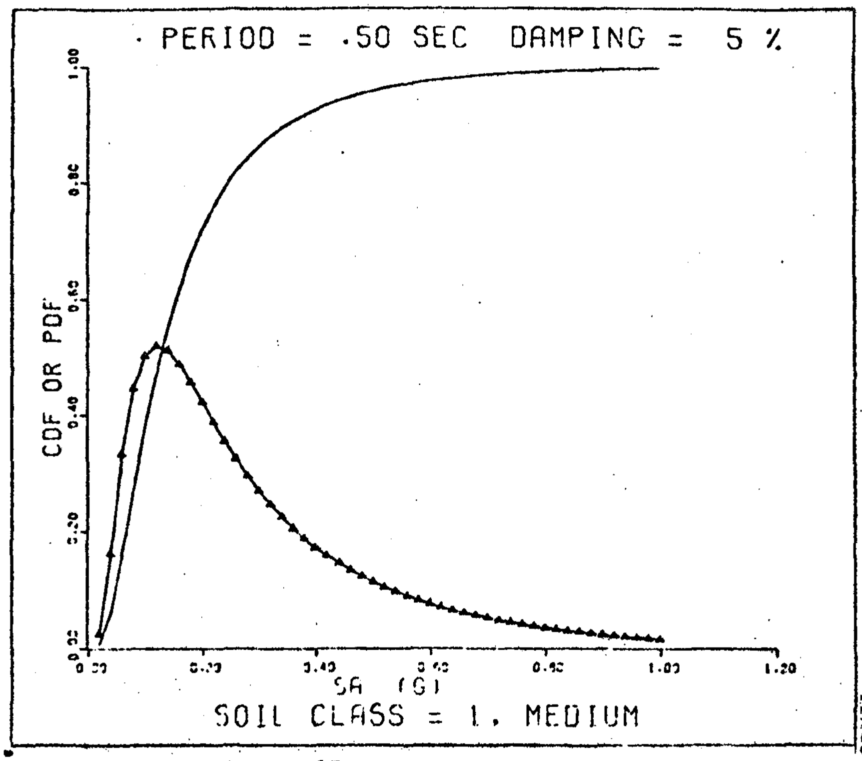

FIGURE 65 CDF(s_a) and PDF(s_a),
Los Angeles Site, Time Period = 50 Yrs.

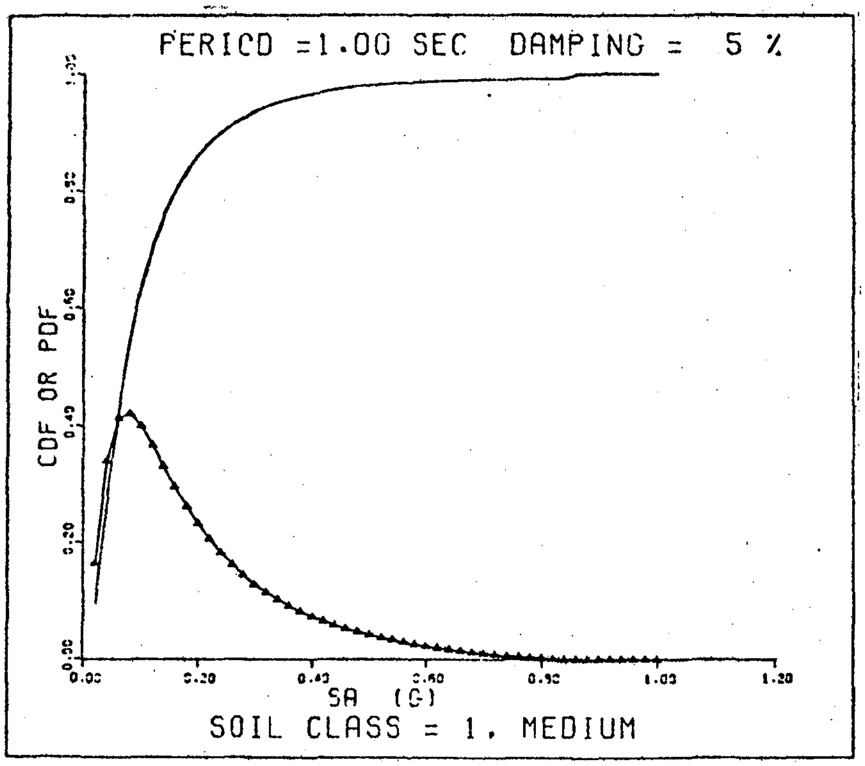

FIGURE 66 CDF(s_a) and PDF(s_a),
Los Angeles Site, Time Period = 50 Yrs.

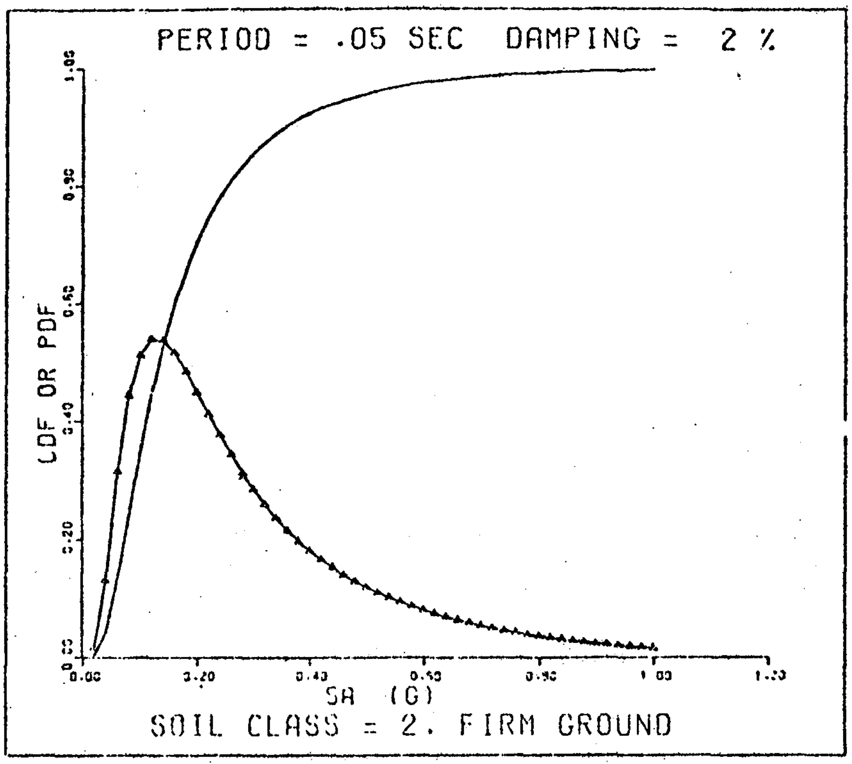

FIGURE 67 CDF(s_a) and PDF(s_a),
Los Angeles Site, Time Period = 50 Yrs.

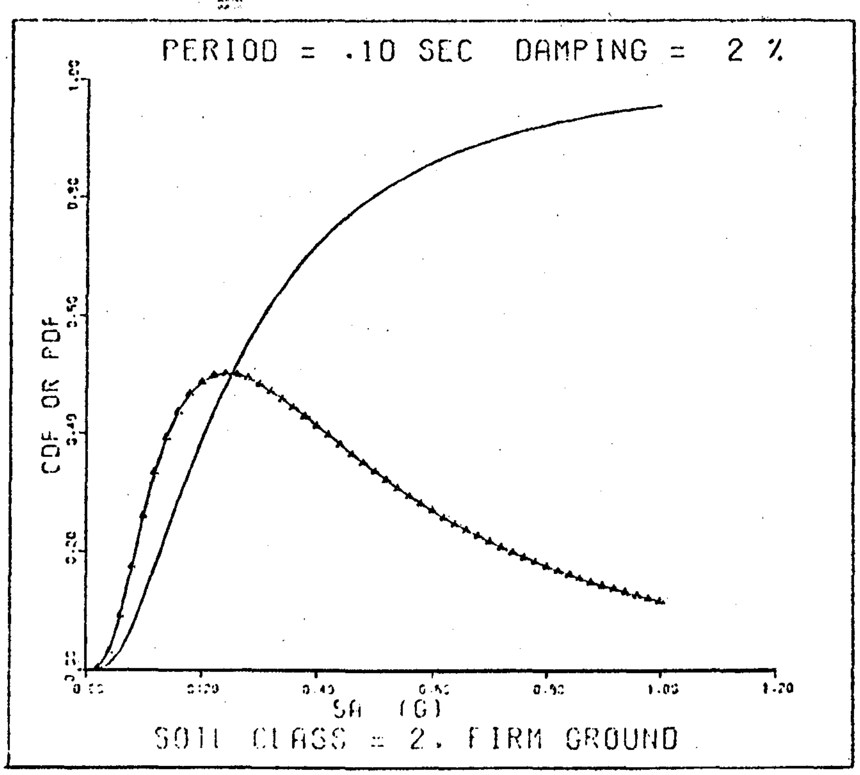

FIGURE 68 CDF(s_a) and PDF(s_a),
Los Angeles Site, Time Period = 50 Yrs.

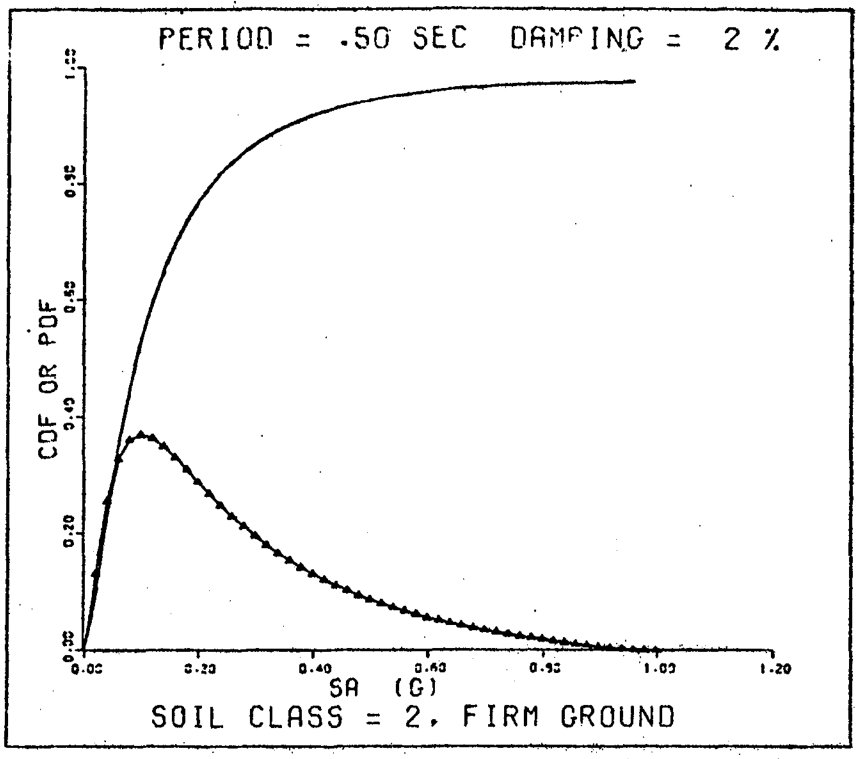

FIGURE 69 CDF(s_a) and PDF(s_a),
Los Angeles Site, Time Period = 50 Yrs.

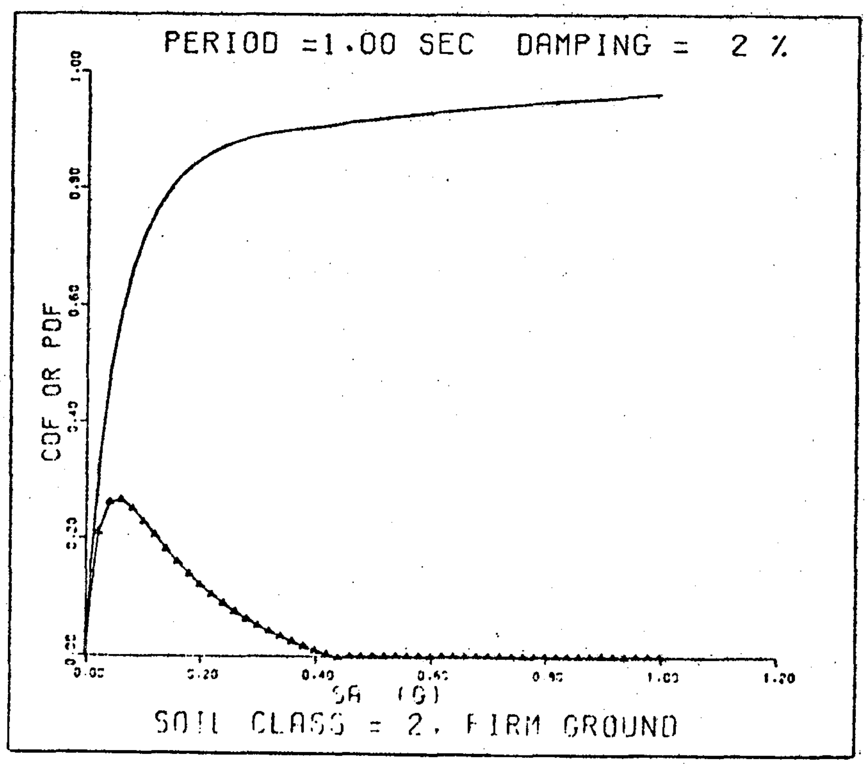

FIGURE 70 CDF(s_a) and PDF(s_a),
Los Angeles Site, Time Period = 50 Yrs.

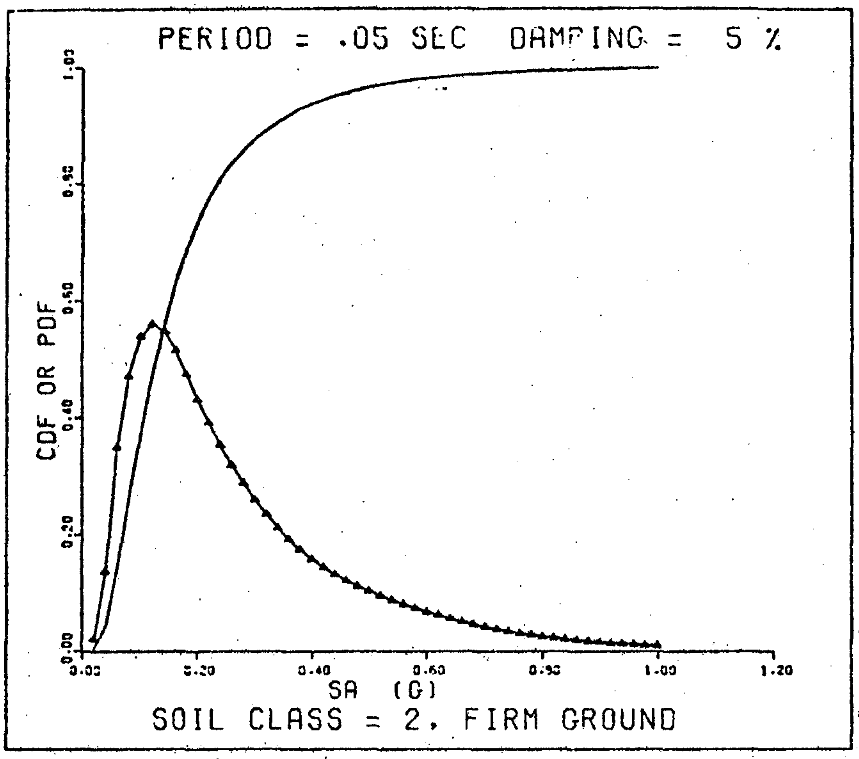

FIGURE 71 CDF(s_a) and PDF(s_a),
Los Angeles Site, Time Period = 50 Yrs.

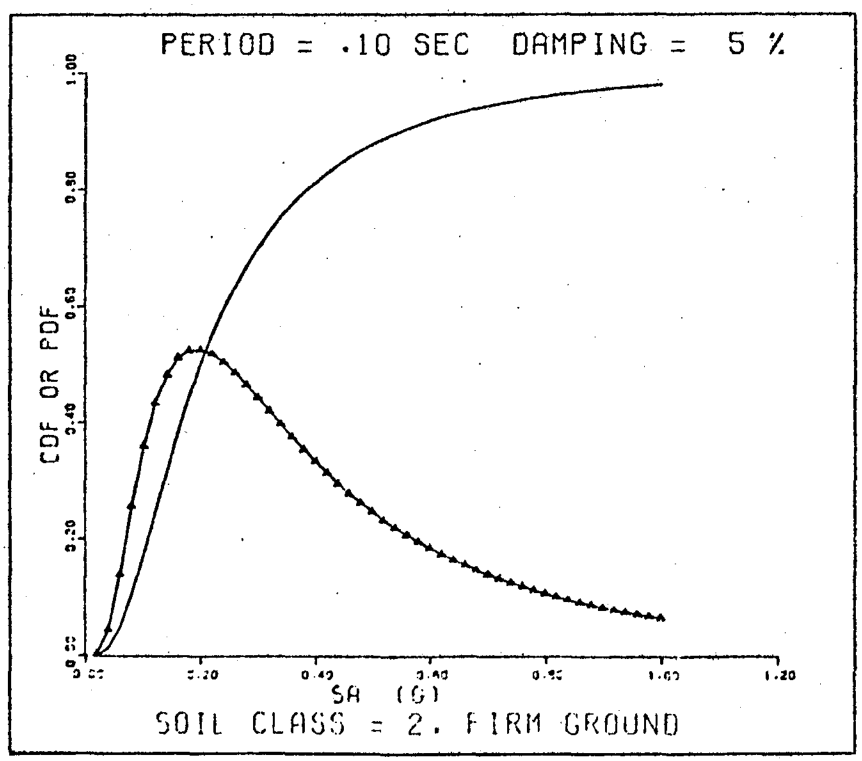

FIGURE 72 CDF(s_a) and PDF(s_a),
Los Angeles Site, Time Period = 50 Yrs.

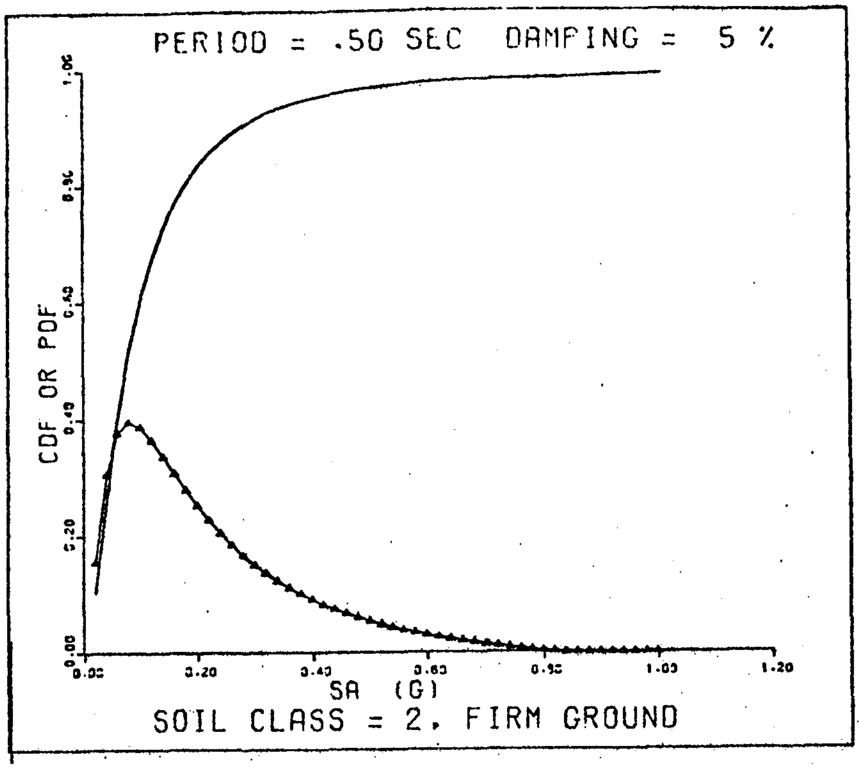

FIGURE 73 CDF(s_a) and PDF(s_a),
Los Angeles Site, Time Period = 50 Yrs.

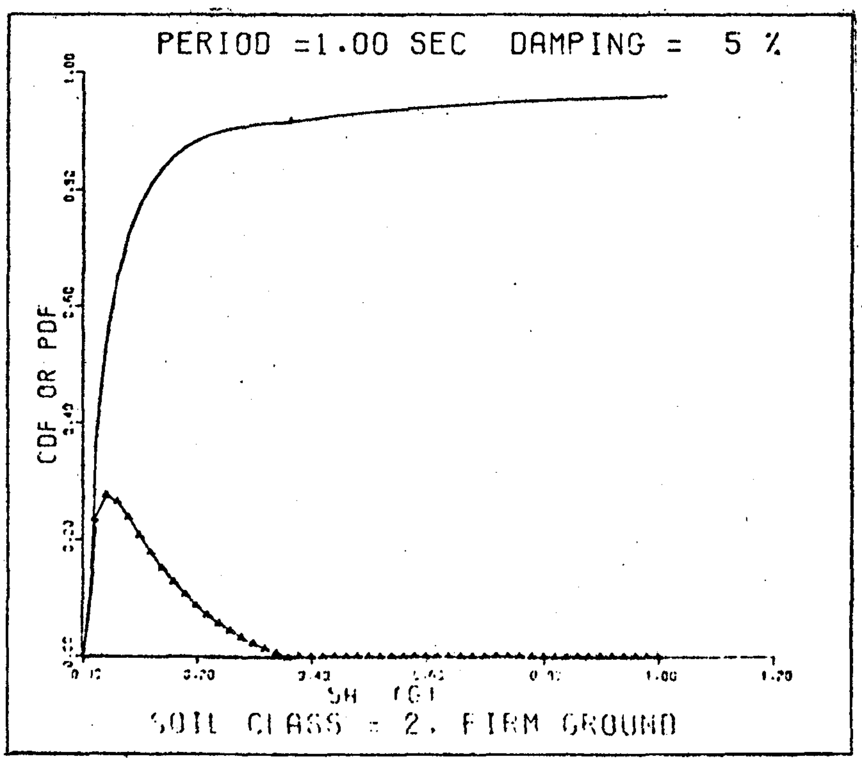

FIGURE 74 CDF(s_a) and PDF(s_a),
Los Angeles Site, Time Period = 50 Yrs.

The cumulative density functions, $F_{S_a}(s_a)$, for the three soil types are next compared to the cumulative density function of peak ground acceleration. Figures 75, 76, and 77 show the two CDF's for soft soils, intermediate soils, and firm ground respectively. The $F_{S_a}(s_a)$ is shown for a damping of 5% and only one value of the natural period T. For soft and intermediate soils, the natural period is taken at T = 0.3 sec. For firm ground the period is taken at T = 0.15 sec. The CDF's of s_a for these natural periods give the highest values of acceleration at a specified risk level. The CDF's of s_a for other values of T will lie above the curves of CDF of s_a shown in Figures 75, 76 and 77. It is important to note the difference in values between peak ground acceleration and response spectrum accelerations at the same risk level. For example, at 5% chance of exceedence the PGA value for soft soils is 0.23g while the s_a value is 0.52g. Similarly, for intermediate soils the PGA value at 5% risk level is 0.29g while the s_a value is 0.65g. For the same risk level the PGA at firm ground is 0.38g and the corresponding value of s_a is 0.87g. Thus, a structural design based on peak ground acceleration rather than on response spectrum acceleration may greatly underestimate the earthquake load resistance requirements for the structure.

Pseudo-acceleration response spectra are obtained for three risk levels. Figures 78 to 80 give the response spectra for 10%, 20%, and 50% chance of exceeding the acceleration values when the structure has 5% damping. In most cases the pseudo-acceleration response spectra for soil class 1 is higher than the others at periods higher than 0.3 sec. In the low period range, $.05 \leq T \leq .3$ sec, the soil class 2 response spectra predominates over the two other curves.

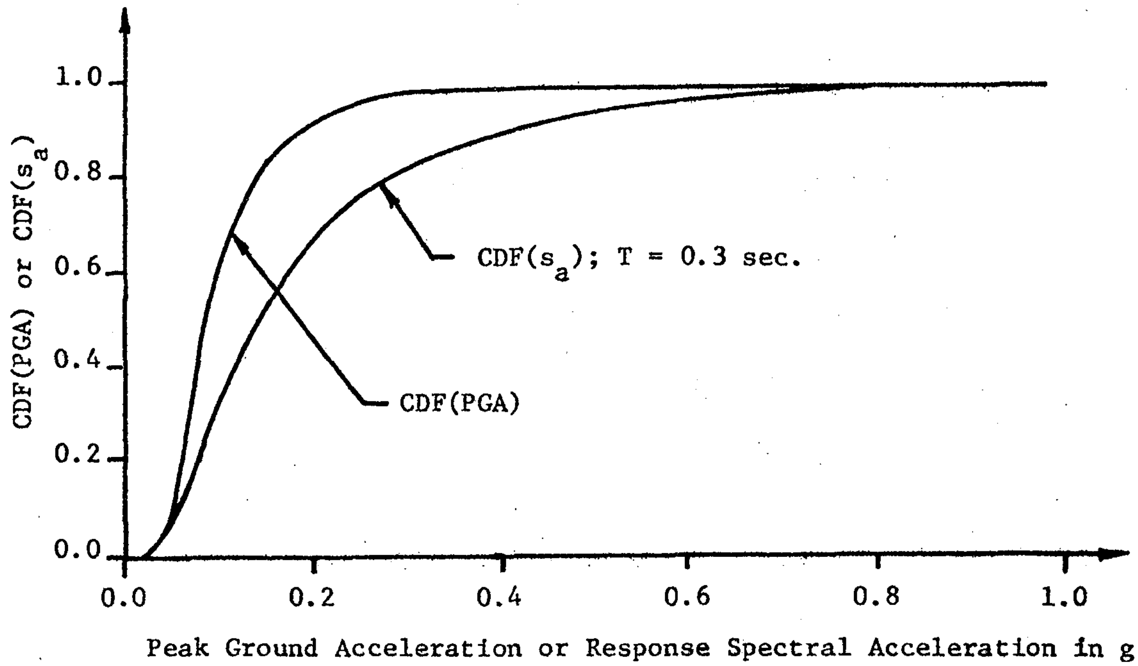

FIGURE 75 Comparison of CDF(PGA) to CDF(s_a) for Los Angeles Site, Soil Class = 0, Damping = 5%, Time = 50 years.

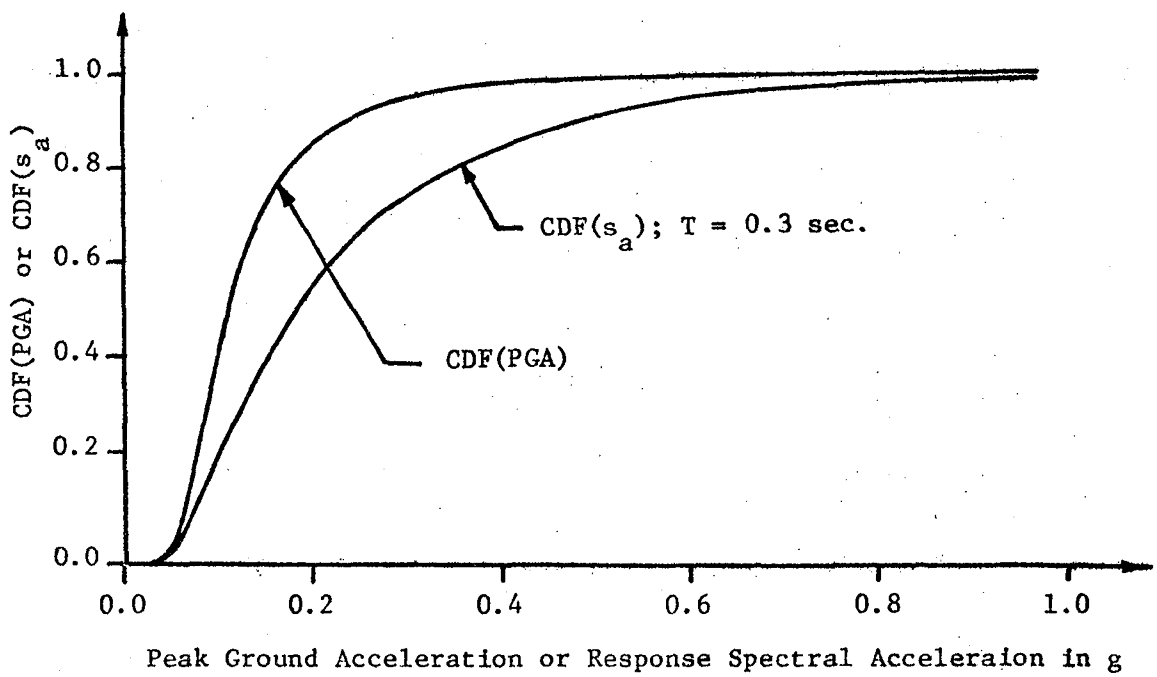

FIGURE 76 Comparison of CDF(PGA) to CDF(s_a) for Los Angeles Site, Soil Class = 1, Damping = 5%, Time = 50 years.

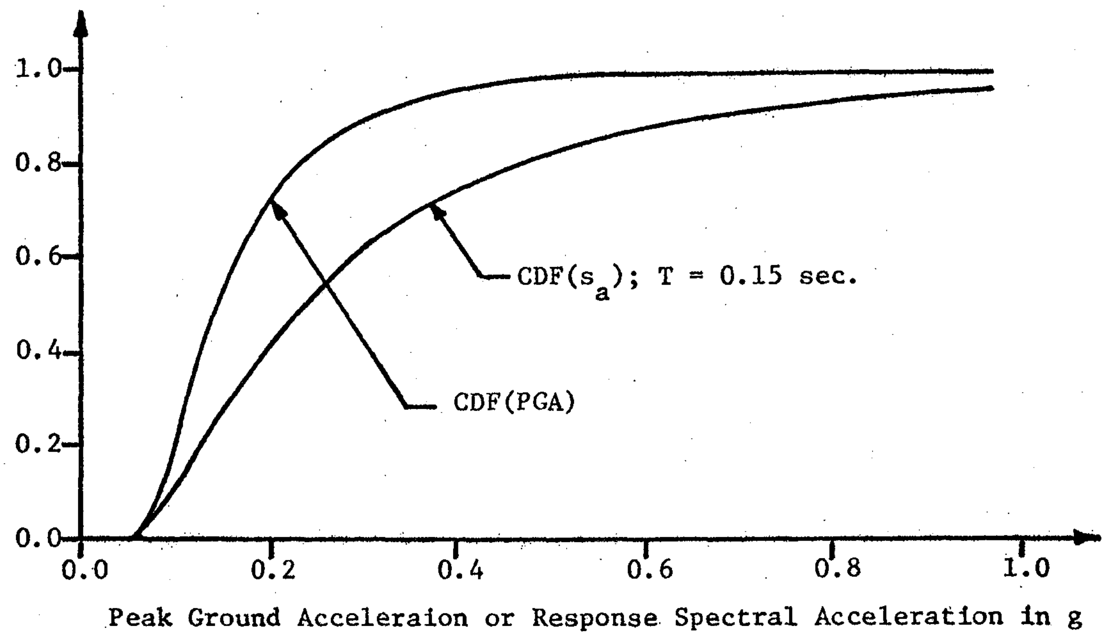

FIGURE 77 Comparison of CDF(PGA) to CDF(s_a) for Los Angeles Site, Soil Class = 2, Damping = 5%, Time = 50 years.

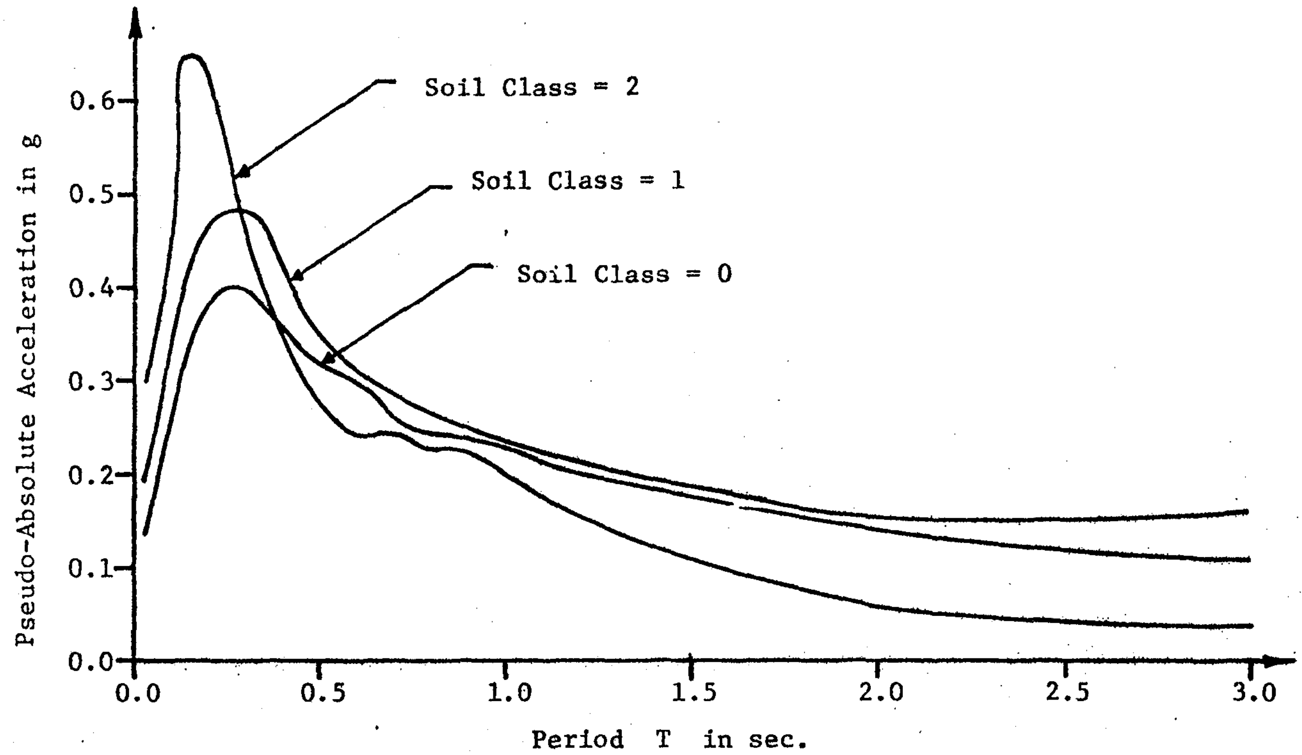

FIGURE 78 Pseudo-Absolute Acceleration Response Spectra for Three Soil Types, Los Angeles Site, $P[S_a > s_a] = 0.1$, Damping = 5%, Time = 50 years

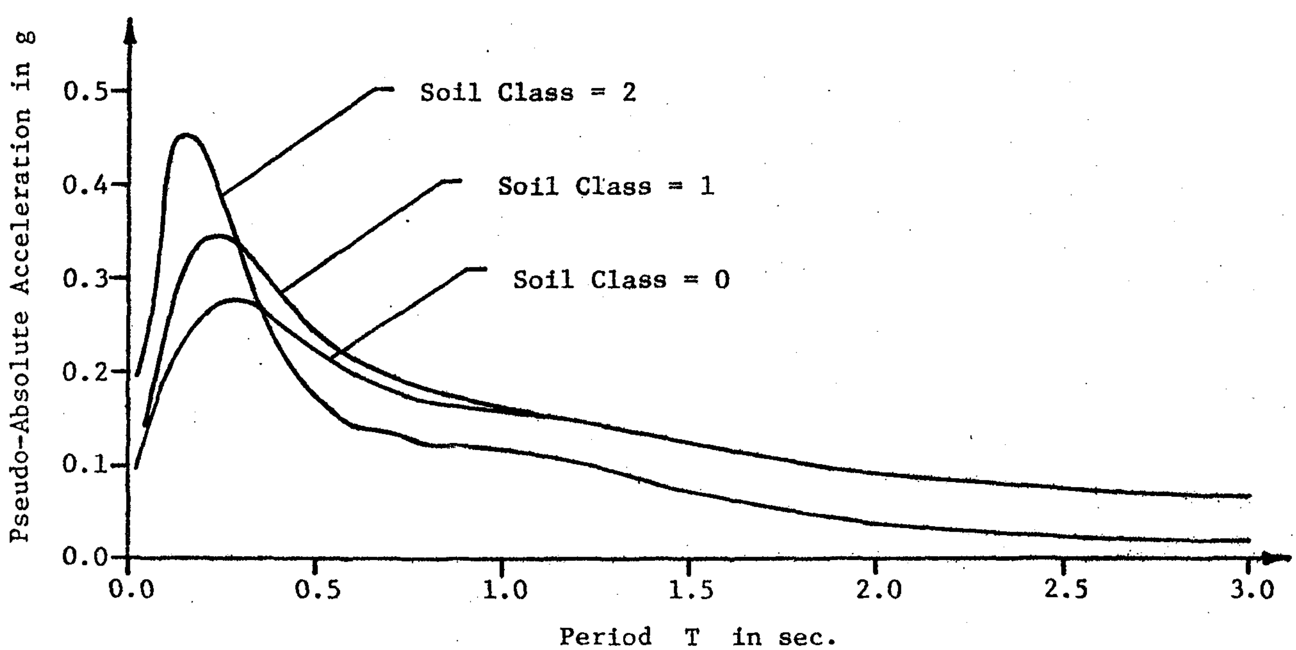

FIGURE 79 Pseudo-Absolute Acceleration Response Spectra for Three Soil Types, Los Angeles Site, $P[S_a > s_a] = 0.2$, Damping = 5%, Time = 50 years.

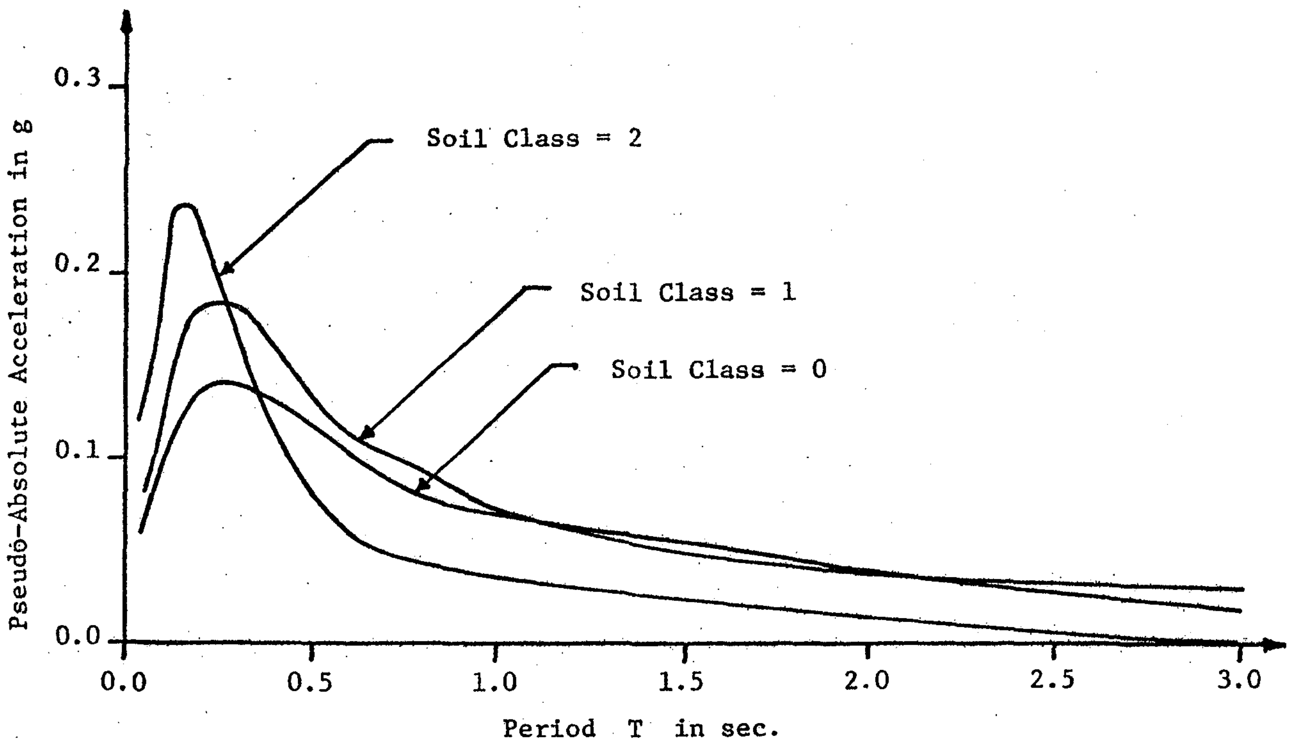

FIGURE 80 Pseudo-Absolute Acceleration Response Spectra for Three Soil Types, Los Angeles Site, $P[S_a > s_a] = 0.5$, Damping = 5%, Time = 50 years.

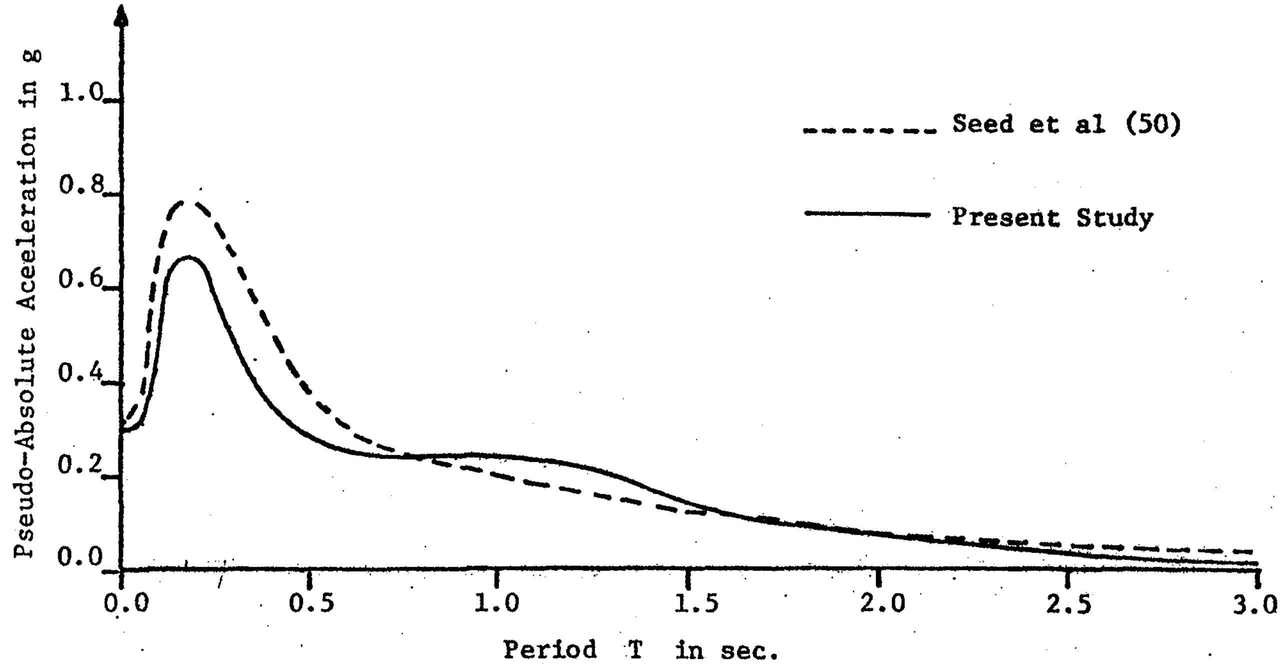

FIGURE 81 Comparison of Pseudo Absolute Acceleration Response Spectra, Los Angeles Site, Soil Class = 2, Damping = 5%, Time = 50 years, $P[S_a > s_a] = 0.1$.

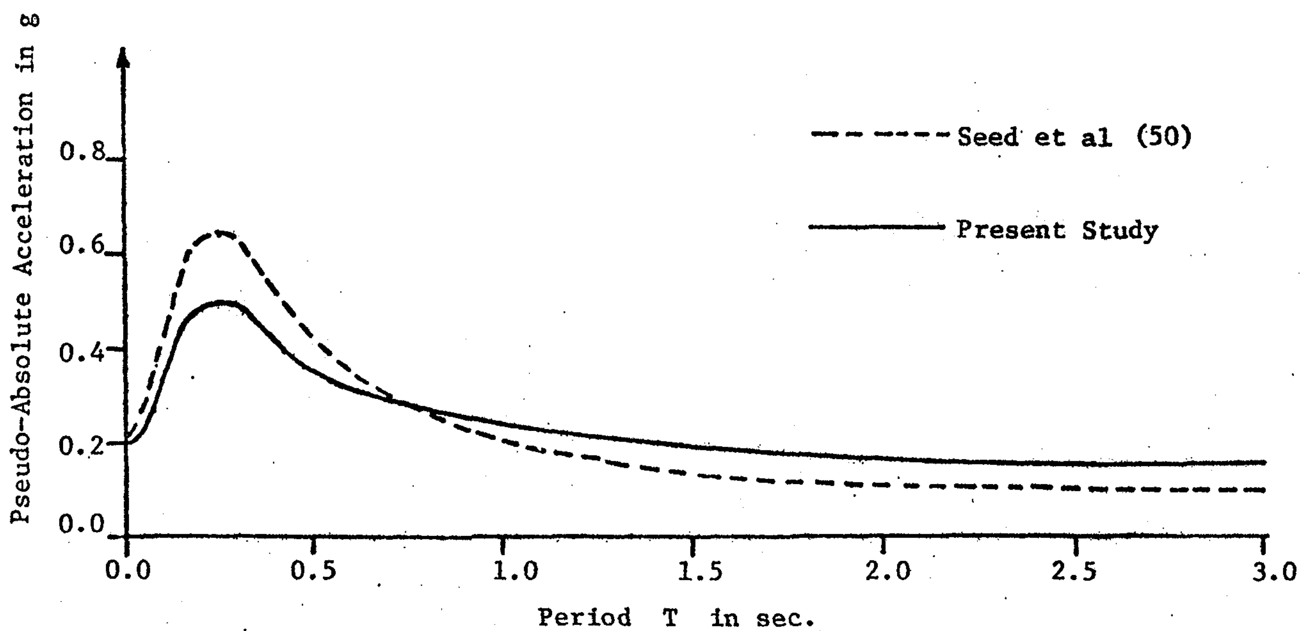

FIGURE 82 Comparison of Pseudo-Absolute Acceleration Response Spectra, Los Angeles Site, Soil Class = 1, Damping = 5%, Time = 50 years, $P[S_a > s_a] = 0.1$

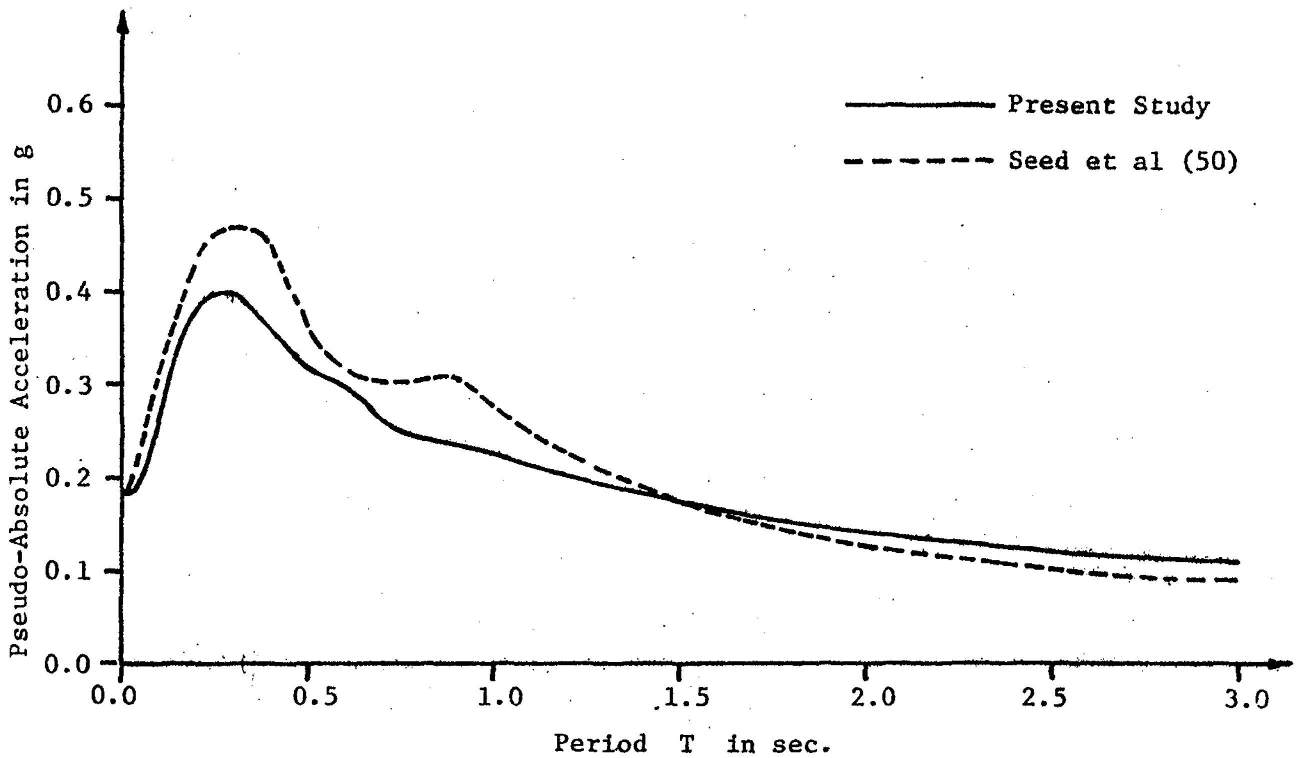

FIGURE 83 Comparison of Pseudo-Absolute Acceleration Response Spectra, Los Angeles Site, Soil Class = 0, Damping = 5%, Time = 50 years, $P[S_a > s_a] = 0.1$.

The response spectra for 50% risk level and 5% damping obtained in this study are compared to the mean spectra for magnitude 6 1/2 earthquake at a distance of 5 miles (8 km) as computed by Seed, et al (14). Figures 81 and 82 show the response spectra for soil classes 2 and 1. The deep cohesionless soils and soft to medium clays and sands are compared to the soil class 0 from this development as presented in Figure 83.

To be able to make a reasonable comparison, the response spectral shape for rocks obtained by Seed, et al (14) is multiplied by 0.30g, the shape for intermediate soils by 0.22g, and the shapes for deep cohesionless soils by 0.18g. These factors correspond to the peak ground acceleration values for 10% chance of exceedence in the next 50 years at a site in Los Angeles having either of soil conditions 2, 1, or 0.

From Figures 81 to 83, the response spectrum curves reported by the present study are lower than the response spectra obtained by Seed, et al (14) in all three cases when the natural period is smaller than about 0.7 sec. For values of T larger than about 0.7 sec the spectra from both studies are quite close. The discrepancy in the low period range results primarily because of the difference in the original strong motion data used in each study.

CHAPTER 6

CONCLUSIONS

The following significant observations can be made from the results of this study:

- Peak ground acceleration from a given earthquake, whose epicenter is within 25 km from the site of interest, diminishes in value by factors of 1.0, 0.75, and 0.60 as the local site conditions change from firm ground to intermediate soils, to alluvial soils. The corresponding factors for distances between 26 km and 50 km are 1.0, 1.16, and 1.09.
- Probability distributions on peak ground acceleration for soil classes 0 and 1 can be derived from the distribution for soil class 2 by applying the soil factors of k_0 and k_1 as given in Table 6.
- Spectral shapes for the three soil types described by classes 0, 1 and 2 are found to be statistically independent of peak ground acceleration. Correlation coefficients relating spectral shapes (dynamic amplification factors) and peak ground acceleration are very low.
- The stochastic behavior of dynamic amplification factors is found to be best represented by the gamma distribution. The fit of the gamma distribution to DAF data is better than either the lognormal or truncated normal distributions used by Dalal (1).

- Probability distributions on response spectra for 3 soil types can be obtained from the distributions on peak ground acceleration and the soil dependent gamma distributions on dynamic amplification factor as shown in Chapter 5.
- From the distributions on response spectra for a Los Angeles site and a future time period of 50 years, the risk is found to be highest for structures on soil class 1 and lowest on soil class 2 for natural periods higher than 0.3 sec. The risk is highest for structures on soil class 2 and lowest on soil class 0 at low periods smaller than about 0.3 sec.
- All of the results presented in this study depend on the quality of the strong motion data used. More than 50% of the data is from the February 9, 1971 San Fernando earthquake, thus any of the above conclusions have a bias towards this earthquake. The effect is strongest for the soil class 0 conclusions. The data for soil class 2, is fairly well represented by different earthquakes, but the majority of them are from Southern California. The application of any findings to other parts of the state should be done with great caution.

REFERENCES

1. Dalal, J. S., "Probabilistic Seismic Exposure and Structural Risk Evaluation", Technical Report No. 169, Dept. of Civil Engineering, Stanford University, February 1973.

2. Duke, C. M., "Effects of Ground on Destructiveness of Large Earthquakes," Journal of the Soil Mechanics and Foundation Division, ASCE, Vol. 84, No. SM3, Paper 1730, August 1958.

3. Gutenberg, B. and Richter, C. F., "Earthquake Magnitude, Intensity, Energy and Acceleration (Second Paper)", Bulletin of the Seismological Society of America, April 1956.

4. Gutenberg, B., "The Effects of Ground on Earthquake Motion," B SSA, Vol. 47, No. 3, July 1957, pp. 221-251.

5. Hansen, W. R., Weiss, R. B., Idriss, I. M. and Cluft, L. S., "Geotechnical Data Compilation for Selected Strong Motion Seismograph Sites in California", Woodward-Lundgren & Associates, Consulting Engineers and Geologists, Oakland, CA., December, 1973.

6. Hudson, D. E., Brady, A. G., Trifunac, M. D. and Vijayaraghavan, "Strong-Motion Earthquake Accelerograms, Corrected Accelerograms and Integrated Ground Velocity and Displacement Curves", Volume II, Part A, EERL71-50, Earthquake Engr. Res. Lab., Calif. Inst. of Tech., Pasadena, 1971.

7. Hudson, D. E., Trifunac, M. D. and Brady, A. G., "Strong-Motion Earthquake Accelerograms, Response Spectra", Volume III, Part A, EERL72-80, Earthquake Engr. Res. Lab., Calif. Inst. of Tech., Pasadena, 1972.

8. Hudson, D. E., editor, "Strong-Motion Instrumental Data on the San Fernando Earthquake of Feb. 9, 1971", Earthquake Engineering-ing Res. Lab., California Institute of Tech., and Seismological Field Survey, National Oceanic and Atmospheric Administration, U. S. Dept. of Commerce, September 1971.

9. Kanai, K., "Semi-empirical Formula for the Seismic Characteristics of the Ground", Bull. of the Earthquake Engineering Research Institute, Vol. 35, Part 2, June 1957, pp. 309-326.

10. Kiremidjian, A. S. and Shah, H. C., "Seismic Hazard Mapping of California", The John A. Blume Earthquake Engineering Center, Report No. 21, Dept. of Civil Engr., Stanford Univ., November 1975.

11. Kiremidjian, A. S., "Probabilistic Hazard Mapping and Development of Site-dependent Seismic Load Parameters", Ph.D. Dissertation, Department of Civil Engineering, Stanford University, Stanford, California, December 1976.

12. Seed, H. B. and Idriss, I. M., "Influence of Soil Conditions on Ground Motions During Earthquakes", Journal of Soil Mechanics and Foundation Division, Proceedings of the ASCE, SM1, pp. 99-137, January 1969.

13. Seed, H. B. and Idriss, I. M., "Influence of Soil Conditions on Building Damage Potential During Earthquakes", Journal of the Structural Division, Proceedings of the ASCE, ST2, pp. 639-663, February 1971.

14. Seed, H. B., Ugas, C. and Lysmer, T., "Site-Dependent Spectra for Earthquake Resistant Design", Report No. EERC 74-12, University of California, Berkeley, November 1974.

15. Shah, H. C., Mortgat, C. P., Kiremidjian, A. and Zsutty, T. C., "A Study of Seismic Risk for Nicaragua", Part I, The J. A. Blume Earthquake Engineering Center, Report No. 11, Dept. of Civil Engr., Stanford University, January 1975.

16. Shah, H. C., Zsutty, T. C., Krawinkler, H., Mortgat, C. P., Kiremidjian, A. S. and Dizon, J. O., "A Study of Seismic Risk for Nicaragua", Part II, The J. A. Blume Earthquake Engineering Center, Report No. 12A and 12B, Dept. of Civil Engr., Stanford University, March 1976.

17. Trifunac, M. D. and Brady, A. G., "On the Correlation of Seismic Intensity Scales With the Peaks of Recorded Strong Ground Motion", Bull. of the Seis. Soc. of Am., Vol. 65, No. 1, pp. 139-162, February 1975.

18. Wiggins, J. H., Effect of Site Conditions on Earthquake Intensity, J. Struct. ASCE, ST2, April 1964.

19. Wood, H. O., "Distribution of Apparent Intensity in San Francisco", in "The California Earthquake of April 18, 1906", Report of the State Earthquake Investigation Commission, Carnegie Institute of Washington, Washington, D. C., pp. 220-245.